UNIVERSIDADE FEDERAL DE PELOTAS
Instituto de Física e Matemática
Programa de Pós-Graduação em Física

Tese

Electroweak gauge boson production in hadronic collisions at forward rapidities in the color - dipole S - matrix framework

Yan B. Bandeira

Pelotas, 2025

Yan B. Bandeira

Electroweak gauge boson production in hadronic collisions at forward rapidities in the color - dipole S - matrix framework

Advisor: Prof. Dr. Victor Gonçalves

Coadvisor: Prof. Hab. Dr. Wolfgang Schäfer

Pelotas, 2025

Yan B. Bandeira

Electroweak gauge boson production in hadronic collisions at forward rapidities in the color - dipole S - matrix framework

Tese aprovada, como requisito parcial, para obtenção do grau de Doutor em Física, Programa de Pós-Graduação em Física, Instituto de Física e Matemática, Universidade Federal de Pelotas.

Data da Defesa: 25 de julho de 2025

Banca Examinadora:

Prof. Dr. Victor Paulo Barros Gonçalves (orientador)
Doutor em Física pela Universidade Federal do Rio Grande do Sul.

Prof. Dr. Fernando Silveira Navarra
Doutor em Física pela Universidade de Marburg.

Prof. Dr. João Thiago de Santana Amaral
Doutor em Física pela Universidade Federal do Rio Grande do Sul.

Prof. Dr. Mario Luiz Lopes da Silva
Doutor em Física pela Universidade Federal do Rio Grande do Sul.

Prof. Dr. Werner Krambeck Sauter
Doutor em Física pela Universidade Federal do Rio Grande do Sul.

I dedicate this work to my grandmother, Iolanda Anselmo Bueno, who, despite never having experienced academic life herself, has always been my greatest inspiration in pursuing this path.

ACKNOWLEDGEMENTS

ABSTRACT

BANDEIRA, Yan B.. **Electroweak gauge boson production in hadronic collisions at forward rapidities in the color - dipole S - matrix framework**. Advisor: Victor Gonçalves. 2025. 121 f. Thesis (Doctorate in Physics) – Institute of Physics and Mathematics, Federal University of Pelotas, Pelotas, 2025.

Understanding the internal structure of the proton in the high-energy regime remains a key challenge in Quantum Chromodynamics (QCD). At small values of Bjorken-x, the proton dynamics becomes saturated with gluons, leading to a nonlinear regime characterized by a high-density QCD dynamics and saturation effects. Forward rapidity processes in hadronic collisions offer a unique opportunity to probe this regime, complementing information obtained from deep inelastic scattering experiments. In this thesis, we study the production of electroweak gauge bosons ($G = W^{\pm}, Z^0, \gamma$) at forward rapidities within the hybrid factorization framework, using the color dipole S-matrix (CDSM) formalism. We derive the differential cross-sections of the processes $qp \to GX$ and $qp \to GJX$, both in impact parameter and transverse momentum spaces, taking into account the longitudinal and transverse polarizations of the gauge bosons. We show that the final results can be expressed in terms of the dipole–proton cross–section or the target unintegrated gluon distribution, enabling a quantitative analysis of saturation effects in the LHC kinematics and beyond. Furthermore, we present, for the first time, the general expressions for electroweak gauge boson + jet at forward rapidities. Our results generalize and reproduce previous findings in the literature for real photon and Z^0 production and we present for the first time the description to $W^{\pm}$ boson production. In addition, we analyze dilepton production at forward rapidities, deriving the angular coefficients associated with the decay of virtual photons, Z^0, and $W^{\pm}$ bosons. Numerical results are presented for $\sqrt{s} = 14$ TeV in the rapidity range $2.0 \le y \le 4.5$, including comparisons between different models for the unintegrated gluon distribution and tests of the Lam–Tung relation. The results presented in this thesis provide novel insight into the dynamics of QCD in the small-x regime and offer new tools for phenomenological studies of forward electroweak processes at current and future high-energy colliders.

Keywords: Forward Electroweak boson production; Color Dipole S-Matrix; Hybrid Factorization; Small-x physics.

RESUMO

Compreender a estrutura interna do próton em altas energias segue como um dos principais desafios da Cromodinâmica Quântica. Para pequenos valores de Bjorken-x, a distribuição interna torna-se saturada com glúons, levando a um regime não linear, caracterizado por dinâmicas da QCD em alta densidade e efeitos de saturação. Processos em rapidez frontal em colisões hadrônicas oferecem uma oportunidade única de investigar esse regime, complementando os dados de espalhamento inelástico profundo. Nesta tese, estudamos a produção de bósons de calibre eletrofracos ($G = W^{\pm}, Z^0, \gamma$) em regiões de rapidez frontal no descrição da fatoração híbrida, utilizando o formalismo da matriz-S de dipolo de cor. Derivamos as seções de choque diferenciais dos processos $qp \rightarrow GX$ e $qp \rightarrow GJX$, tanto no espaço do parâmetro de impacto quanto no espaço de momento, considerando as polarizações longitudinal e transversal. Mostramos que os resultados podem ser expressos em termos da seção de choque dipolo–próton ou da distribuição de glúons não integrada, possibilitando uma análise quantitativa dos efeitos de saturação nas cinemáticas do LHC e além. Além disso, apresentamos, pela primeira vez, as expressões gerais para a produção associada de bósons de calibre eletrofracos com jatos em regiões de rapidez frontal. Nossos resultados generalizam e reproduzem expressões anteriores da literatura para a produção de fótons reais e bósons Z^0, e introduzem pela primeira vez a descrição teórica da produção do bóson $W^{\pm}$ nesse formalismo. Adicionalmente, analisamos a produção de pares de léptons em regiões de rapidez frontal, derivando os coeficientes angulares associados ao decaimento dos bósons virtuais γ^*, Z^0 e $W^{\pm}$. Apresentamos resultados numéricos para $\sqrt{s} = 14$ TeV no intervalo de rapidez $2.0 \leq y \leq 4,5$, incluindo comparações entre diferentes modelos para a distribuição não integrada de glúons e uma análise da relação de Lam–Tung. Os resultados apresentados nesta tese oferecem novas perspectivas sobre a dinâmica da QCD no regime de pequeno-x e fornecem ferramentas inéditas para o estudo fenomenológico de processos eletrofracos em regiões de rapidez frontal nos atuais e futuros colisores de altas energias.

Palavras-chave: Produção de bósons eletrofracos em rapidez frontal; Matriz S de dipolo de cor; Fatoração híbrida; Física de pequeno-x.

LIST OF FIGURES

CONTENTS

1 INTRODUCTION

Since antiquity, the nature of matter's fundamental constituents has captivated human inquiry, evolving into a rigorous scientific pursuit by the 19th century with the establishment of atomic theory and the identification of the electron by J. J. Thomson. Subsequent discoveries, including the atomic nucleus by Rutherford, the neutron by Chadwick, and the positron and neutrino in the 1930s, progressively revealed the growing complexity of the subatomic world. These findings challenged existing models and led to the formulation of nuclear theories describing protons and neutrons as composite systems bound by the strong force, mediated by mesons. However, the increasing number of strongly interacting particles observed in high-energy experiments necessitated a new classification – hadrons, encompassing baryons and mesons. In the early 1960s, the quark model emerged as a framework to describe hadrons as composites of more elementary constituents. Although initially viewed with skepticism, quarks gained substantial empirical support in the late 1960s through deep inelastic electron-proton scattering experiments conducted at the Stanford Linear Accelerator Center (SLAC). These groundbreaking experiments revealed point-like substructures within the proton, providing the first direct evidence for the existence of quarks and revolutionizing our understanding of hadronic matter. These discoveries laid the foundation for Quantum Chromodynamics (QCD), which explains key phenomena such as color confinement and asymptotic freedom, and it is now a central component of the Standard Model (SM) of particle physics. This insight, combined with the development of accelerator technologies, paved the way for the modern understanding of hadronic matter in terms of partons – quarks and gluons.

However, many open questions remain, requiring an extension of our understanding of the Standard Model and/or its future modification. One of the unresolved problems or mysteries is the description of hadrons in the high-energy regime of the strong interactions theory. QCD predicts that, for large atomic numbers and high energies, the hadronic system is characterized by a high parton density. This leads from a linear dynamic regime, where only emission processes are considered, to a nonlinear regime where parton recombination becomes significant.

The lepton-hadron process was fundamental to improving the proton structure. In Deep Inelastic Scattering (DIS), the large momentum transfer between the lepton and the target allows one to resolve the individual partons — quarks and gluons — inside the proton. Measurements from DIS have been essential in establishing the parton model and in determining parton distribution functions (PDFs), which encode the momentum distribution of partons within the proton. Experiments such as those at HERA extended the reach of DIS into previously unexplored kinematic regions, further refining our understanding of quantum chromodynamics (QCD) and the internal dynamics of the proton. One main result from HERA is that in the low-x regime, the gluon distribution becomes larger, and then in this region, the gluon densities dominate. As the HERA experiment ceased operations in 2007, hadron colliders such as the Large Hadron Collider (LHC) now provide our most powerful experimental platform for probing proton structure, via hadronic interactions.

In this context, a natural path toward advancing our understanding of the proton's internal structure is through the Drell–Yan (DY) process, $pp \rightarrow [GX \rightarrow l\bar{l}]X$, in which a lepton–antilepton pair is produced via an intermediate electroweak boson ($G = \gamma, Z^0, W^{\pm}$) originating from a quark–antiquark annihilation in hadronic collisions (pp or $p\bar{p}$). These processes are particularly valuable because the electroweak bosons involved are color-neutral, which suppresses final-state QCD interactions. This feature allows for a cleaner interpretation of the observed final states in terms of the initial-state parton dynamics, making electroweak boson production a powerful probe of parton distribution functions (PDFs), especially in kinematic regimes that complement those accessed via DIS.

Moreover, the electroweak gauge boson production in association with hadronic jets is among the most important processes studied at hadron colliders. Electroweak gauge bosons — photons, Z, and W — mediate electroweak (EW) interactions, while the associated hadronic jets arise from QCD processes, specifically from the fragmentation and hadronization of high-energy partons (quarks and gluons) produced in the collision. Therefore, the study of $G+$ jets events constitutes an ideal probe for testing QCD and electroweak interactions as well as a major source of backgrounds to searches for new physics. Measurements of $G +$ jets also validate the adequacy of the approximations used in theoretical calculations and models used for background estimates in precision measurements. Thanks to their large cross-sections, the colorless nature of the γ, W, and Z bosons as carriers of electromagnetic and weak forces, respectively, and their high sample purities, accurate studies of $G +$ jets are of paramount importance for the success of a hadron collider physics program (Tricoli; Schönherr; Azzurri, 2021). In this scenario, the proton structure dynamics remains an open question.

For hadronic collisions, the proton structure dynamics can be investigated at forward rapidities where there is an imbalance between the projectile parton's and the target's

energy scale, allowing us to investigate the small x region of the proton dynamics. At forward rapidities, we have an asymmetric kinematic configuration, dominated by the interaction between partons with a large momentum fraction, x, in one of the hadrons with partons with small x in the other. As the number of partons increases with decreasing x, in this kinematic configuration, we have the interaction between a diluted system (the hadron with large x) and a dense system (the hadron with small x). Such processes are considered ideal for proving the dynamics of strong interactions in the nonlinear regime (Gelis; Iancu; Jalilian-marian; Venugopalan, 2010; Weigert, 2005; Jalilian-marian; Kovchegov, 2006).

The primary HERA result is the proton structure picture at small x, where it is densely populated. This physical system description is an open question. In this thesis, our objective is to enhance our understanding of proton dynamics in this regime, which can be investigated at forward rapidities in hadronic collisions. However, evaluating cross-sections in hadronic collisions is inherently nontrivial, since hadrons are not point-like objects, but composite systems governed by QCD. Then, partons exhibit both perturbative and nonperturbative dynamics, manifested through two fundamental properties of QCD: asymptotic freedom at high energies, where interactions become weak and perturbative calculations are reliable, and confinement at low energies, where the strong coupling prevents the isolation of individual partons. Fortunately, factorization schemes provide a robust theoretical framework that allows the separation of perturbative and nonperturbative contributions, ensuring that the total cross-section can be expressed as a convolution of these components. The most widely used framework is collinear factorization, which assumes that partons are collinearly distributed relative to the parent hadron. In this scheme, all nonperturbative information is encapsulated in the parton distribution functions (PDFs) of the hadrons, while the hard scattering cross-section is computed perturbatively. However, in specific kinematic regimes — particularly at forward rapidities and small x — the assumptions underlying collinear factorization may break down, then one expects a violation of collinear factorization due to the emergence of high gluon densities and significant transverse momentum components. Consequently, in recent years, several groups have proposed generalized factorization schemes, which involve new objects in addition to the usual (un)integrated parton distribution functions. In this thesis, we'll explore the hybrid factorization formalism as given in the Color Dipole S-Matrix framework (CDSM) proposed in the Refs. (Nikolaev; Schafer; Zakharov; Zoller, 2003; Nikolaev; Schafer, 2005; Nikolaev; Schafer; Zakharov; Zoller, 2005a; Nikolaev; Schafer; Zakharov, 2005a; Nikolaev; Schafer; Zakharov; Zoller, 2005b; Nikolaev; Schafer; Zakharov, 2005b). In this framework the hadronic cross-section for the dihadron production at forward rapidities is given as a convolution of the standard parton distributions for the dilute projectile, the parton–target cross-section (which includes the high-density effects) and the parton fragmentation functions. This

formalism connects perturbative QCD at high momentum transfer with the nonlinear small x dynamics, offering a consistent framework to study forward rapidity phenomena in collider experiments.

In this thesis, motivated by the challenges in describing proton dynamics in the high-energy regime where high-density effects are expected to play a significant role, our main objective is to improve the understanding of the proton structure and its impact on physical observables. As discussed, this kinematic region is best accessed in hadronic collisions at forward rapidities. Furthermore, the Drell–Yan process has been identified as a powerful probe to investigate and disentangle the internal structure of the proton. In this context, we present, for the first time, a detailed analysis of electroweak gauge boson production at forward rapidities in hadronic collisions within the hybrid factorization framework. In Refs. (Bandeira; Goncalves; Schäfer, 2024, 2025), we presented, for the first time in the literature, a full derivation of the general formulae for inclusive electroweak gauge boson production at forward rapidities within the Color Dipole S-Matrix framework. We demonstrated that, in the appropriate limits and representations, our results consistently reduce to those previously employed in Refs. (Kopeliovich; Rezaeian; Pirner; Schmidt, 2007; Kopeliovich; Levin; Rezaeian; Schmidt, 2009; Santos; Silveira; Machado, 2020; Gelis; Jalilian-marian, 2002a; Jalilian-marian; Rezaeian, 2012; Ducloué; Lappi; Mäntysaari, 2018; Goncalves; Lima; Pasechnik; Šumbera, 2020; Lima; Giannini; Goncalves, 2024; Kopeliovich; Raufeisen; Tarasov, 2001; Raufeisen; Peng; Nayak, 2002; Kopeliovich; Raufeisen; Tarasov; Johnson, 2003; Betemps; Gay ducati, 2004; Betemps; Ducati; Machado; Raufeisen, 2003; Golec-biernat; Lewandowska; Stasto, 2010; Ducati; Griep; Machado, 2014; Schäfer; Szczurek, 2016; Ducloué, 2017; Gelis; Jalilian-marian, 2002b; Baier; Mueller; Schiff, 2004; Stasto; Xiao; Zaslavsky, 2012; Kang; Xiao, 2013; Basso; Goncalves; Krelina; Nemchik; Pasechnik, 2016; Basso; Goncalves; Nemchik; Pasechnik; Sumbera, 2016; Marquet; Wei; Xiao, 2020) for estimating real photon and Z^0 production. Moreover, the cross-section for $W^\pm$ boson production within the hybrid factorization framework was derived for the first time, representing a novel contribution to the theoretical description of electroweak processes at forward rapidities. Lastly, in Ref. (Bandeira; Goncalves; Schäfer, 2025), we investigate the angular distributions of leptonic pairs $(\bar{l}_1 l_2)$, extending the results of Ref. (Schäfer; Szczurek, 2016) to cases where the dilepton system originates from the decay of Z^0 or $W^\pm$ gauge boson. We present the main theoretical ingredients required to explore spin-vector and tensor polarization effects, among other polarization observables. As a result, we provide a comprehensive framework to study proton dynamics in hadronic collisions at forward rapidities through inclusive observables, offering new insights into the interplay between QCD dynamics and electroweak processes in the high-energy, small x regime.

This document is structured as follows. In the next chapter, we introduce the

fundamental concepts of Quantum Chromodynamics (QCD), including confinement and asymptotic freedom. As a direct consequence of these properties, the calculation of hadronic cross-sections becomes nontrivial and requires the use of factorization schemes. We will discuss the collinear factorization framework in detail, followed by an overview of the kinematics involved in hadronic collisions. Special attention will be given to the forward rapidity region, where the asymmetric momentum configuration leads to the breakdown of collinear factorization and necessitates alternative approaches.

In Chap. 3, the color dipole S-matrix framework which is a hybrid factorization scheme will be presented where the hadronic cross-section is described as a convolution of the dilute incoming parton PDF and the parton-target cross-section. Although a series of analysis was performed using such framework, we will extend it to the electroweak gauge boson production — which was a gap in the literature. For such extension, the parton-target cross section depends on the dipole-proton cross-section and the light front wave function (LFWF) of an electroweak gauge boson radiated off a quark. We will derive for the first time the generic LFWF's.

From the derivation present before, in Chap. 4 we will derive both isolated and gauge boson + jet parton-target cross-section. We will also demonstrate that, in the appropriate limits and representations, our expressions consistently reduce to those found in the literature for real photon and Z^0 production, thereby validating the formalism. Additionally, we will present, for the first time within this framework, the derivation of the cross-section for $W^\pm$ boson production.

Furthermore, in Chap. 5, we extend our formalism showed so far to a less inclusive observable, the lepton pair angular distribution. We will demonstrate that our formalism implies that the angular distribution is fully characterized by six nonvanishing angular coefficients. In addition, we present the results for the transverse momentum dependence of the distinct angular coefficients considering pp collisions. Finally, in Chap. 6 we will summarize our main results and conclusions.

Some remarks are in order. All figures in this document that do not have an explicitly indicated source were produced by the author. The conventions and notations adopted throughout this thesis are summarized in Appendix A. Additionally, this document was reviewed with the assistance of AI tools to enhance the clarity and grammar of the English text. To maintain the narrative focus and flow, we have chosen not to include the study performed in Ref. (Bandeira; Goncalves, 2023), which analyzed higher-twist contributions in eA collisions within the context of the EIC proposal. Lastly, it is worth mentioning that a six-month research internship was conducted at the Institute of Nuclear Physics (INP/PAN) in Kraków, Poland, with funding provided by CAPES. During this period, the author had the opportunity to present and discuss several of the results reported in this thesis.

2 BASIC CONCEPTS

The current understanding of the fundamental constituents of matter is encapsulated in the Standard Model. This theory provides a comprehensive description of elementary particles and their interactions. There are four fundamental forces known to exist: gravitational, electromagnetic, weak, and strong. Notably, the Standard Model does not encompass gravity. Fig. 1 presents a schematic overview of the Standard Model, delineating between fermions and bosons, characterized by their fractional or integer spins, respectively. Fermions are further categorized into quarks and leptons. These three particle types — quarks, leptons, and bosons — form the basis of the Standard Model.

Bosons are classified into gauge bosons and the Higgs boson. Gauge bosons mediate the interactions described by quantum field theories, while the Higgs boson is responsible for endowing other particles with mass (Thomson, 2013). Quarks and leptons are organized into three generations, with each subsequent generation having particles with identical quantum numbers but larger masses.

The photon (γ), a gauge boson, mediates electromagnetic interactions as described by quantum electrodynamics (QED). Any charged fermion can participate in electromagnetic interactions. The Z and W bosons, on the other hand, mediate the weak force, which is responsible for certain types of radioactive decay. Fermions possess a quantum number known as "flavor", which distinguishes different types of quarks and leptons. For instance, leptons have flavors such as electron, electron neutrino, muon, muon neutrino, tau, and tau neutrino. Quarks, conversely, have flavors like up, down, charm, strange, top, and bottom. The electromagnetic and weak forces can be unified into a single electroweak theory.

Finally, the gluon, another gauge boson, mediates the strong force, which is described by quantum chromodynamics (QCD). Quarks possess a quantum number called "color charge", which allows them to interact via the strong force. Unlike the other forces, color charge is unique to quarks and gluons. A distinguishing feature of quarks is that they are always bound together in composite particles, such as protons and neutrons, because of the confining nature of the strong force. This phenomenon will be explored

Figure 1 – Illustration of the Standard Model.

	three generations of matter (fermions)			three generations of antimatter (antifermions)			interactions / forces (bosons)	
	I	II	III	I	II	III		
mass charge spin	$\simeq$ 2.2 MeV +2/3 1/2 **u** up	$\simeq$ 1.3 GeV +2/3 1/2 **c** charm	$\simeq$ 173 GeV +2/3 1/2 **t** top	$\simeq$ 2.2 MeV −2/3 1/2 **ū** antiup	$\simeq$ 1.3 GeV −2/3 1/2 **c̄** anticharm	$\simeq$ 173 GeV −2/3 1/2 **t̄** antitop	0 0 1 **g** gluon	$\simeq$ 125 GeV 0 0 **H** Higgs
	$\simeq$ 4.7 MeV −1/3 1/2 **d** down	$\simeq$ 96 MeV −1/3 1/2 **s** strange	$\simeq$ 4.2 GeV −1/3 1/2 **b** bottom	$\simeq$ 4.7 MeV +1/3 1/2 **d̄** antidown	$\simeq$ 96 MeV +1/3 1/2 **s̄** antistrange	$\simeq$ 4.2 GeV +1/3 1/2 **b̄** antibottom	0 0 1 **γ** photon	
	$\simeq$ 0.511 MeV −1 1/2 **e⁻** electron	$\simeq$ 106 MeV −1 1/2 **μ⁻** muon	$\simeq$ 1.777 GeV −1 1/2 **τ⁻** tau	$\simeq$ 0.511 MeV +1 1/2 **e⁺** positron	$\simeq$ 106 MeV +1 1/2 **μ⁺** antimuon	$\simeq$ 1.777 GeV +1 1/2 **τ⁺** antitau	$\simeq$ 91.2 GeV 0 1 **Z⁰** Z boson	
	< 1.0 eV 0 1/2 **ν_e** electron neutrino	< 0.17 eV 0 1/2 **ν_μ** muon neutrino	< 18.2 MeV 0 1/2 **ν_τ** tau neutrino	< 1.0 eV 0 1/2 **$\bar{\nu}_e$** electron antineutrino	< 0.17 eV 0 1/2 **$\bar{\nu}_\mu$** muon antineutrino	< 18.2 MeV 0 1/2 **$\bar{\nu}_\tau$** tau antineutrino	$\simeq$ 80.4 GeV −1 1 **W⁻** W boson	$\simeq$ 80.4 GeV +1 1 **W⁺** W boson

in more detail in the subsequent section.

2.1 Quantum Chromodynamics

Quantum Chromodynamics (QCD) is a quantum field theory that describes the strong interactions occurring within hadrons between quarks and gluons, endowed with a non-Abelian gauge symmetry of the SU(3) color group. That is, all color carriers are subject to strong interactions. The Lagrangian density for QCD, invariant under SU(3) group transformations, is ($\slashed{D} = \gamma^\mu D_\mu$)

$$\mathcal{L}_{\text{QCD}} = \sum_f \overline{\psi}_f \left(i\slashed{D} - m_f I\right)\psi_f - \frac{1}{4}F_{\mu\nu}^a F^{a\mu\nu} + \mathcal{L}_{\text{GF}} + \mathcal{L}_{\text{FPG}}. \tag{1}$$

The first term describes quarks, where the quark field is represented by ψ with mass m_f, and the sum is over all six flavors f. I represents the identity matrix and D_μ is the covariant derivative, defined as follows

$$D_\mu \equiv I\partial_\mu + igt^a A_\mu^a, \tag{2}$$

where g determines the coupling of both the quark field and the gluon field, as well as of the gluons among themselves. The color matrix t a acts as a generator of the SU(3) color group. In a fundamental representation, the color matrices are related to

the Gell-Mann matrices as follows $t^a = \lambda^a/2$ (Muta, 2010), which satisfy

$$\left[t^a, t^b\right] = i f^{abc} t^c \qquad \text{and} \qquad \text{Tr}\left(t^a t^b\right) = \frac{1}{2}\delta^{ab}, \qquad (3)$$

where $a, b, c = 1, 2, \ldots 8$. The structure constants f^{abc} are antisymmetric under the exchange of two indices, i.e., $f^{abc} = -f^{bac}$ and satisfy the Jacobi identity:

$$f^{adc} f^{bcd} + f^{bdc} f^{cad} + f^{cde} f^{abd} = 0. \qquad (4)$$

The tensor $F^a_{\mu\nu}$ in the second term of Eq. (1), which represents the interaction between the gluon fields, is defined as follows

$$F^a_{\mu\nu} \equiv \partial_\mu A^a_\nu - \partial A^a_\mu + g f^{abc} A^b_\mu A^c_\nu. \qquad (5)$$

From a simple comparison between the tensor $F_{\mu\nu}$ of QED and the tensor $F^a_{\mu\nu}$ of QCD, we see that in the case of QCD there is the presence of the term $g f^{abc} A^b_\mu A^c_\nu$, which allows the self-interaction of the gluon field, that is, in QCD the gauge bosons self-interact. This property is fundamental to justify the properties and effects that will be seen later.

To finalize our analysis of the QCD Lagrangian density, we have that the last two terms in Eq. (1) correspond to gauge fixing (GF) and the Faddeev-Popov ghost (FPG) field. For more details, see Ref. (Muta, 2010).

A crucial feature of QCD arises from the renormalization process, employed to address infinities that emerge in quantum field theories such as QCD. In QED, renormalization is used to manage infinities arising from loop diagrams, as illustrated in Fig. 2. These calculations reveal that the coupling constant varies with distance and is inversely proportional to the scale Q. The explicit summation of loop diagrams, depicted in Fig. 2, produces an expression for electromagnetic coupling, $\alpha_{\text{em}}(Q^2)$. The distance dependence in the electromagnetic case is weak, which implies that the approximation $\alpha_{em} \simeq 1/137$ is sufficiently accurate (Griffiths, 2008). In QED, the electron is surrounded by virtual photons and virtual electron-positron pairs that continually annihilate and create each other (Greiner; Reinhardt, 2008). Due to the attraction between opposite charges, virtual positrons tend to approach the electron, thereby screening the electron's charge. This phenomenon is analogous to the polarization of a dielectric medium in the presence of an electric charge and is termed vacuum polarization. This interpretation accounts for the fact that in QED, the coupling becomes stronger as the charges approach each other (larger Q^2).

In QCD, the same interpretation cannot be inferred, as the QCD vacuum is not solely composed of virtual $q\bar{q}$ pairs but also contains gluons, given that gluons are self-interacting. Consequently, unlike QED, in QCD, in addition to quark-quark-gluon vertices

Figure 2 – Renormalization in QED
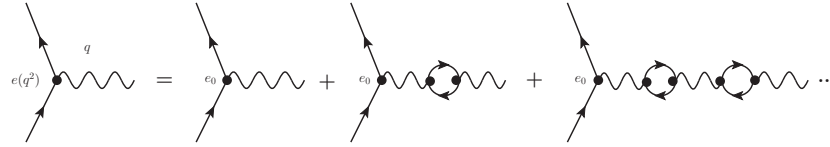
Figure 3 – Renormalization in QCD
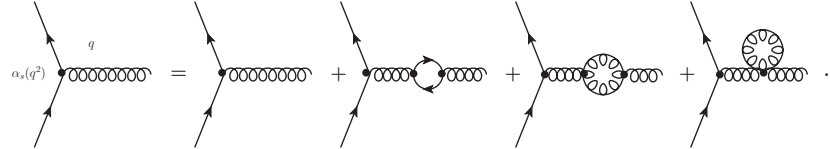
(quark loops), which screen the quark's color charge, leading to a strong increase in the strong interaction coupling constant at short distances, there are also direct gluon-gluon vertices (gluon loops), as seen in Figure 3, which have an opposite effect to quark loops, producing antiscreening that decreases the coupling at short distances. The resulting form of the QCD coupling constant is given by (Muta, 2010):

$$\alpha_s(Q^2) = \frac{12\pi}{(11N_c - 2N_f)\ln\left(Q^2/\Lambda^2\text{QCD}\right)}\,, \qquad \text{for } Q \gg \Lambda\text{QCD}, \qquad (6)$$

where the parameter Λ_{QCD} is introduced as a scale characterizing the non-perturbative region. The value $\Lambda_{\text{QCD}} \approx 200 \sim 300$ MeV is not predicted theoretically but is determined experimentally and depends on the renormalization scheme used (Bethke, 2009).

From the Standard Model, we have that for quarks $N_c = 3$ and $N_f = 6$, hence $11N_c > 2N_f$, causing the antiscreening effect to dominate and, consequently, the coupling constant to decrease with increasing Q^2. This leads to quarks confined within hadrons acting almost as free particles when probed at sufficiently high energies. This property of strong interactions is called asymptotic freedom. Asymptotic freedom enables the use of perturbation theory, leading to quantitative predictions for physical observables in hadronic interactions. Conversely, as the distance increases, the coupling becomes so strong that it becomes impossible to isolate a quark from a hadron. This mechanism is called confinement.

The behavior of the coupling constant given by Eq. (6) is presented in Figure 4, where the properties of asymptotic freedom and confinement are explicitly shown by the asymptotic limits of the coupling constant. A comprehensive discussion of this topic is presented in Ref. (d'enterria et al., 2024), which provides an updated perspective. Furthermore, Figure 4 shows that the intensity of the QCD coupling varies considerably within the range of Q relevant to particle physics in the high energy regime. The low transverse momentum regime, $Q \ll \Lambda_{\text{QCD}}$, where $\alpha_s \approx 1$, is the regime in which the use of perturbation theory is not valid (*soft QCD*). This is the regime of color confinement. On the other hand, the high transverse momentum regime, $Q \gg \Lambda_{\text{QCD}}$, where α_s is

Figure 4 – The evolution of the QCD coupling α_s as a function of the scale Q
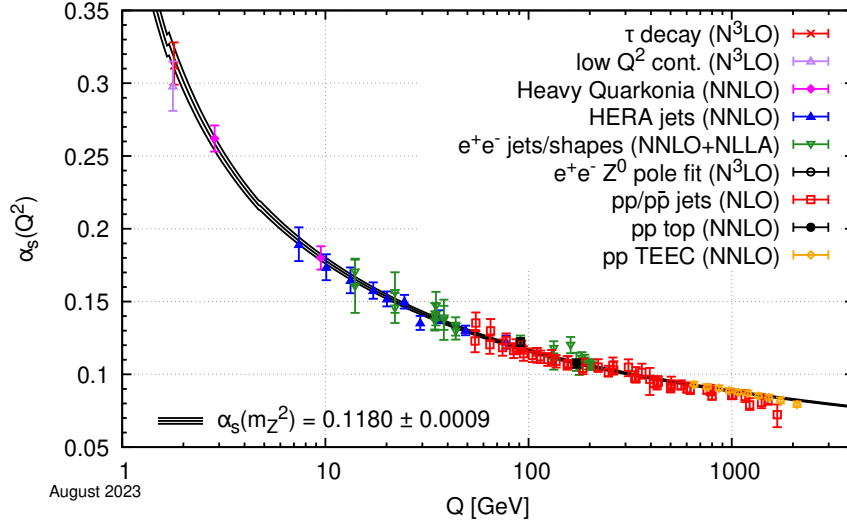
Source: Extracted from (Zyla et al., 2020).

sufficiently small, allows for the use of perturbation theory, hence we have perturbative QCD (pQCD) (Collins, 2023).

Therefore, QCD predicts two opposed behaviors for the coupling, implying that in collision processes, both short-distance (pQCD) and long-distance non-perturbative QCD effects will be present. Consequently, the calculation of cross-sections for these processes that depend on QCD dynamics becomes complex. However, factorization theorems allow for the separation of these contributions and the realization of precise calculations of the observables.

The hadron structure dynamics is ruled by QCD and its evolution is given by the DGLAP evolution equation (Dokshitzer, 1977; Altarelli; Parisi, 1977; Gribov; Lipatov, 1971),

$$\frac{\partial q_i(x, Q^2)}{\partial \ln Q^2} = \frac{\alpha_s}{2\pi} \int_x^1 \frac{dy}{y} \left[q_i(y, Q^2) P_{qq}(x/y) + g(y, Q^2) P_{qg}(x/y) \right] \tag{7}$$

for the quark sector and

$$\frac{\partial g(x, Q^2)}{\partial \ln Q^2} = \frac{\alpha_s}{2\pi} \int_x^1 \frac{dy}{y} \left[\sum_i q_i(y, Q^2) P_{gq}(x/y) + g(y, Q^2) P_{gg}(x/y) \right]. \tag{8}$$

for the gluon sector. In eq. (7) and eq. (8), $q_i(x, Q^2)$ and $g(x, Q^2)$ are the quark distribution of flavor i and the gluon distribution, respectively. These evolution equations govern the scale dependence of the parton distribution functions (PDFs), allowing them to be evolved to a given virtuality Q^2.

Using global fits that account for both nonperturbative and perturbative contributions,

Figure 5 – Parton densities as extracted from HERA data by H1, ZEUS and CTEQ collaborations at $Q^2 = 10$ GeV^2. The sea quark and gluon densities are reduced by a factor of 20.
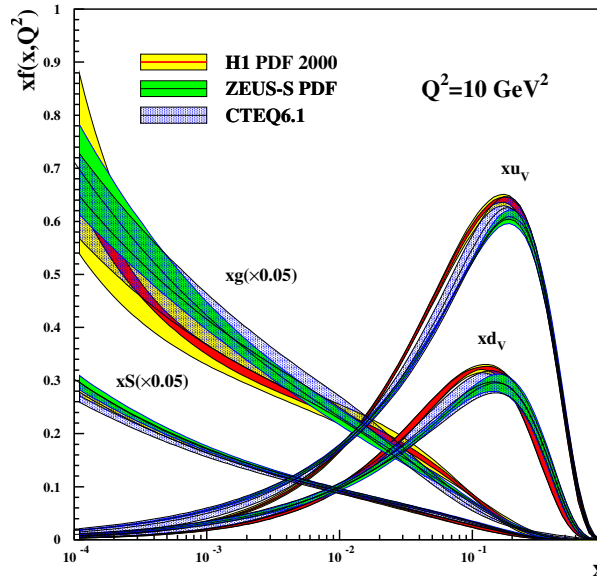
Source: Extracted form (Newman, 2004)

one can reconstruct the internal structure of the proton in terms of its parton content. Figure 5 illustrates this, presenting the valence quark densities, the total sea quark contribution, and the gluon distribution, as extracted by the HERA collaborations H1 and ZEUS (Adloff et al., 2003; Chekanov et al., 2003), compared with the CTEQ global fit results (Pumplin; Stump; Huston; Lai; Nadolsky; Tung, 2002), which incorporate a wide range of DIS data. It is important to note that, in Fig. 5, both the sea quark and gluon distributions have been rescaled by a factor of 20 for visualization purposes. This rescaling emphasizes that, at small values of x, the proton becomes densely populated by gluons.

2.2 Factorization

The fundamental problem that factorization theorems address is how to compute high-energy scattering cross-sections. In the following, we will consider the example of hadron-hadron interactions. More specifically, we will address the production of dihadrons in pp collisions, $p + p \rightarrow H_1 + H_2 + X$, as depicted in Fig. 6, using the collinear factorization scheme, where partons inside the hadron move collinearly with the hadron. Thus, the partons have momenta approximately xP, where $x \in (0, 1)$ and P is the momentum of the hadron. The description of partons inside the hadron is given by parton distribution functions $f_i(x, Q^2)$, which are non-perturbative quantities that characterize the probability of finding a parton of a given flavor i with a momentum fraction x. However, the interaction between partons from different incident hadrons

Figure 6 – Illustration of the collinear factorization theorem for a dihadron production in a pp collision.
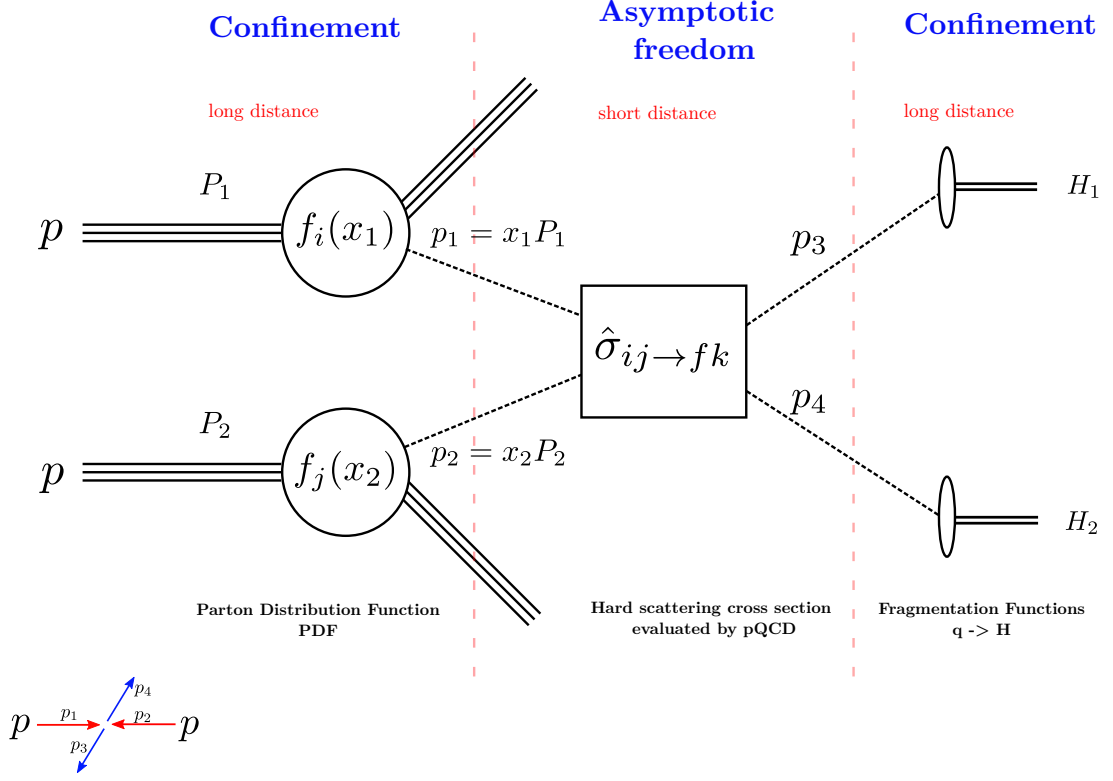
occurs at short distances and is therefore amenable to a perturbative description. Such a description is given by the cross-section for the partonic process $i + j \rightarrow q + \overline{q}$, $\hat{\sigma}_{ij}$. The partons will form hadrons in the final state due to the confinement property. This hadronization is generally described by fragmentation functions (FFs), $\mathcal{D}^{k/h}$, which provide the probability that a flavor parton k will generate a given hadron h. The factorization theorem is based on the fact that the description of the initial state, the interaction, and the formation of hadrons in the final state occurs at different distance scales, which can be factorized and described by PDFs, partonic cross-sections, and FFs. Therefore, the cross-section of the discussed process is:

$$\sigma_{pp \rightarrow H_1 H_2 X} = \sum_{i,j} \int_0^1 \mathrm{d}x_1 \mathrm{d}x_2 f_i(x_1,\, \mu_F) f_j(x_2,\, \mu_F) \hat{\sigma}_{ij \rightarrow fk}(\mu_F, \mu)$$

$$\times \int_{z_{\min}}^1 \frac{\mathrm{d}z}{z^2} \mathcal{D}^{H_1}(z, \mu^2) \int_{z'_{\min}}^1 \frac{\mathrm{d}z'}{z'^2} \mathcal{D}^{H_2}(z', \mu^2), \tag{9}$$

where μ_F is the factorization scale. Thus, the pp collision is divided into three steps: the collinear distribution of partons inside the protons, the hard interaction between partons (perturbative part), and the fragmentation of the produced heavy quark. This separation and convolution of the elements are a consequence of factorization.

In the case of the Drell–Yan process, $pp \to [G\,X \to l\bar{l}]\,X$, where $G = \gamma,\,Z^0,\,W^{\pm}$, the collinear factorization framework implies that the cross-section can be expressed as a convolution of the proton parton distribution functions (PDFs), the partonic cross-section $i + j \to G + X$, denoted by $\mathrm{d}\hat{\sigma}_{ij}$, and a function $\mathcal{F}_G(M)$, which encodes the decay of the electroweak gauge boson into a lepton pair. The function $\mathcal{F}_G(M)$ plays a role analogous to fragmentation functions (FFs) in dihadron production processes discussed previously.

Therefore, summarizing, in the collinear factorization the cross-section for lepton pair production is written as a convolution of the partonic cross-section with the PDFs for each of the colliding protons as

$$
\begin{aligned}
\frac{\mathrm{d}\sigma(pp \to [G \to l\bar{l}]X)}{\mathrm{d}Q^2\mathrm{d}y\mathrm{d}M^2} &= \mathcal{F}_G(M)\frac{\mathrm{d}\sigma(pp \to GX)}{\mathrm{d}Q^2\mathrm{d}y}, \\
&= \mathcal{F}_G(M)\sum_{i,j}\int_0^1 \mathrm{d}x_1\mathrm{d}x_2 f_i(x_1,\mu_F)f_j(x_2,\,\mu_F)\frac{\mathrm{d}\hat{\sigma}_{ij \to GX}(\mu_F, Q^2)}{\mathrm{d}Q^2\mathrm{d}y},
\end{aligned}
\tag{10}
$$

where μ_F is the factorization scale. In the collinear factorization, the pp collision — whether in dihadron or Drell–Yan processes — is typically described in three stages: (i) the collinear distribution of partons inside the protons, (ii) the hard scattering between partons, which is treated perturbatively, and (iii) the decay of the produced particle. This separation, and the convolution of these components, is a direct consequence of the factorization theorem.

Despite its many successes, collinear factorization is expected to break down in the high-energy regime and/or in collisions involving nuclei (Gelis; Iancu; Jalilian-marian; Venugopalan, 2010; Weigert, 2005; Jalilian-marian; Kovchegov, 2006). Such breakdown is anticipated when the transverse momentum of partons becomes non-negligible and the parton density reaches high values. This motivates the development and application of alternative factorization schemes, which will be explored in the following chapters.

2.3 Hadron scattering variables

In hadron–hadron collisions, the momentum fractions x_1 and x_2 of the two interacting partons are unknown, and the event kinematics have to be described by three variables, for example Q^2, x_1 and x_2. These three independent kinematic variables can be related to three experimentally well-measured quantities. In hadron collider experiments, the scattered partons are observed as jets. In a process such as $pp \to$ two jets $+ X$, the angles of the two-jets with respect to the beam axis are relatively well measured. In this context, the most commonly used variables to describe the event kinematics are the transverse momentum p_T and the rapidities of the final-state particles. The transverse

Figure 7 – A simpler picture of detector's angular relation at pp collisions, and how it connects with the rapidity variable.

$$\eta = -\ln\left[\tan\left(\frac{\theta}{2}\right)\right]$$
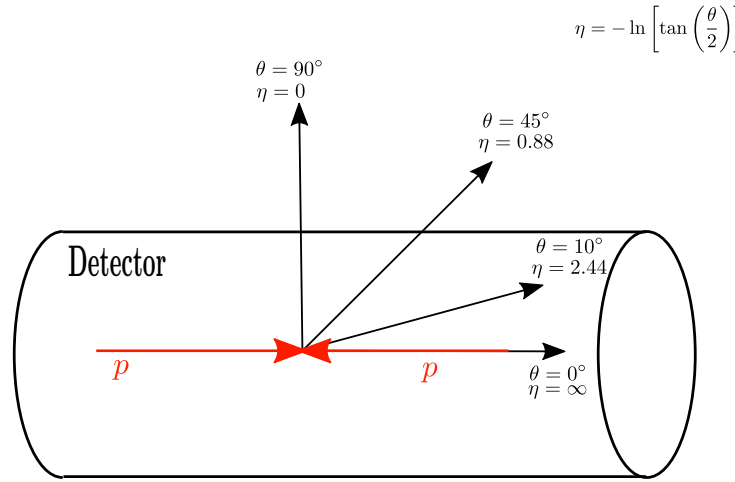
momentum is defined as the component of momentum perpendicular to the beam axis,

$$p_T = \sqrt{p_x + p_y}\,, \tag{11}$$

and is a Lorentz-invariant quantity under boosts along the beam direction. Rapidity is defined as

$$y = \frac{1}{2}\ln\left(\frac{E + p_z}{E - p_z}\right), \tag{12}$$

and is essential to treat the very high energy product of a collision, in the highly relativistic regime. If a particle is directed mainly in the transverse plane, perpendicular to the beam, then p_z is small and the rapidity is close to zero. On the other hand, if the particle moves predominantly along the beam axis ($+z$ direction), then $E \simeq p_z$ and $y \to \infty$. Similarly, if the particle travels in the $-z$ direction, $y \to -\infty$. Thus, rapidity is near zero for transverse particles and tends to $\pm\infty$ for particles collimated with the beam axis.

The angles of the outgoing jets relative to the beam are often expressed in terms of pseudorapidity which is defined as,

$$\eta = -\ln\left[\tan\left(\frac{\theta}{2}\right)\right], \tag{13}$$

and depends only on the polar angle θ with respect to the beam axis. For highly relativistic particles, $y \simeq \eta$. Hence, in high-energy hadron colliders such as the LHC, the two quantities are effectively equivalent.

In Fig. 7, we have the pp collision description within the detector and how the angle between the jet, the product of the collision, and the collision plane is used to determine the rapidity. Additionally, particles produced perpendicularly with the collision plane

imply in $\eta \approx 0$ and this is called the *central* region, in contrast when the particle produced is close to the collision plane and the rapidity goes into larger values it is in what is called the *forward rapidity* region.

The momentum fractions x_1 and x_2 can be directly related to the final-state observables via the expressions (Thomson, 2013)

$$x_1 = \frac{p_T}{\sqrt{s}} \left(e^{y_1} + e^{y_2} \right) , \tag{14}$$

$$x_2 = \frac{p_T}{\sqrt{s}} \left(e^{-y_1} + e^{-y_2} \right) , \tag{15}$$

where $\sqrt{s}$ is the center-of-mass energy of the proton-proton system, y_1 and y_2 are the rapidities of the two final-state particles (e.g., jets, gauge bosons).

In the forward rapidity region, we have an asymmetric kinematic configuration, dominated by the interaction between partons with a large momentum fraction, x, in one of the hadrons with partons with small x in the other. As the number of partons increases with decreasing x, in this kinematic configuration, we have an interaction between a diluted system (the hadron with large x) and a dense system (the hadron with small x). This is precisely the kinematic regime where the study of small-x dynamics, high gluon densities, and nonlinear QCD effects becomes essential.

In addition, as mentioned in the previous section, nonlinear effects are expected to become comparable in magnitude to linear ones at small values of x, due to the high gluon density in the proton. As a result, the QCD dynamics in this regime cannot be properly described by linear evolution equations such as DGLAP, which neglect these effects.

2.4 Conclusion

In this chapter, we provided a comprehensive review of the foundational concepts underlying the calculation of hadronic collision cross-sections. We began by presenting the Standard Model, detailing the current understanding of the fundamental constituents of matter, categorized into fermions and bosons. Furthermore, we discussed the quantum field theories that govern the behavior and interactions of these particles. Of particular importance is Quantum Chromodynamics (QCD), the theory describing the strong interaction between quarks and gluons — the color-charged fundamental building blocks of matter.

Hadronic observables governed by QCD dynamics cannot be calculated directly from first principles and are therefore treated using perturbative QCD at a given perturbative scale. Although perturbative QCD provides mathematical results, physical processes such as proton-proton (pp) collisions depend on more than just these perturbative calculations. Consequently, factorization schemes are employed, allowing the description

of these processes as a convolution of perturbative and non-perturbative contributions. Additionally, QCD dynamics describe the internal structure of hadrons, and it has been shown that at small values of the momentum fraction x, the proton is densely populated with gluons.

The collinear factorization scheme is often used to describe hadron-hadron scattering, however at forward rapidities we have an asymmetric kinematic configuration, dominated by the interaction between partons with a large momentum fraction, x, in one of the hadrons with partons with small x in the other. As the number of partons increases with decreasing x, in this kinematic configuration, we have an interaction between a diluted system (the hadron with large x) and a dense system (the hadron with small x). Consequently, one expects that nonlinear effects become of the same order as linear ones in the dense system (small x) which leads to collinear factorization violation.

Thus, at forward rapidities region, others schemes of factorization are proposed. In what follows, it will be presented the hybrid factorization scheme which provides a consistent framework for processes at forward rapidities. It incorporates both the dilute nature of the projectile (described by standard PDFs) and the dense, nonlinear dynamics of the small x target (encoded in unintegrated gluon distributions or dipole cross-sections). This framework will be the focus of the following chapters, where we explore its application to electroweak gauge boson production in hadronic collisions.

3   THE COLOR - DIPOLE S - MATRIX FRAMEWORK AND THE GAUGE BOSON PRODUCTION

The description of particle production at forward rapidities in hadronic collisions at high energies and nuclear targets is still an open question. In recent years, several groups have proposed generalized factorization schemes, which involve new objects in addition to the usual (un)integrated parton distribution functions (Nikolaev; Schafer; Zakharov; Zoller, 2003; Nikolaev; Schafer, 2005; Nikolaev; Schafer; Zakharov; Zoller, 2005a; Nikolaev; Schafer; Zakharov, 2005a; Nikolaev; Schafer; Zakharov; Zoller, 2005b; Nikolaev; Schafer; Zakharov, 2005b; Fujii; Gelis; Venugopalan, 2005; Dominguez; Marquet; Xiao; Yuan, 2011; Dominguez; Marquet; Stasto; Xiao, 2013; Kotko; Kutak; Marquet; Petreska; Sapeta; Hameren, 2015). In particular, in the hybrid factorization scheme, the hadronic cross-section for the dihadron production at forward rapidities is schematically expressed as a convolution of the standard parton distribution function for the dilute projectile, $f_{a/A}(x_1)$, the parton-target cross-section, $\mathrm{d}\sigma(aB \to bc)$, which includes the QCD dynamics effects, and the parton fragmentation functions, $D_{H_1/b}$ and $D_{H_2/b}$, i.e.,

$$\mathrm{d}\sigma(h_A h_B \to H_1 H_2 X) \propto f_{a/A}(x_1) \otimes \mathrm{d}\sigma(aB \to bc) \otimes D_{H_1/b} \otimes D_{H_2/b}. \tag{16}$$

The references mentioned above have demonstrated the parton-target cross-section derivation where the final state particles are partons is not trivial and implies, depending on the approach considered for estimating this quantity, the presence of quadrupole correlators of fundamental Wilson lines or the contribution of a four partons S matrix.

In this chapter, we introduce a hybrid factorization framework used to describe the parton–target cross-section, known as the *Color Dipole S-Matrix* (CDSM), originally proposed by Nikolaev and collaborators. We then focus on a simplified case in which one of the final-state particles is an electroweak gauge boson ($G = W^{\pm}, Z^0, \gamma$), a configuration that has not been explored in the literature so far. Additionally, this chapter serves as a brief review of the results presented in Ref. (Bandeira; Goncalves; Schäfer, 2024).

Figure 8 – The color dipole structure (left-hand side) of the generic three-parton state and (right-hand side) of the three-parton state entering the color-dipole description of fragmentation $a \to bc$ with formation of the bc dipole of size $\boldsymbol{r}$.
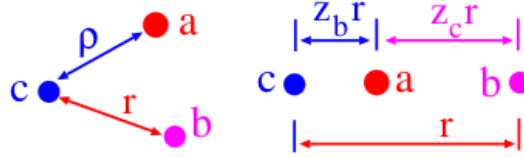
Source: extract from (Nikolaev; Schafer, 2005).

3.1 The color - dipole S - matrix framework

At forward rapidity, the projectile parton has a large longitudinal momentum x_1 and the target structure is dominated by gluons, since $x_2 \ll 1$. As a consequence, the pp cross-section is determined by the $ag \to bc$ subprocess, where b and c can be both partons or a combination of a quark and an electroweak gauge boson for an incident quark ($a = q_f$). In the laboratory frame, such a process can be viewed as an excitation of the perturbative $|bc\rangle$ Fock state of the physical projectile $|a\rangle$ by a one - gluon exchange with the target proton (Nikolaev; Piller; Zakharov, 1995, 1996). At high energies, the parton a can be assumed to propagate along an arbitrary line with a fixed impact parameter. The perturbative transition $a \to bc$ can be described in terms of the Fock state expansion for the physical state $|a\rangle_{phys}$, which at the lowest order is given by (Nikolaev; Schafer; Zakharov; Zoller, 2003)

$$|a\rangle_{phys} = |a\rangle_0 + \Psi(z_b, \boldsymbol{r})|bc\rangle_0 \ , \tag{17}$$

where $|...\rangle_0$ refers to bare partons and $\Psi(z_b, \boldsymbol{r})$ is the probability amplitude to find the bc system with separation $\boldsymbol{r}$ in the two-dimensional impact parameter space. Considering that the impact parameter is conserved in the process, the action of the S matrix on $|a\rangle_{phys}$ can be expressed as follows (Nikolaev; Schafer; Zakharov; Zoller, 2003)

$$
\begin{aligned}
S|a\rangle_{phys} &= S_a(\boldsymbol{b})|a\rangle_0 + S_b(\boldsymbol{b}_b)S_c(\boldsymbol{b}_c)\Psi(z_b, \boldsymbol{r})|bc\rangle_0 \\
&= S_a(\boldsymbol{b})|a\rangle_{phys} + [S_b(\boldsymbol{b}_b)S_c(\boldsymbol{b}_c) - S_a(\boldsymbol{b})]\Psi(z_b, \boldsymbol{r})|bc\rangle \ ,
\end{aligned} \tag{18}
$$

where in the last line we have decomposed the final state into the elastically scattered $|a\rangle_{phys}$ and the excited state $|bc\rangle$. Moreover, one has assumed that the impact parameter of the parton a is $\boldsymbol{b}$, which implies $\boldsymbol{b}_b = \boldsymbol{b} + z_c\boldsymbol{r}$ and $\boldsymbol{b}_c = \boldsymbol{b} - z_b\boldsymbol{r}$, with z_i the fraction of the longitudinal momentum of parton a carried by the particle i (for $i = b, c$), see Fig. 8.

The last two terms in eq. (18) describe the scattering on the proton of the bc system,

Figure 9 – Two-body density matrix S-matrix structure for $a \to bc$ excitation.
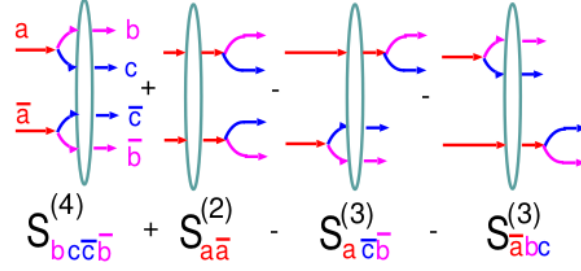
which was formed before the interaction, and the transition $a \to bc$ after the interaction of a with the proton. It is important to emphasize that the contribution associated with the transition $a \to bc$ inside the target vanishes in the high - energy limit. The differential cross-section for the production of a dijet system, with momenta $\boldsymbol{p}_b$ and $\boldsymbol{p}_c$, is proportional to the modulus square of the scattering amplitude for the $ag \to bc$ process, which is given by (Nikolaev; Schafer, 2005)

$$\mathcal{A} = \int \mathrm{d}^2 \boldsymbol{b}_b \, \mathrm{d}^2 \boldsymbol{b}_c \exp\left[-i(\boldsymbol{p}_b \cdot \boldsymbol{b}_b + \boldsymbol{p}_c \cdot \boldsymbol{b}_c)\right] [S_b(\boldsymbol{b}_b) S_c(\boldsymbol{b}_c) - S_a(\boldsymbol{b})] \Psi(z_b, \boldsymbol{r}) \ . \tag{19}$$

As a consequence, the master formula for the dijet production in the color - dipole S - matrix framework is given by (Nikolaev; Schafer; Zakharov; Zoller, 2003)

$$
\begin{aligned}
\frac{d\sigma(a \to b(p_b)c(p_c))}{dz d^2 \boldsymbol{p}_b d^2 \boldsymbol{p}_c} &= \frac{1}{(2\pi)^4} \int d^2 \boldsymbol{b}_b d^2 \boldsymbol{b}_c d^2 \boldsymbol{b}'_b d^2 \boldsymbol{b}'_c \exp[i\boldsymbol{p}_b \cdot (\boldsymbol{b}_b - \boldsymbol{b}'_b) + i\boldsymbol{p}_c \cdot (\boldsymbol{b}_c - \boldsymbol{b}'_c)] \\
&\times \ \Psi(z, \boldsymbol{b}_b - \boldsymbol{b}_c) \Psi^*(z, \boldsymbol{b}'_b - \boldsymbol{b}'_c) \left\{ S^{(4)}_{\bar{b}\bar{c}cb}(\boldsymbol{b}'_b, \boldsymbol{b}'_c, \boldsymbol{b}_b, \boldsymbol{b}_c) \right. \\
&\times \ \left. + S^{(2)}_{\bar{a}a}(\boldsymbol{b}', \boldsymbol{b}) - S^{(3)}_{\bar{b}\bar{c}a}(\boldsymbol{b}, \boldsymbol{b}'_b, \boldsymbol{b}'_c) - S^{(3)}_{\bar{a}bc}(\boldsymbol{b}', \boldsymbol{b}_b, \boldsymbol{b}_c) \right\} \ ,
\end{aligned}
\tag{20}
$$

where we have defined the quantities

$$
\begin{aligned}
S^{(2)}_{a\bar{a}}(\boldsymbol{b}', \boldsymbol{b}) &= S^\dagger_a(\boldsymbol{b}') S_a(\boldsymbol{b}) \ , & (21) \\
S^{(3)}_{\bar{a}bc}(\boldsymbol{b}', \boldsymbol{b}_b, \boldsymbol{b}_c) &= S^\dagger_a(\boldsymbol{b}') S_b(\boldsymbol{b}_b) S_c(\boldsymbol{b}_c) \ , & (22) \\
S^{(3)}_{\bar{b}\bar{c}a}(\boldsymbol{b}, \boldsymbol{b}'_b, \boldsymbol{b}'_c) &= S^\dagger_b(\boldsymbol{b}'_b) S^\dagger_c(\boldsymbol{b}'_c) S_a(\boldsymbol{b}) \ , & (23) \\
S^{(4)}_{\bar{b}\bar{c}cb}(\boldsymbol{b}'_b, \boldsymbol{b}'_c, \boldsymbol{b}_b, \boldsymbol{b}_c) &= S^\dagger_b(\boldsymbol{b}'_b) S^\dagger_c(\boldsymbol{b}'_c) S_c(\boldsymbol{b}_c) S_b(\boldsymbol{b}_b) \ . & (24)
\end{aligned}
$$

As the hermitian conjugate $S^\dagger$ can be viewed as the S matrix for an antiparticle, one has that $S^{(2)}_{a\bar{a}}(\boldsymbol{b}', \boldsymbol{b})$ represents the S matrix for the interaction of the $a\bar{a}$ state with the target, with $\bar{a}$ propagating at the impact parameter $\boldsymbol{b}'$. The averaging over the color states of the beam parton a implies that one has a color - singlet $a\bar{a}$ state. Similarly, $S^{(3)}_{\bar{a}bc}$ and $S^{(4)}_{\bar{b}\bar{c}cb}$ can be associated with the interaction of the color - singlet $\bar{a}bc$ and $\bar{b}\bar{c}cb$ systems,

respectively. This is shown schematically in Fig. 9. From the optical theorem, one can connect the S matrix with the dipole cross-section. Therefore, the $S^{(2)}$ and $S^{(3)}$ are readily calculated in terms of the 2-parton and 3-parton dipole cross-section (Nikolaev; Schafer, 2005).

A detailed discussion about how to calculate these quantities ($S^{(3)}_{\bar{a}bc}$ and $S^{(4)}_{\bar{b}\bar{c}cb}$) in the general case was presented in a series of publications (Nikolaev; Schafer; Zakharov; Zoller, 2003; Nikolaev; Schafer, 2005; Nikolaev; Schafer; Zakharov; Zoller, 2005a; Nikolaev; Schafer; Zakharov, 2005a; Nikolaev; Schafer; Zakharov; Zoller, 2005b; Nikolaev; Schafer; Zakharov, 2005b), which we refer for the interested reader. In what follows, we focus on the $a \to Gc$ process, where G denotes an electroweak gauge boson. This channel, which had not been previously addressed in the literature, was investigated in Ref. (Bandeira; Goncalves; Schäfer, 2024), filling an important gap in the theoretical description.

3.2 Electroweak gauge boson production

In what follows, we will consider one simplest case, where one of the particles in the final state is an electroweak gauge boson ($G = W^{\pm}, Z^0, \gamma$), as represented in Fig. 10, where q_f is the incoming quark and q_k is the outgoing quark. For producing an electroweak gauge boson, one has that the master equation simplifies, since they are color - singlet objects. In particular, for $b = G$ and $c = q$, we have the following simplifications: $S^{(4)}_{\bar{b}\bar{c}cb} \to S^{(2)}_{q\bar{q}}$ and $S^{(3)}_{\bar{a}bc} \to S^{(2)}_{q\bar{q}}$. Therefore, the differential cross-section for the production of gauge boson associated with a quark is given by

$$
\begin{aligned}
\frac{d\sigma^f_{T,L}(q_f p \to G(p_G)q_k(p_q))}{dz d^2\boldsymbol{p}_G d^2\boldsymbol{p}_q} =& \frac{1}{(2\pi)^4} \int d^2\boldsymbol{b}_G d^2\boldsymbol{b}_q d^2\boldsymbol{b}'_G d^2\boldsymbol{b}'_q \\
& \times \exp\left[i\boldsymbol{p}_G \cdot (\boldsymbol{b}_G - \boldsymbol{b}'_G) + i\boldsymbol{p}_q \cdot (\boldsymbol{b}_q - \boldsymbol{b}'_q)\right] \\
& \times \Psi_{T,L}(z, \boldsymbol{b}_G - \boldsymbol{b}_q)\Psi^*_{T,L}(z, \boldsymbol{b}'_G - \boldsymbol{b}'_q) \\
& \times \left\{ S^{(2)}_{q\bar{q}}(\boldsymbol{b}'_q, \boldsymbol{b}_q) + S^{(2)}_{q\bar{q}}(\boldsymbol{b}', \boldsymbol{b}) - S^{(2)}_{q\bar{q}}(\boldsymbol{b}, \boldsymbol{b}'_q) - S^{(2)}_{q\bar{q}}(\boldsymbol{b}', \boldsymbol{b}_q) \right\} .
\end{aligned}
\tag{25}
$$

Here, the G-boson and the final state quark share the light-cone plus momentum of the incoming quark in fractions z and $1 - z$, respectively. Conservation of orbital angular momentum leads to the relations

$$
\boldsymbol{b} = z\boldsymbol{b}_G + (1 - z)\boldsymbol{b}_q \,,\; \boldsymbol{b}' = z\boldsymbol{b}'_G + (1 - z)\boldsymbol{b}'_q \,,
\tag{26}
$$

between the impact parameters of incoming and outgoing partons in amplitude and

Figure 10 – Typical diagram contributing for the gauge boson + hadron production in hadronic collisions, where the gauge boson is irradiated by a quark of flavor f after the interaction with the target color field (denoted by a shaded circle). For the $W^{\pm}$ radiation one has $q_k \neq q_f$.
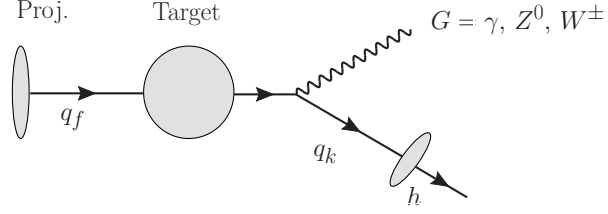
complex conjugate amplitude, respectively. Introducing

$$r = b_G - b_q \, , \; r' = b'_G - b'_q \, , \tag{27}$$

we can thus express the relevant impact parameters as

$$
\begin{aligned}
b_G &= b + (1-z)r \, , \; b_q = b - zr \\
b'_G &= b' + (1-z)r' \, , \; b'_q = b' - zr' \, .
\end{aligned}
\tag{28}
$$

Changing variables in the impact parameter space integration, we can write

$$
\begin{aligned}
\frac{d\sigma^f_{T,L}(q_f \to G(p_G)q_k(p_q))}{dz d^2\boldsymbol{p}_G d^2\boldsymbol{p}_q} &= \frac{1}{(2\pi)^4} \int d^2\boldsymbol{r} d^2\boldsymbol{r}' \exp\big[i((1-z)\boldsymbol{p}_G - z\boldsymbol{p}_q) \cdot (\boldsymbol{r} - \boldsymbol{r}')\big] \\
&\times \Psi_{T,L}(z,\boldsymbol{r})\Psi^*_{T,L}(z,\boldsymbol{r}') \\
&\times \int d^2\boldsymbol{b} d^2\boldsymbol{b}' \exp\big[i(\boldsymbol{p}_G + \boldsymbol{p}_q) \cdot (\boldsymbol{b} - \boldsymbol{b}')\big] \\
&\times \Big\{ S^{(2)}_{q\bar{q}}(\boldsymbol{b}' - z\boldsymbol{r}', \boldsymbol{b} - z\boldsymbol{r}) + S^{(2)}_{q\bar{q}}(\boldsymbol{b}', \boldsymbol{b}) \\
&- S^{(2)}_{q\bar{q}}(\boldsymbol{b}' - z\boldsymbol{r}', \boldsymbol{b}) - S^{(2)}_{q\bar{q}}(\boldsymbol{b}', \boldsymbol{b} - z\boldsymbol{r}) \Big\} \, .
\end{aligned}
\tag{29}
$$

One has that the conjugate variable to $\boldsymbol{r} - \boldsymbol{r}'$ is the light-cone relative momentum

$$\boldsymbol{k} = (1-z)\boldsymbol{p}_G - z\boldsymbol{p}_q \, . \tag{30}$$

Introducing the transverse momentum decorrelation $\boldsymbol{\Delta} = \boldsymbol{p}_G + \boldsymbol{p}_q$, as well as

$$s = b - b' \, , \; B = \frac{b + b'}{2} \, , \tag{31}$$

allows us to express the differential cross-section in terms of the $q\bar{q}$ dipole cross-section after integrating out B. To simplify the notation, we express the cross-section in terms

of the variables k and $\boldsymbol{\Delta}$, for which it takes the form

$$
\begin{aligned}
\frac{d\sigma_{T,L}^f(q_f \to G(p_G)q_k(p_q))}{dz d^2\boldsymbol{k} d^2\boldsymbol{\Delta}} &= \frac{1}{2(2\pi)^4} \int d^2\boldsymbol{r} d^2\boldsymbol{r}' \exp[i\boldsymbol{k}\cdot(\boldsymbol{r}-\boldsymbol{r}')] \\
&\times \Psi_{T,L}(z,\boldsymbol{r})\Psi_{T,L}^*(z,\boldsymbol{r}') \int d^2\boldsymbol{s} \exp[i\boldsymbol{\Delta}\cdot\boldsymbol{s}] \\
&\times \left\{ \sigma_{q\bar{q}}(\boldsymbol{s}+z\boldsymbol{r}') + \sigma_{q\bar{q}}(\boldsymbol{s}-z\boldsymbol{r}) - \sigma_{q\bar{q}}(\boldsymbol{s}-z(\boldsymbol{r}-\boldsymbol{r}')) - \sigma_{q\bar{q}}(\boldsymbol{s}) \right\},
\end{aligned}
\tag{32}
$$

where we made use of the definition of the dipole cross-section in terms of the $q\bar{q}$ S-matrix:

$$
\sigma(\boldsymbol{r}) = 2 \int d^2\boldsymbol{B} \left[1 - S_{q\bar{q}}^{(2)}\left(\boldsymbol{B}+\frac{\boldsymbol{r}}{2}, \boldsymbol{B}-\frac{\boldsymbol{r}}{2}\right) \right].
\tag{33}
$$

The equation (32) is the main ingredient to estimate the associated production of an electroweak gauge boson with a hadron. Assuming that the projectile quark is unpolarized, we can write parton-target cross-section for the electroweak gauge boson production as

$$
\begin{aligned}
\frac{d\sigma_{T,L}^f(q_f \to G(p_G)q_k(p_q))}{dz d^2\boldsymbol{k} d^2\boldsymbol{\Delta}} &= \frac{1}{2(2\pi)^4} \int d^2\boldsymbol{r} d^2\boldsymbol{r}' \exp[i\boldsymbol{k}\cdot(\boldsymbol{r}-\boldsymbol{r}')] \\
&\times \left(\rho_{T,L}^V(z,\boldsymbol{r},\boldsymbol{r}') + \rho_{T,L}^A(z,\boldsymbol{r},\boldsymbol{r}')\right) \int d^2\boldsymbol{s} \exp[i\boldsymbol{\Delta}\cdot\boldsymbol{s}] \\
&\times \left\{ \sigma_{q\bar{q}}(\boldsymbol{s}+z\boldsymbol{r}') + \sigma_{q\bar{q}}(\boldsymbol{s}-z\boldsymbol{r}) - \sigma_{q\bar{q}}(\boldsymbol{s}-z(\boldsymbol{r}-\boldsymbol{r}')) - \sigma_{q\bar{q}}(\boldsymbol{s}) \right\},
\end{aligned}
\tag{34}
$$

where $\boldsymbol{r}$ and $\boldsymbol{r}'$ are the quark-G transverse separations in the total radiation amplitude and its conjugated, respectively. Moreover, the average over quark polarization implies that

$$
\rho_{T,L}^V(z,\boldsymbol{r},\boldsymbol{r}') + \rho_{T,L}^A(z,\boldsymbol{r},\boldsymbol{r}') = \overline{\sum}_{\text{quark pol.}} \Psi_{T,L}(z,\boldsymbol{r})\Psi_{T,L}^*(\boldsymbol{r}'),
\tag{35}
$$

with

$$
\rho_V^T(z,\boldsymbol{r},\boldsymbol{r}') = \frac{1}{2} \sum_{\lambda,\lambda',\lambda_G} \Psi_V^{T,\lambda_G}(z,\boldsymbol{r})\Psi_V^{T,\lambda_G*}(z,\boldsymbol{r}'),
\tag{36a}
$$

$$
\rho_A^T(z,\boldsymbol{r},\boldsymbol{r}') = \frac{1}{2} \sum_{\lambda,\lambda',\lambda_G} \Psi_A^{T,\lambda_G}(z,\boldsymbol{r})\Psi_A^{T,\lambda_G*}(z,\boldsymbol{r}'),
\tag{36b}
$$

$$
\rho_V^L(z,\boldsymbol{r},\boldsymbol{r}') = \frac{1}{2} \sum_{\lambda,\lambda'} \Psi_V^L(z,\boldsymbol{r})\Psi_V^{L*}(z,\boldsymbol{r}'),
\tag{36c}
$$

$$\rho_A^L(z, \boldsymbol{r}, \boldsymbol{r}') = \frac{1}{2} \sum_{\lambda,\lambda'} \Psi_A^L(z, \boldsymbol{r}) \Psi_A^{L*}(z, \boldsymbol{r}') \,. \tag{36d}$$

Therefore, the transverse momentum spectrum for the electroweak gauge boson production in the $qp \rightarrow GX$ channel is fully determined by the dipole - proton cross - section $\sigma_{q\bar{q}}$, which encodes the QCD dynamics, and by the squared light cone wave functions, represented by the functions ρ_i^j, defined in eq. (36). Since the dipole - proton cross - section can be determined, e.g., using the HERA data (Golec-biernat; Wusthoff, 1998, 1999; Iancu; Itakura; Munier, 2004; Rezaeian; Siddikov; Klundert; Venugopalan, 2013; Kowalski; Teaney, 2003; Kowalski; Motyka; Watt, 2006), the main unknown component for evaluating the parton-target cross - section for electroweak gauge boson production is the wave function, $\Psi_{T,L}(z, \boldsymbol{r})$, associated with an electroweak gauge boson radiated off a quark, $q_f \rightarrow G q_k$. This calculation was performed in detail in Ref. (Bandeira; Goncalves; Schäfer, 2024).

3.3 Light cone wave function of the gauge boson radiation off a quark

To estimate the light front wave function for the gauge boson radiation off a quark, let us consider the diagram presented in Fig. 11, which represents the $q_a \rightarrow q_b G$ transition[1], where quarks a, b are allowed to have different masses m_a, m_b which generalizes the transition to flavor exchange from the production of a $W^\pm$ boson.

The gauge boson polarization vectors are

$$E_\mu^T(\lambda_G) = E_\mu^\perp(\lambda_G) - \frac{p_G \cdot E^\perp(\lambda_G)}{p_G^+} n_\mu^- \,, \qquad E_\mu^L = \frac{1}{M_G} p_{G\mu} - \frac{M_G}{p_G^+} n_\mu^- \,, \tag{37}$$

where λ_G is the gauge boson helicity. We denote the LF components of four-vectors as $a = [a^+, a^-, \boldsymbol{a}]$, so that the polarization vectors take the form

$$E^T(\lambda_G) = \left[0 \,, \; \frac{\boldsymbol{p}_G \cdot \boldsymbol{E}(\lambda_G)}{p_G^+} \,, \; \boldsymbol{E}(\lambda_G) \right] \,, \qquad E^L = \frac{1}{M_G} \left[p_G^+, \; \frac{\boldsymbol{p}_G^2 - M_G^2}{2 p_G^+}, \; \boldsymbol{p}_G \right] \,, \tag{38}$$

with

$$\boldsymbol{E}(\lambda) = -\frac{1}{\sqrt{2}} (\lambda \hat{e}_x + i \hat{e}_y) \,. \tag{39}$$

Therefore, the four momenta of the on-shell particles read in component form:

$$p_a^\mu = \left[p_a^+, \frac{m_d^2}{2 p_a^+}, \boldsymbol{0} \right] \,, \; k^\mu \equiv p_c = \left[z p_a^+, \frac{\boldsymbol{k}^2 + M_W^2}{2 z p_a^+}, \boldsymbol{k} \right] \,, \; p_b^\mu = \left[(1-z) p_a^+, \frac{\boldsymbol{k}^2 + m_u^2}{2(1-z) p_a^+}, -\boldsymbol{k} \right] \,, \tag{40}$$

---

[1] In what follows, the indexes a and b are equals to the f and k indexes used previously.

Figure 11 – Diagram representing the emission of a gauge boson of mass M_G and polarization λ_G by an incident quark of mass m_a and polarization λ that becomes a quark of mass m_b and polarization λ'. For γ and Z^0 radiation one has $q_a = q_b$, which implies $m_a = m_b$.
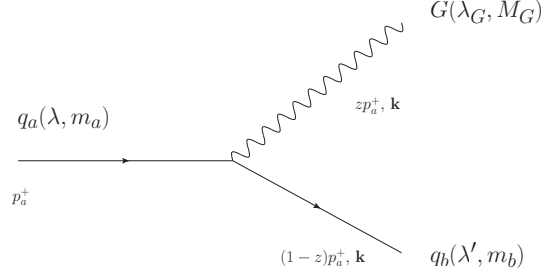
so that we obtain for the LF-"energy denominator"

$$p_a^- - p_b^- - k^- = -\frac{\boldsymbol{k}^2 + \epsilon^2}{2z(1-z)p_a^+}\,, \tag{41}$$

with

$$\epsilon^2 = (1-z)M_G^2 + zm_b^2 - z(1-z)m_a^2 = (1-z)M_G^2 + z(m_b^2 - m_a^2) + z^2 m_b^2\,. \tag{42}$$

From the light cone perturbative theory (LCPT), the light cone wave function for an electroweak gauge boson emission has the general structure

$$\Psi(z, \boldsymbol{k}) \propto C_f^G g_{(V,A),f}^G\, j_\mu E^\mu\,, \tag{43}$$

where $C_f^G g_{(V,A),f}^G$ are the couplings, j_μ denotes the current associated with the process and E^μ is the polarization vector of the gauge boson. The relevant couplings for this study – namely $C_f^G, g_{V,f}^G, g_{A,f}^G$ for $G = W^\pm, Z^0, \gamma^*$ – are summarized in Table 1. A detailed discussion of the photon case can be found in Ref.(Kovchegov; Levin, 2013), and in Brazilian Portuguese in Ref.(Bandeira, 2021).

Finally, to encapsulate our results uniformly for all gauge bosons ($G = W^\pm, Z^0, \gamma^*$), we introduce the light-cone wave functions (LCWFs) of effective "vector" and "axial vector" boson as in the $q_a \to q_b G$ transition. The factor $1/\sqrt{z(1-z)}$ is absorbed into the wave function, so that the phase space is $\propto dz$. Our effective wave functions, are given by:

$$\Psi_V(z, \boldsymbol{k}) = C_f^G g_{V,f}^G\, \sqrt{z(1-z)}\, \frac{j_\mu E^{*\mu}}{\boldsymbol{k}^2 + \epsilon^2}\,, \quad \Psi_A(z, \boldsymbol{k}) = C_f^G g_{A,f}^G\, \sqrt{z(1-z)}\, \frac{j_\mu^A E^{*\mu}}{\boldsymbol{k}^2 + \epsilon^2}\,, \tag{44}$$

with

$$j_\mu = \overline{u}_{\lambda'}(p_b)\gamma_\mu u_\lambda(p_a)\,, \quad j_\mu^A = \overline{u}_{\lambda'}(p_b)\gamma_\mu\gamma_5 u_\lambda(p_a)\,, \tag{45}$$

Table 1 – Vector and axial couplings and coefficients for the distinct gauge bosons, with θ_W being the Weinberg angle, $f_u = u, c, t$ and $f_d = d, s, b$ are the flavors of up- and down-type quarks, respectively, and $V_{f_u f_d}$ the corresponding CKM matrix elements.

Gauge Boson	$\mathcal{C}_f^G$	$g_{v,f}^G$	$g_{a,f}^G$
Z^0	$\mathcal{C}_f^Z = \frac{\sqrt{\alpha_{em}}}{\sin 2\theta_W}$	$g_{v,f_u}^Z = \frac{1}{2} - \frac{4}{3}\sin^2\theta_W$	$g_{a,f_u}^Z = \frac{1}{2}$
		$g_{v,f_d}^Z = -\frac{1}{2} + \frac{2}{3}\sin^2\theta_W$	$g_{a,f_d}^Z = -\frac{1}{2}$
$W^\pm$	$\mathcal{C}_f^{W^+} = \frac{\sqrt{\alpha_{em}}}{2\sqrt{2}\sin\theta_W} V_{f_u f_d}$	$g_{v,f}^W = 1$	$g_{a,f}^W = 1$
	$\mathcal{C}_f^{W^-} = \frac{\sqrt{\alpha_{em}}}{2\sqrt{2}\sin\theta_W} V_{f_d f_u}$		
Photon	$\mathcal{C}_f^\gamma = \sqrt{\alpha_{em}} e_f$	$g_{v,f}^\gamma = 1$	$g_{a,f}^\gamma = 0$

which we evaluate using the Lepage and Brodsky spinors (Lepage; Brodsky, 1980), adjusted for the fact that we define the light front components as $p^\pm = (p^0 \pm p^3)/\sqrt{2}$. In general, the spinors for initial and final state quarks can belong to different masses,

$$\bar{u}(p_b, \lambda', m_b)\mathbb{1}u_\lambda(p_a, \lambda, m_a) = \sqrt{p_b^+ p_a^+}\, \chi_{\lambda'}^\dagger \left\{ \left(\frac{m_a}{p_a^+} + \frac{m_b}{p_b^+}\right)\mathbb{1} - \frac{\boldsymbol{\sigma}\cdot\boldsymbol{p}_b}{p_b^+}(\boldsymbol{\sigma}\cdot\boldsymbol{n}) \right\}\chi_\lambda \quad (46)$$

$$\bar{u}(p_b, \lambda', m_b)\gamma_5 u(p_a, \lambda, m_a) = \sqrt{p_a^+ p_b^+}\, \chi_{\lambda'}^\dagger \left\{ \left(\frac{m_b}{p_b^+} - \frac{m_a}{p_a^+}\right)(\boldsymbol{\sigma}\cdot\boldsymbol{n}) - \frac{\boldsymbol{\sigma}\cdot\boldsymbol{p}_b}{p_b^+} \right\}\chi_\lambda, \quad (47)$$

the evaluation of these simpler results are presented in details in the Appendix B. For $j = [j^+, j^-, \boldsymbol{j}]$, we obtain for the vector and axial vector bilinear are given, respectively, by

$$j_{\lambda'\lambda}^{V+} = 2\sqrt{p_b^+ p_a^+}\, \chi_{\lambda'}^\dagger \mathbb{1}\chi_\lambda$$

$$j_{\lambda'\lambda}^{V-} = \sqrt{p_b^+ p_a^+}\, \chi_{\lambda'}^\dagger \left\{ \frac{m_a m_b}{p_a^+ p_b^+}\mathbb{1} - \frac{m_a}{p_a^+ p_b^+}(\boldsymbol{\sigma}\cdot\boldsymbol{p}_b)(\boldsymbol{\sigma}\cdot\boldsymbol{n}) \right\}\chi_\lambda$$

$$\boldsymbol{j}_{\lambda'\lambda}^V \cdot \boldsymbol{a} = \sqrt{p_a^+ p_b^+}\, \chi_{\lambda'}^\dagger \left\{ \left(\frac{\boldsymbol{p}_b\cdot\boldsymbol{a}}{p_b^+} + i\frac{[\boldsymbol{p}_b, \boldsymbol{a}]}{p_b^+}(\boldsymbol{\sigma}\cdot\boldsymbol{n})\right)\mathbb{1} \right.$$
$$\left. + \frac{p_a^+ m_b - p_b^+ m_a}{p_a^+ p_b^+}(\boldsymbol{\sigma}\cdot\boldsymbol{a})(\boldsymbol{\sigma}\cdot\boldsymbol{n}) \right\}\chi_\lambda, \quad (48)$$

and

$$j_{\lambda'\lambda}^{A+} = 2\sqrt{p_a^+ p_b^+}\, \chi_{\lambda'}^\dagger (\boldsymbol{\sigma}\cdot\boldsymbol{n})\chi_\lambda$$

$$j_{\lambda'\lambda}^{A-} = \sqrt{p_a^+ p_b^+}\, \chi_{\lambda'}^\dagger \left\{ -\frac{m_a m_b}{p_a^+ p_b^+}(\boldsymbol{\sigma}\cdot\boldsymbol{n}) + \frac{m_a}{p_a^+ p_b^+}\boldsymbol{\sigma}\cdot\boldsymbol{p}_b \right\}\chi_\lambda$$

$$\boldsymbol{j}_{\lambda'\lambda}^A \cdot \boldsymbol{a} = \sqrt{p_a^+ p_b^+}\, \chi_{\lambda'}^\dagger \left\{ \left(\frac{\boldsymbol{p}_b\cdot\boldsymbol{a}}{p_b^+}(\boldsymbol{\sigma}\cdot\boldsymbol{n}) + i\frac{[\boldsymbol{p}_b, \boldsymbol{a}]}{p_b^+}\right)\mathbb{1} \right.$$

$$+\frac{p_a^+ m_b + p_b^+ m_a}{p_a^+ p_b^+}\,\boldsymbol{\sigma}\cdot\boldsymbol{a}\Big\}\chi_\lambda\,. \tag{49}$$

Above, vectors $\boldsymbol{p}_b$ is the transverse momentum of quark b, $\boldsymbol{a}$ is an arbitrary transverse vector, and $\boldsymbol{n}=(0,0,1)$. Pauli spinors χ_λ are eigenstates of $\boldsymbol{\sigma}\cdot\boldsymbol{n}$:

$$(\boldsymbol{\sigma}\cdot\boldsymbol{n})\chi_\lambda = \lambda\,\chi_\lambda,\quad \lambda=\pm 1, \tag{50}$$

so that $\lambda/2$ is the quark helicity.

Let us collect explicitly the LFWFs by inserting the results above into the definitions presented in eq. (44). Firstly, for transverse polarizations $\lambda_G=\pm 1$, we have

$$\Psi_V^{T,\lambda_G}(z,\boldsymbol{k}) \;=\; \mathcal{C}_f^G g_{V,f}^G\,\frac{\sqrt{z(1-z)}}{\boldsymbol{k}^2+\epsilon^2}\,\chi_{\lambda'}^\dagger\Big(-\boldsymbol{j}\cdot\boldsymbol{E}^*(\lambda_G)+\frac{\boldsymbol{k}\cdot\boldsymbol{E}^*(\lambda_G)}{zp_a^+}j^+\Big)\chi_\lambda \tag{51}$$

$$\Psi_V^{T,\lambda_G}(z,\boldsymbol{k}) \;=\; \mathcal{C}_f^G g_{V,f}^G\,\frac{\sqrt{z}}{\boldsymbol{k}^2+\epsilon^2}\,\chi_{\lambda'}^\dagger\Big\{\Big(\frac{2-z}{z}\boldsymbol{k}\cdot\boldsymbol{E}^*(\lambda_G)+i\lambda[\boldsymbol{k},\boldsymbol{E}^*(\lambda_G)]\Big)\mathbb{1}$$
$$-\;(m_b-(1-z)m_a)\,\lambda\boldsymbol{\sigma}\cdot\boldsymbol{E}^*(\lambda_G)\Big\}\chi_\lambda\,, \tag{52}$$

where the polarization state of the quark is given by the Pauli-spinor χ_λ. For longitudinal gauge boson polarizations, we have

$$\Psi_V^L(z,\boldsymbol{k}) \;=\; \mathcal{C}_f^G g_{V,f}^G\,\frac{1}{\sqrt{z}}\frac{1}{M_G}\chi_{\lambda'}^\dagger\Big\{\Big(\frac{z^2 m_a(m_b-m_a)-z(m_b^2-m_a^2)-2(1-z)M_G^2}{\boldsymbol{k}^2+\epsilon^2}\Big)\mathbb{1}$$
$$+\;z(m_b-m_a)\frac{\lambda\,\boldsymbol{\sigma}\cdot\boldsymbol{k}}{\boldsymbol{k}^2+\epsilon^2}\Big\}\chi_\lambda \tag{53}$$

For the axial vector coupling, we obtain for the transverse polarizations

$$\Psi_A^{T,\lambda_G}(z,\boldsymbol{k}) \;=\; \mathcal{C}_f^G g_{A,f}^G\,\frac{\sqrt{z}}{\boldsymbol{k}^2+\epsilon^2}\,\chi_{\lambda'}^\dagger\Big\{\Big(\frac{2-z}{z}\boldsymbol{k}\cdot\boldsymbol{E}^*(\lambda_G)+i\lambda[\boldsymbol{k},\boldsymbol{E}^*(\lambda_G)]\Big)\lambda\mathbb{1}$$
$$-(m_b+(1-z)m_a)\,\boldsymbol{\sigma}\cdot\boldsymbol{E}^*(\lambda_G)\Big\}\chi_\lambda\,, \tag{54}$$

and for the longitudinal case, we have

$$\Psi_A^L(z,\boldsymbol{k}) \;=\; \mathcal{C}_f^G g_{A,f}^G\,\frac{1}{\sqrt{z}}\frac{1}{M_G}\chi_{\lambda'}^\dagger\Big\{\Big(-\frac{z^2 m_a(m_b+m_a)+z(m_b^2-m_a^2)+2(1-z)M_G^2}{\boldsymbol{k}^2+\epsilon^2}\Big)\lambda\mathbb{1}$$
$$-z(m_b+m_a)\frac{\boldsymbol{\sigma}\cdot\boldsymbol{k}}{\boldsymbol{k}^2+\epsilon^2}\Big\}\chi_\lambda\,. \tag{55}$$

We now obtain the LCWFs in the mixed $z, \boldsymbol{r}$ representation

$$\Psi(z, \boldsymbol{r}) = \int \frac{d^2\boldsymbol{k}}{(2\pi)^2} \, \exp(-i\boldsymbol{k} \cdot \boldsymbol{r}) \, \Psi(z, \boldsymbol{k}) \,. \tag{56}$$

For the transverse wave functions, we obtain

$$\begin{aligned}
\Psi_V^{T,\lambda_G}(z, \boldsymbol{r}) &= \mathcal{C}_f^G g_{V,f}^G \frac{1}{2\pi} \frac{1}{\sqrt{z}} \chi_{\lambda'}^\dagger \Big\{ \Big((2-z) \frac{\boldsymbol{r} \cdot \boldsymbol{E}^*(\lambda_g)}{r} + zi\lambda \frac{[\boldsymbol{r}, \boldsymbol{E}^*(\lambda_g)]}{r} \Big) \mathbb{1} \, i\epsilon K_1(\epsilon r) \\
&\quad - \lambda \boldsymbol{\sigma} \cdot \boldsymbol{E}^*(\lambda_G) \left(z(m_b - m_a) + z^2 m_a \right) K_0(\epsilon r) \Big\} \chi_\lambda \,, \tag{57} \\
\Psi_A^{T,\lambda_G}(z, \boldsymbol{r}) &= \mathcal{C}_f^G g_{A,f}^G \frac{1}{2\pi} \frac{1}{\sqrt{z}} \chi_{\lambda'}^\dagger \Big\{ \Big((2-z) \frac{\boldsymbol{r} \cdot \boldsymbol{E}^*(\lambda_g)}{r} + zi\lambda \frac{[\boldsymbol{r}, \boldsymbol{E}^*(\lambda_g)]}{r} \Big) \lambda \mathbb{1} \, i\epsilon K_1(\epsilon r) \\
&\quad - \boldsymbol{\sigma} \cdot \boldsymbol{E}^*(\lambda_G) \left(z(m_b + m_a) - z^2 m_a \right) K_0(\epsilon r) \Big\} \chi_\lambda \,, \tag{58}
\end{aligned}$$

while the longitudinal functions become

$$\begin{aligned}
\Psi_V^L(z, \boldsymbol{r}) &= \mathcal{C}_f^G g_{V,f}^G \frac{1}{2\pi} \frac{1}{\sqrt{z}} \frac{1}{M_G} \chi_{\lambda'}^\dagger \Big\{ \Big(z^2 m_a(m_b - m_a) - z(m_b^2 - m_a^2) \\
&\quad - 2(1-z)M_G^2 \Big) \mathbb{1} \, K_0(\epsilon r) + z(m_b - m_a) \lambda \frac{\boldsymbol{\sigma} \cdot \boldsymbol{r}}{r} i\epsilon K_1(\epsilon r) \Big\} \chi_\lambda \,, \tag{59} \\
\Psi_A^L(z, \boldsymbol{r}) &= \mathcal{C}_f^G g_{A,f}^G \frac{1}{2\pi} \frac{1}{\sqrt{z}} \frac{1}{M_G} \chi_{\lambda'}^\dagger \Big\{ - \Big(z^2 m_a(m_b + m_a) + z(m_b^2 - m_a^2) \\
&\quad + 2(1-z)M_G^2 \Big) \lambda \mathbb{1} \, K_0(\epsilon r) - z(m_b + m_a) \frac{\boldsymbol{\sigma} \cdot \boldsymbol{r}}{r} i\epsilon K_1(\epsilon r) \Big\} \chi_\lambda \,. \tag{60}
\end{aligned}$$

Calculating all the combinations presented in eq. (36),

$$\begin{aligned}
\rho_V^T(z, \boldsymbol{r}, \boldsymbol{r}') &= \frac{1}{2} \sum_{\lambda, \lambda', \lambda_G} \Psi_V^{T,\lambda_G}(z, \boldsymbol{r}) \Psi_V^{T,\lambda_G *}(z, \boldsymbol{r}'), \\
\rho_A^T(z, \boldsymbol{r}, \boldsymbol{r}') &= \frac{1}{2} \sum_{\lambda, \lambda', \lambda_G} \Psi_A^{T,\lambda_G}(z, \boldsymbol{r}) \Psi_A^{T,\lambda_G *}(z, \boldsymbol{r}') \,, \\
\rho_V^L(z, \boldsymbol{r}, \boldsymbol{r}') &= \frac{1}{2} \sum_{\lambda, \lambda'} \Psi_V^L(z, \boldsymbol{r}) \Psi_V^{L *}(z, \boldsymbol{r}'), \\
\rho_A^L(z, \boldsymbol{r}, \boldsymbol{r}') &= \frac{1}{2} \sum_{\lambda, \lambda'} \Psi_A^L(z, \boldsymbol{r}) \Psi_A^{L *}(z, \boldsymbol{r}') \,. \tag{61}
\end{aligned}$$

one has that

$$\begin{aligned}
\rho_V^T(z, \boldsymbol{r}, \boldsymbol{r}') &= \frac{(\mathcal{C}_f^G)^2 (g_{V,f}^G)^2}{2\pi^2} \Big\{ \frac{1 + (1-z)^2}{z} \frac{\boldsymbol{r} \cdot \boldsymbol{r}'}{rr'} \epsilon^2 K_1(\epsilon r) K_1(\epsilon r') \\
&\quad + z \Big((m_b - m_a) + z m_a \Big)^2 K_0(\epsilon r) K_0(\epsilon r') \Big\} \\
\rho_A^T(z, \boldsymbol{r}, \boldsymbol{r}') &= \frac{(\mathcal{C}_f^G)^2 (g_{A,f}^G)^2}{2\pi^2} \Big\{ \frac{1 + (1-z)^2}{z} \frac{\boldsymbol{r} \cdot \boldsymbol{r}'}{rr'} \epsilon^2 K_1(\epsilon r) K_1(\epsilon r')
\end{aligned}$$

$$+z\Big((m_b+m_a)-zm_a\Big)^2 \mathrm{K}_0(\epsilon r)\mathrm{K}_0(\epsilon r')\Big\}$$

$$\rho_V^L(z,\boldsymbol{r},\boldsymbol{r}') = \frac{(\mathcal{C}_f^G)^2(g_{V,f}^G)^2}{4\pi^2}\Big\{\frac{z(m_b-m_a)^2}{M_G^2}\frac{\boldsymbol{r}\cdot\boldsymbol{r}'}{rr'}\epsilon^2\mathrm{K}_1(\epsilon r)\mathrm{K}_1(\epsilon r')$$

$$+\frac{(z^2m_a(m_b-m_a)-z(m_b^2-m_a^2)-2(1-z)M_G^2)^2}{zM_G^2}\mathrm{K}_0(\epsilon r)\mathrm{K}_0(\epsilon r')\Big\}$$

$$\rho_A^L(z,\boldsymbol{r},\boldsymbol{r}') = \frac{(\mathcal{C}_f^G)^2(g_{A,f}^G)^2}{4\pi^2}\Big\{\frac{z(m_b+m_a)^2}{M_G^2}\frac{\boldsymbol{r}\cdot\boldsymbol{r}'}{rr'}\epsilon^2\mathrm{K}_1(\epsilon r)\mathrm{K}_1(\epsilon r')$$

$$+\frac{(z^2m_a(m_b+m_a)+z(m_b^2-m_a^2)+2(1-z)M_G^2)^2}{zM_G^2}\mathrm{K}_0(\epsilon r)\mathrm{K}_0(\epsilon r')\Big\} \quad (62)$$

3.4 Summary

In this chapter, within the hybrid factorization scheme we have the CDSM formalism which was proposed in a series of publications (Nikolaev; Schafer; Zakharov; Zoller, 2003; Nikolaev; Schafer, 2005; Nikolaev; Schafer; Zakharov; Zoller, 2005a; Nikolaev; Schafer; Zakharov, 2005a; Nikolaev; Schafer; Zakharov; Zoller, 2005b; Nikolaev; Schafer; Zakharov, 2005b) where they presented a general formula to describe the $ag \to bc$ subprocess in hadronic collisions at forward rapidities which depends on a quadrupole S-matrix term. However, evaluating such a formula for the electroweak gauge boson production $q_a g \to G q_b$ was a completely new unexplored subprocess which was analyzed in this chapter.

The parton-target master formula simplifies due to the electroweak gauge boson's non-colored nature reducing the higher S-matrix order to $S^{(2)}$ which is readily calculated in terms of the two-parton dipole cross-section. As a result, we can write the hard cross-section in terms of the dipole cross-section, model dependent, and the emission light front wave function, eq. (34). However, the generalized electroweak boson radiated from a quark light front wave function wasn't presented in the literature. Therefore, we have derived, for the first time, the generic expressions for the LFWF's in ref. (Bandeira; Goncalves; Schäfer, 2024).

From this result, one can construct the parton-target cross-sections for the isolated electroweak gauge boson production as well as the electroweak gauge boson + jet production. In the following chapters, we will present those parton-level cross-sections which are the main ingredient to prove our understanding of the hadronic dynamics.

4 ELECTROWEAK GAUGE BOSON PRODUCTION AT FORWARD RAPIDITIES IN COLOR - DIPOLE S - MATRIX FRAMEWORK IN THE MOMENTUM REPRESENTATION

In the previous chapter, we have seen that in the CDSM framework the electroweak gauge boson production parton-target cross-section, eq. (34), is expressed in terms of the squared LFWF's, derived previously, and the dipole - proton cross-section $\sigma_{q\bar{q}}$. As this quantity is usually derived in the impact parameter space, e.g., by solving the Balitsky - Kovchegov equation (Balitsky, 1996, 1998, 1999, 2001; Balitsky; Belitsky, 2002; Kovchegov, 1999, 2000), a natural representation of the spectrum is at this same space. However, it is also possible to use the relation between the dipole - proton cross-section and the unintegrated gluon distribution $f(x, \boldsymbol{k})$ given by

$$\sigma(\boldsymbol{r}, x) = \frac{1}{2} \int d^2 \boldsymbol{k} f(x, \boldsymbol{k}) \left(2 - e^{i\boldsymbol{k}\cdot\boldsymbol{r}} - e^{-i\boldsymbol{k}\cdot\boldsymbol{r}} \right) , \qquad (63)$$

and represent the spectrum in the transverse momentum space. It is important to emphasize that both representations are equivalent, and approximated limits of both have been used in the literature to estimate the Drell - Yan process and the real photon production. The choice of one particular representation is, in general, associated with a description of the QCD dynamics, which sometimes is performed in terms of $\sigma_{q\bar{q}}$ and in other cases of $f(x, \boldsymbol{k})$.

Furthermore, in this chapter, we will construct the final expression for the generic electroweak gauge boson dipole-target cross-section within the momentum space for the isolated and associated production. In the Appendix D we present the parton-target cross-section derivation in the impact parameter space for didactic purposes. Additionally, this chapter is based on the following publications (Bandeira; Goncalves; Schäfer, 2024, 2025).

4.1 Isolated gauge boson production

The equation (34) is the main ingredient to estimate the associated production of an electroweak gauge boson with a hadron, which will be discussed in the forthcoming section. Here, we focus on the isolated gauge boson production, which has a cross-section that can be derived integrating the master equation over the transverse momentum of the quark in the final state or, equivalently, integrating eq. (34) over Δ. Assuming that the projectile quark is unpolarized and integrating eq. (34) over Δ, one has that the differential cross-section for the $q_f p \to GX$ process reads

$$
\begin{aligned}
\frac{d\sigma_{T,L}^f(q_f\, p \to GX)}{dzd^2\boldsymbol{p}} &= \frac{1}{(2\pi)^2} \overline{\sum}_{\text{quark pol.}} \int d^2\boldsymbol{r}\mathrm{d}^2\boldsymbol{r}' \exp[i\boldsymbol{p}\cdot(\boldsymbol{r}-\boldsymbol{r}')]\,\Psi_{T,L}(z,\boldsymbol{r})\Psi_{T,L}^*(z,\boldsymbol{r}') \\
&\times \frac{1}{2}\left[\sigma_{q\bar{q}}(z\boldsymbol{r},x) + \sigma_{q\bar{q}}(z\boldsymbol{r}',x) - \sigma_{q\bar{q}}(z|\boldsymbol{r}-\boldsymbol{r}'|,x)\right].
\end{aligned}
\tag{64}
$$

Using the relation between the dipole - hadron cross-section and the unintegrated gluon distribution, given in Eq. (63), one has that the differential cross-section will be given by

$$
\begin{aligned}
\frac{d\sigma_{T,L}^f}{dzd^2\boldsymbol{p}} &= \frac{1}{2(2\pi)^2} \overline{\sum}_{\text{quark pol.}} \int d^2\boldsymbol{r}\mathrm{d}^2\boldsymbol{r}' e^{i\boldsymbol{p}\cdot(\boldsymbol{r}-\boldsymbol{r}')}\,\Psi_{T,L}(z,\boldsymbol{r})\Psi_{T,L}^*(z,\boldsymbol{r}') \\
&\int d^2\boldsymbol{k} f(x,\boldsymbol{k})\left[1 - e^{iz\boldsymbol{k}\cdot\boldsymbol{r}} - e^{iz\boldsymbol{k}\cdot\boldsymbol{r}'} + e^{iz\boldsymbol{k}\cdot(\boldsymbol{r}-\boldsymbol{r}')}\right].
\end{aligned}
\tag{65}
$$

Remembering that $\overline{\sum}_{\text{quark pol.}}\Psi_{T,L}(z,\boldsymbol{r},\boldsymbol{r}')\Psi_{T,L}^*(z,\boldsymbol{r},\boldsymbol{r}') = \rho_{T,L}^V(z,\boldsymbol{r},\boldsymbol{r}') + \rho_{T,L}^A(z,\boldsymbol{r},\boldsymbol{r}')$, for transverse polarization, one has that

$$
\begin{aligned}
\frac{d\sigma_T^f}{dzd^2\boldsymbol{p}} &= \frac{1}{2(2\pi)^2}\int d^2\boldsymbol{r}\,\mathrm{d}^2\boldsymbol{r}' e^{i\boldsymbol{p}\cdot(\boldsymbol{r}-\boldsymbol{r}')}\rho_V^T(z,\boldsymbol{r},\boldsymbol{r}') \\
&\times \int d^2\boldsymbol{k} f(x,\boldsymbol{k})\left[1 - e^{iz\boldsymbol{k}\cdot\boldsymbol{r}} - e^{iz\boldsymbol{k}\cdot\boldsymbol{r}'} + e^{iz\boldsymbol{k}\cdot(\boldsymbol{r}-\boldsymbol{r}')}\right] \\
&+ \frac{1}{2(2\pi)^2}\int d^2\boldsymbol{r}\,\mathrm{d}^2\boldsymbol{r}' e^{i\boldsymbol{p}\cdot(\boldsymbol{r}-\boldsymbol{r}')}\rho_A^T(z,\boldsymbol{r},\boldsymbol{r}') \\
&\times \int d^2\boldsymbol{k} f(x,\boldsymbol{k})\left[1 - e^{iz\boldsymbol{k}\cdot\boldsymbol{r}} - e^{iz\boldsymbol{k}\cdot\boldsymbol{r}'} + e^{iz\boldsymbol{k}\cdot(\boldsymbol{r}-\boldsymbol{r}')}\right]
\end{aligned}
\tag{66}
$$

In what follows, we'll consider only the vector contribution $(\mathrm{d}\sigma_T^f|_V)$. Thus, substituting the expression for the squared LFWF, ρ_V^T, presented at eq. (62) one gets

$$
\begin{aligned}
\frac{d\sigma_T^f}{dzd^2\boldsymbol{p}}\Big|_V &= \frac{(\mathcal{C}_f^G)^2(g_{V,f}^G)^2}{(2\pi)^4}\int d^2\boldsymbol{k} f(x,\boldsymbol{k})\Bigg\{ \\
&\times \frac{1 + (1-z)^2}{z}\,\epsilon^2\int d^2\boldsymbol{r}\,\mathrm{d}^2\boldsymbol{r}'\,e^{i\boldsymbol{p}\cdot(\boldsymbol{r}-\boldsymbol{r}')}\,\frac{\boldsymbol{r}\cdot\boldsymbol{r}'}{rr'}\mathrm{K}_1(\epsilon r)\mathrm{K}_1(\epsilon r')
\end{aligned}
$$

$$\times \left[1 - e^{iz\boldsymbol{k}\cdot\boldsymbol{r}} - e^{iz\boldsymbol{k}\cdot\boldsymbol{r'}} + e^{iz\boldsymbol{k}\cdot(\boldsymbol{r}-\boldsymbol{r'})} \right]$$

$$+ \quad z \left[(m_b + m_a - zm_a) \right]^2 \int d^2\boldsymbol{r}\, d^2\boldsymbol{r'}\, e^{i\boldsymbol{p}\cdot(\boldsymbol{r}-\boldsymbol{r'})}\, \mathrm{K}_0(\epsilon r)\mathrm{K}(\epsilon r')$$

$$\times \left[1 - e^{iz\boldsymbol{k}\cdot\boldsymbol{r}} - e^{iz\boldsymbol{k}\cdot\boldsymbol{r'}} + e^{iz\boldsymbol{k}\cdot(\boldsymbol{r}-\boldsymbol{r'})} \right] \Bigg\}, \tag{67}$$

from the equation above, one gets a series of eight integrals over r and r' to evaluate which depends on the Bessel functions and the exponentials products. In the Appendix C we present the results for each one of them considering that the integral over $e^{iz\boldsymbol{k}\cdot\boldsymbol{r}}$ is similar to the integral over $e^{iz\boldsymbol{k}\cdot\boldsymbol{r'}}$. Additionally, each integral is evaluated using Bessel function integrals, which are included in this appendix for reference. Thus, as a result, we obtain that the transverse parton-level differential cross-section vector contribution is expressed as follows:

$$z\frac{d\sigma_T^f}{dzd^2\boldsymbol{p}}\bigg|_V = \frac{(\mathcal{C}_f^G)^2(g_{v,f}^G)^2}{2\pi^2} \int d^2\boldsymbol{k} f(x,\boldsymbol{k}) \Bigg\{ z^2[(m_b - m_a) + zm_a]^2\, \mathcal{E}_1(\boldsymbol{p},\boldsymbol{k},\epsilon,z)$$
$$+ [1 + (1-z)^2]\mathcal{E}_2(\boldsymbol{p},\boldsymbol{k},\epsilon,z) \Bigg\}, \tag{68}$$

where we have defined the auxiliary functions:

$$\mathcal{E}_1(\boldsymbol{p},\boldsymbol{k},\epsilon,z) \equiv \left[\frac{1}{2}\frac{1}{(p^2+\epsilon^2)^2} - \frac{1}{[(\boldsymbol{p}-z\boldsymbol{k})^2+\epsilon^2]}\frac{1}{(p^2+\epsilon^2)} + \frac{1}{2}\frac{1}{[(\boldsymbol{p}-z\boldsymbol{k})^2+\epsilon^2]^2} \right]$$
$$= \frac{1}{2}\left[\frac{1}{p^2+\epsilon^2} - \frac{1}{(\boldsymbol{p}-z\boldsymbol{k})^2+\epsilon^2} \right]^2 \tag{69}$$

$$\mathcal{E}_2(\boldsymbol{p},\boldsymbol{k},\epsilon,z) \equiv \left[\frac{1}{2}\frac{p^2}{(p^2+\epsilon^2)^2} - \frac{\boldsymbol{p}\cdot(\boldsymbol{p}-z\boldsymbol{k})}{(p^2+\epsilon^2)[(\boldsymbol{p}-z\boldsymbol{k})^2+\epsilon^2]} + \frac{1}{2}\frac{(\boldsymbol{p}-z\boldsymbol{k})^2}{[(\boldsymbol{p}-z\boldsymbol{k})^2+\epsilon^2]^2} \right]$$
$$= \frac{1}{2}\left[\frac{\boldsymbol{p}}{p^2+\epsilon^2} - \frac{\boldsymbol{p}-z\boldsymbol{k}}{(\boldsymbol{p}-z\boldsymbol{k})^2+\epsilon^2} \right]^2 \tag{70}$$

Similarly, substituting the expression for ρ_A^T, one has that the axial contribution is given by:

$$z\frac{d\sigma_T^f}{dzd^2\boldsymbol{p}}|_A = \frac{(\mathcal{C}_f^G)^2(g_{a,f}^G)^2}{2\pi^2} \int d^2\boldsymbol{k} f(x,\boldsymbol{k}) \Bigg\{ z^2[(m_b + m_a) - zm_a]^2\mathcal{E}_1(\boldsymbol{p},\boldsymbol{k},\epsilon,z)$$
$$+ [1 + (1-z)^2]\mathcal{E}_2(\boldsymbol{p},\boldsymbol{k},\epsilon,z) \Bigg\}. \tag{71}$$

Following similar steps, one can derive that the vector and axial contributions for the

longitudinal cross-section will be given by

$$
z\frac{d\sigma_L^f}{dzd^2\boldsymbol{p}}|_V = \frac{(\mathcal{C}_f^G)^2(g_{v,f}^G)^2}{4\pi^2}\int d^2\boldsymbol{k}f(x,\boldsymbol{k})\Big\{\frac{z^2(m_b-m_a)^2}{M_G^2}\mathcal{E}_2(\boldsymbol{p},\boldsymbol{k},\epsilon,z)
$$
$$
+\frac{(z^2m_a(m_b-m_a)-z(m_b^2-m_a^2)-2(1-z)M_G^2)^2}{M_G^2}\mathcal{E}_1(\boldsymbol{p},\boldsymbol{k},\epsilon,z)\Big\} \quad (72)
$$

and

$$
z\frac{d\sigma_L^f}{dzd^2\boldsymbol{p}}|_A = \frac{(\mathcal{C}_f^G)^2(g_{a,f}^G)^2}{4\pi^2}\int d^2\boldsymbol{k}f(x,\boldsymbol{k})\Big\{\frac{z^2(m_b+m_a)^2}{M_G^2}\mathcal{E}_2(\boldsymbol{p},\boldsymbol{k},\epsilon,z)
$$
$$
+\frac{(z^2m_a(m_b+m_a)+z(m_b^2-m_a^2)+2(1-z)M_G^2)^2}{M_G^2}\mathcal{E}_1(\boldsymbol{p},\boldsymbol{k},\epsilon)\Big\} \quad (73)
$$

The eqs. (68), (71), (72) and (73) are the main results of this section. They allow us to estimate the vector and axial contributions for the spectrum associated with the isolated gauge boson production in the transverse momentum space. At the Appendix D, we present the eqs. (232), (235), (236), (237), which are the results in the impact parameter space.

The expressions are valid for massive (Z^0 and $W^\pm$) and massless (γ) electroweak gauge bosons and take into account the transverse and longitudinal polarizations as well as do not disregard the masses of the quarks, which is fundamental to derive realistic predictions for the $W^\pm$ production. However, as we will demonstrate in the next section, some particular cases of our expressions already have been used in the literature, with a successful description of the current data.

4.1.1 Particular cases

4.1.1.1 Real photon production

The simplest case to which we can apply the expressions derived in the previous section is the real photon production in the $qp \to \gamma X$ process. For the production of a real photon, one has that $g_{a,f}^\gamma = 0$, $g_{v,f}^\gamma = 1$, $\mathcal{C}_f^\gamma = \sqrt{\alpha_{em}}e_f$, $M_G^2 = 0$ and $m_a = m_b = m_f$. Moreover, the longitudinal polarization does not contribute. Consequently, the differential cross-section is given in the transverse momentum space by:

$$
z\frac{d\sigma_T^f}{dzd^2\boldsymbol{p}}\bigg|_{qp\to\gamma X} = \frac{\alpha_{em}e_f^2}{2\pi^2}\int d^2\boldsymbol{k}f(x,\boldsymbol{k})\left\{m_f^2z^4\,\mathcal{E}_1(\boldsymbol{p},\boldsymbol{k},\epsilon,z)+[1+(1-z)^2]\mathcal{E}_2(\boldsymbol{p},\boldsymbol{k},\epsilon,z)\right\}.
$$
$$(74)$$

Neglecting the quark mass, this expression reduces to those used e.g. in Refs. (Gelis; Jalilian-marian, 2002a; Jalilian-marian; Rezaeian, 2012; Ducloué; Lappi; Mäntysaari,

2018; Goncalves; Lima; Pasechnik; Šumbera, 2020; Lima; Giannini; Goncalves, 2024)
considering the CGC formalism to estimate the isolated photon production.

4.1.1.2 Drell - Yan process

Another possible application of our results is the emission of an off-mass shell gauge
boson G^* that decays into a dilepton system with invariant mass M, characteristic of the
Drell - Yan (DY) process. For $G^* = \gamma^*$ and Z^*, one has the production of l^+l^- system
in the final state and such a process was analyzed in Refs. (Kopeliovich; Raufeisen;
Tarasov, 2001; Raufeisen; Peng; Nayak, 2002; Kopeliovich; Raufeisen; Tarasov; John-
son, 2003; Betemps; Gay ducati, 2004; Betemps; Ducati; Machado; Raufeisen, 2003;
Golec-biernat; Lewandowska; Stasto, 2010; Ducati; Griep; Machado, 2014; Schäfer;
Szczurek, 2016; Ducloué, 2017; Gelis; Jalilian-marian, 2002b; Baier; Mueller; Schiff,
2004; Stasto; Xiao; Zaslavsky, 2012; Kang; Xiao, 2013; Basso; Goncalves; Krelina;
Nemchik; Pasechnik, 2016) using the color dipole and CGC formalisms. The results
derived in the previous section can be directly applied to this case, if we take into
account that the decay process can be factorized as follows

$$\frac{d\sigma(qp \to [G^* \to l\bar{l}]X)}{dzd^2\boldsymbol{p}dM^2} = \mathcal{F}_G(M) \frac{d\sigma(qp \to G^*X)}{dzd^2\boldsymbol{p}} \,, \tag{75}$$

where the function $\mathcal{F}_G(M)$ describes the process $G^* \to l^+l^-$ and is given by

$$\begin{align}
\mathcal{F}_\gamma(M) &= \frac{\alpha_{em}}{3\pi M^2} && \text{for } G^* = \gamma^* \,, \tag{76} \\
\mathcal{F}_Z(M) &= \text{Br}(Z^0 \to l\bar{l})\rho_Z(M) && \text{for } G^* = Z^* \,, \tag{77}
\end{align}$$

where $\rho_Z(M)$ is the invariant mass distribution of the Z^0 boson in the narrow width
approximation (Basso; Goncalves; Nemchik; Pasechnik; Sumbera, 2016)

$$\rho_Z(M) = \frac{1}{\pi} \frac{M\Gamma_Z(M)}{(M^2 - m_Z^2)^2 + [M\Gamma_Z(M)]^2} \,, \qquad \Gamma_Z(M)/M \ll 1 \,, \tag{78}$$

with generalized total Z^0 decay width being given by

$$\Gamma_Z(M) = \frac{\alpha_{em}M}{6\sin^2 2\theta_W}\left(\frac{160}{3}\sin^4\theta_W - 40\sin^2\theta_W + 21\right), \tag{79}$$

where θ_W is the Weinberg gauge boson mixing angle in the SM.

For the particular case of a virtual photon ($G^* = \gamma^*$) with virtuality M^2, one has that
the axial contributions vanishes and differential cross-section for the $qp \to [\gamma^* \to l\bar{l}]X$

process will be given in the transverse momentum space by:

$$
z \frac{d\sigma^f_{total}}{dz d^2 \boldsymbol{p} dM^2}\bigg|_{DY} = \frac{\alpha_{em} e_f^2}{2\pi^2} \mathcal{F}_\gamma(M) \int d^2 \boldsymbol{k} f(x, \boldsymbol{k}) \Big\{ [m_f^2 z^4 + 2M^2(1-z)^2] \, \mathcal{E}_1(\boldsymbol{p}, \boldsymbol{k}, \epsilon, z)
$$
$$
+ [1 + (1-z)^2] \mathcal{E}_2(\boldsymbol{p}, \boldsymbol{k}, \epsilon, z) \Big\} , \tag{80}
$$

which was derived in the massless limit in Ref. (Gelis; Jalilian-marian, 2002b) using the CGC formalism and applied for pp/pA collisions at the LHC, e.g., in Refs. (Baier; Mueller; Schiff, 2004; Stasto; Xiao; Zaslavsky, 2012; Kang; Xiao, 2013; Basso; Goncalves; Krelina; Nemchik; Pasechnik, 2016). Finally, it is important to emphasize that we have verified that our results also reproduce the expressions presented in Ref. (Basso; Goncalves; Nemchik; Pasechnik; Sumbera, 2016) for the $G^* = Z^*$ case.

4.2 Associated gauge boson production in the transverse momentum and impact parameter representations

In the previous section, we have derived using the CDSM framework, the general formulae for the inclusive electroweak gauge boson production at forward rapidities and demonstrated that it reduces to those used in Refs. (Kopeliovich; Rezaeian; Pirner; Schmidt, 2007; Kopeliovich; Levin; Rezaeian; Schmidt, 2009; Santos; Silveira; Machado, 2020; Gelis; Jalilian-marian, 2002a; Jalilian-marian; Rezaeian, 2012; Ducloué; Lappi; Mäntysaari, 2018; Goncalves; Lima; Pasechnik; Šumbera, 2020; Lima; Giannini; Goncalves, 2024; Kopeliovich; Raufeisen; Tarasov, 2001; Raufeisen; Peng; Nayak, 2002; Kopeliovich; Raufeisen; Tarasov; Johnson, 2003; Betemps; Gay ducati, 2004; Betemps; Ducati; Machado; Raufeisen, 2003; Golec-biernat; Lewandowska; Stasto, 2010; Ducati; Griep; Machado, 2014; Schäfer; Szczurek, 2016; Ducloué, 2017; Gelis; Jalilian-marian, 2002b; Baier; Mueller; Schiff, 2004; Stasto; Xiao; Zaslavsky, 2012; Kang; Xiao, 2013; Basso; Goncalves; Krelina; Nemchik; Pasechnik, 2016; Basso; Goncalves; Nemchik; Pasechnik; Sumbera, 2016; Marquet; Wei; Xiao, 2020) to estimate the real photon and Z^0 production in the appropriate limits and representations. Moreover, for the first time, we have derived the cross-section for the $W^\pm$ production in the hybrid factorization formalism. Such results are an important improvement in describing the inclusive electroweak gauge boson production. They are useful to investigate the impact of the nonlinear effects in the transverse momentum and rapidity distributions of the gauge boson probed in the kinematical range of the LHCb detector.

A more detailed information about the QCD dynamics is expected to be provided through the study of processes where two particles are tagged in the final state (See, e.g., Ref. (Morreale; Salazar, 2021) for a recent review). Such expectation is directly associated with the presence in the dense target of a characteristic momentum scale –

the saturation scale Q_s –, which implies that the incident partons acquire a momentum imbalance due to its multiple scattering with the target (Gelis; Iancu; Jalilian-marian; Venugopalan, 2010; Weigert, 2005; Jalilian-marian; Kovchegov, 2006). As a consequence, the nonlinear effects are expected to generate a depletion of the back-to-back peak predicted by the collinear formalism (Marquet, 2007; Albacete; Marquet, 2010; Stasto; Xiao; Yuan, 2012; Stasto; Wei; Xiao; Yuan, 2018). Such an expectation has been confirmed by the analyses performed in Refs. (Dominguez; Marquet; Xiao; Yuan, 2011; Stasto; Xiao; Zaslavsky, 2012; Jalilian-marian; Rezaeian, 2012; Basso; Goncalves; Nemchik; Pasechnik; Sumbera, 2016; Ducloué; Lappi; Mäntysaari, 2018; Goncalves; Lima; Pasechnik; Šumbera, 2020; Taels, 2024), which have estimated the azimuthal angle correlation for the associated hadron + γ and hadron + Z^0 production considering different frameworks and distinct approximations in the calculation of the $qp \rightarrow qGX$ cross-section. Our goal, in this section, is to extend the formalism presented previously for the associated jet plus electroweak gauge boson production at forward rapidities in hadronic collisions and present the general formulae for the $qp \rightarrow qGX$ cross-section considering the longitudinal and transverse polarizations of the gauge boson.

The treatment of the two - particle production at forward rapidities in hadronic collisions at high energies and the derivation of the corresponding cross-sections is still a challenge, especially when both particles in the final state are generated by partons, since in this case it depends in a non-trivial way on quadrupole correlators of fundamental Wilson lines or four partons S matrix, depending on the approach considered estimating this quantity (Nikolaev; Schafer; Zakharov, 2005b; Dominguez; Marquet; Xiao; Yuan, 2011), as seen in eq. (25). We have seen that the calculation of these objects in the general case is a hard task, in contrast if one of the particles in the final state is an electroweak gauge boson, which does not interact strongly, these quantities can be expressed in terms of dipole correlators or two partons S matrix, as seen in previous chapter. As explicitly demonstrated so far, the cross-sections for the isolated electroweak gauge boson production in pp collisions can be expressed in terms of the unintegrated gluon distribution or, equivalently, of the dipole - proton cross-section, which can be constrained using experimental data for ep collisions. Such characteristic motivates a more detailed investigation of the associated jet + electroweak gauge boson production.

The hadronic cross-section for the associated jet + G production, represented in Fig. 12, can be schematically expressed as follows

$$d\sigma(h_A h_B \rightarrow G\,J\,X) \propto q_{a/A} \otimes d\sigma(q_a h_B \rightarrow q_b GX) \,, \tag{81}$$

i.e., as a convolution of the standard quark distributions for the dilute projectile, $q_{f/A}$, and the parton - target cross-section, $d\sigma(q_a h_B \rightarrow q_b GX)$, which includes the nonlinear

Figure 12 – Typical diagram contributing for the associated G + jet production in hadronic collisions, where the gauge boson is irradiated by a quark of flavor f after the interaction with the target color field (denoted by a shaded circle). The quark q_k generates the jet J. For the $W^{\pm}$ radiation $q_k \neq q_f$.
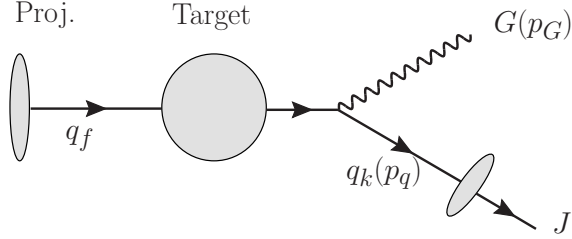
QCD effects, with the quark q_b generating the jet J. We already presented the master formulae for the parton -target cross-section, $d\sigma(q_a h_B \to q_b G X)$, in eq. (34) which in the momentum space is written as

$$
\begin{aligned}
\frac{\mathrm{d}\sigma_{T,L}^{f}(q_a \to Gq_b)}{\mathrm{d}z\mathrm{d}^2\boldsymbol{p}\mathrm{d}^2\boldsymbol{\Delta}} = {} & \frac{1}{2(2\pi)^4} \int \mathrm{d}^2\boldsymbol{k}\, f(x,\boldsymbol{k}) \int \mathrm{d}^2\boldsymbol{r}\, \mathrm{d}^2\boldsymbol{r}'\, e^{-i\boldsymbol{p}\cdot(\boldsymbol{r}-\boldsymbol{r}')} \\
& \times \left[\rho_V^{T,L}(z,\boldsymbol{r},\boldsymbol{r}') + \rho_A^{T,L}(z,\boldsymbol{r},\boldsymbol{r}') \right] \int \mathrm{d}^2\boldsymbol{s}\, e^{-i\boldsymbol{\Delta}\cdot\boldsymbol{s}} \\
& \times \left\{ e^{i\boldsymbol{k}\cdot\boldsymbol{s}} + e^{i\boldsymbol{k}\cdot(\boldsymbol{s}-z(\boldsymbol{r}-\boldsymbol{r}'))} - e^{i\boldsymbol{k}\cdot(\boldsymbol{s}+z\boldsymbol{r}')} - e^{i\boldsymbol{k}\cdot(\boldsymbol{s}-z\boldsymbol{r})} \right\}.
\end{aligned}
\tag{82}
$$

In comparison with the isolated electroweak gauge boson production case, the associated production differs by not neglecting the jet momentum, i.e., by including the integral over $\boldsymbol{s}$, which accounts for the correlation between the electroweak gauge boson and the final-state quark. From the master equation, the transverse dipole-target cross-section is given by

$$
\begin{aligned}
\frac{\mathrm{d}\sigma_T^{f}(q_f \to Gq_k)}{\mathrm{d}z\mathrm{d}^2\boldsymbol{p}\mathrm{d}^2\boldsymbol{\Delta}} = {} & \frac{1}{2(2\pi)^4} \int \mathrm{d}^2\boldsymbol{k}\, f(x,\boldsymbol{k}) \int \mathrm{d}^2\boldsymbol{r}\, \mathrm{d}^2\boldsymbol{r}'\, e^{-i\boldsymbol{p}\cdot(\boldsymbol{r}-\boldsymbol{r}')} \\
& \times \rho_V^{T}(z,\boldsymbol{r},\boldsymbol{r}') \int \mathrm{d}^2\boldsymbol{s}\, e^{-i\boldsymbol{\Delta}\cdot\boldsymbol{s}} \\
& \times \left\{ e^{i\boldsymbol{k}\cdot\boldsymbol{s}} + e^{i\boldsymbol{k}\cdot(\boldsymbol{s}-z(\boldsymbol{r}-\boldsymbol{r}'))} - e^{i\boldsymbol{k}\cdot(\boldsymbol{s}+z\boldsymbol{r}')} - e^{i\boldsymbol{k}\cdot(\boldsymbol{s}-z\boldsymbol{r})} \right\} \\
& + \frac{1}{2(2\pi)^4} \int \mathrm{d}^2\boldsymbol{k}\, f(x,\boldsymbol{k}) \int \mathrm{d}^2\boldsymbol{r}\, \mathrm{d}^2\boldsymbol{r}'\, e^{-i\boldsymbol{p}\cdot(\boldsymbol{r}-\boldsymbol{r}')} \\
& \times \rho_A^{T}(z,\boldsymbol{r},\boldsymbol{r}') \int \mathrm{d}^2\boldsymbol{s}\, e^{-i\boldsymbol{\Delta}\cdot\boldsymbol{s}} \\
& \times \left\{ e^{i\boldsymbol{k}\cdot\boldsymbol{s}} + e^{i\boldsymbol{k}\cdot(\boldsymbol{s}-z(\boldsymbol{r}-\boldsymbol{r}'))} - e^{i\boldsymbol{k}\cdot(\boldsymbol{s}+z\boldsymbol{r}')} - e^{i\boldsymbol{k}\cdot(\boldsymbol{s}-z\boldsymbol{r})} \right\},
\end{aligned}
\tag{83}
$$

using the definition of ρ_V^T, eq. (62), evaluated on the previous chapters, one gets

$$
\begin{aligned}
\left.\frac{d\sigma_T^f(q_f \to Gq_k)}{dz\, d^2\boldsymbol{p}\, d^2\boldsymbol{\Delta}}\right|_V &= \frac{2}{2(2\pi)^4}\frac{(C_f^G)^2(g_{V,f}^G)^2}{2\pi^2}\int d^2\boldsymbol{k}\, f(x,\boldsymbol{k})\Bigg\{\int d^2\boldsymbol{r}\, d^2\boldsymbol{r}'\, e^{-i\boldsymbol{p}\cdot(\boldsymbol{r}-\boldsymbol{r}')} \\
&\quad\times \int d^2\boldsymbol{s}\, e^{-\boldsymbol{\Delta}\cdot\boldsymbol{s}}\,\frac{[1+1(1-z)^2]}{z}\,\frac{\boldsymbol{r}\cdot\boldsymbol{r}'}{rr'}\,\epsilon^2\, \mathrm{K}_1(\epsilon r)\mathrm{K}_1(\epsilon r') \\
&\quad\times \left(e^{i\boldsymbol{k}\cdot\boldsymbol{s}} + e^{i\boldsymbol{k}\cdot(\boldsymbol{s}-z(\boldsymbol{r}-\boldsymbol{r}'))} - e^{i\boldsymbol{k}\cdot(\boldsymbol{s}+z\boldsymbol{r}')} - e^{i\boldsymbol{k}\cdot(\boldsymbol{s}-z\boldsymbol{r})}\right) \\
&\quad+ \int d^2\boldsymbol{r}\, d^2\boldsymbol{r}'\, e^{-i\boldsymbol{p}\cdot(\boldsymbol{r}-\boldsymbol{r}')} \int d^2\boldsymbol{s}\, e^{-\boldsymbol{\Delta}\cdot\boldsymbol{s}} \\
&\quad\times z\big[(m_b - m_a) + zm_a\big]^2\, \mathrm{K}_0(\epsilon r)\mathrm{K}_0(\epsilon r') \\
&\quad\times \left(e^{i\boldsymbol{k}\cdot\boldsymbol{s}} + e^{i\boldsymbol{k}\cdot(\boldsymbol{s}-z(\boldsymbol{r}-\boldsymbol{r}'))} - e^{i\boldsymbol{k}\cdot(\boldsymbol{s}+z\boldsymbol{r}')} - e^{i\boldsymbol{k}\cdot(\boldsymbol{s}-z\boldsymbol{r})}\right)\Bigg\},
\end{aligned}
\tag{84}
$$

then, the vector contribution to the transverse cross-section depends on a series of integrals over $\boldsymbol{r}$, $\boldsymbol{r}'$ and $\boldsymbol{s}$. In the Appendix C we present the results for each one of them which were obtained using the Bessel functions integral which are also present in the Appendix. Therefore, as a result, the vector contribution to the transverse gauge boson + jet dipole-target cross-section is:

$$
\begin{aligned}
\left.\frac{d\sigma_T^f(q_f \to Gq_k))}{dz\, d^2\boldsymbol{p}\, d^2\boldsymbol{\Delta}}\right|_V &= \frac{(C_f^G)^2(g_{V,f}^G)^2}{(2\pi)^6}\int d^2\boldsymbol{k}\, f(x,\boldsymbol{k})\,\delta^{(2)}(\boldsymbol{\Delta}-\boldsymbol{k}) \\
&\quad\times \Bigg\{\frac{[1+(1-z)^2]}{z}\,\epsilon^2\Bigg[-\frac{2(2\pi)^2}{\epsilon^2}\,\frac{\boldsymbol{p}\cdot(\boldsymbol{p}-z\boldsymbol{k})}{(p^2+\epsilon^2)[(\boldsymbol{p}-z\boldsymbol{k})^2+\epsilon^2]} \\
&\quad+\frac{(2\pi)^4}{\epsilon^2}\,\frac{(\boldsymbol{p}-z\boldsymbol{k})^2}{[(\boldsymbol{p}-z\boldsymbol{k})^2+\epsilon^2]^2} + \frac{(2\pi)^4}{\epsilon^2}\,\frac{p^2}{(p^2+\epsilon^2)^2}\Bigg] \\
&\quad+ z\big[(m_b-m_a)+zm_a\big]^2\Bigg[-\frac{2(2\pi)^4}{(p^2+\epsilon^2)[(\boldsymbol{p}-z\boldsymbol{k})^2+\epsilon^2]} \\
&\quad+\frac{(2\pi)^4}{[(\boldsymbol{p}-z\boldsymbol{k})^2+\epsilon^2]^2} + \frac{(2\pi)^4}{(p^2+\epsilon^2)}\Bigg]\Bigg\},
\end{aligned}
\tag{85}
$$

using the delta function to evaluate the integral over $\boldsymbol{k}$, one gets

$$
\begin{aligned}
\left.z\frac{d\sigma_T^f(q_f \to Gq_k)}{dz\, d^2\boldsymbol{p}\, d^2\boldsymbol{\Delta}}\right|_V &= \frac{(C_f^G)^2(g_{V,f}^G)^2}{2\pi^2}\, f(x,\boldsymbol{\Delta})\Bigg\{z^2\big[(m_b-m_a)+zm_a\big]^2\,\mathcal{E}_1(\boldsymbol{p},\boldsymbol{\Delta},\epsilon,z) \\
&\quad+ \big[1+(1-z)^2\big]\,\mathcal{E}_2(\boldsymbol{p},\boldsymbol{\Delta},\epsilon,z)\Bigg\},
\end{aligned}
\tag{86}
$$

where

$$\mathcal{E}_1(\boldsymbol{p}, \boldsymbol{\Delta}, \epsilon, z) = \frac{1}{2} \left[\frac{1}{p^2 + \epsilon^2} - \frac{1}{(\boldsymbol{p} - z\boldsymbol{\Delta}) + \epsilon^2} \right]^2, \tag{87}$$

$$\mathcal{E}_2(\boldsymbol{p}, \boldsymbol{\Delta}, \epsilon, z) = \frac{1}{2} \left[\frac{p}{p^2 + \epsilon^2} - \frac{\boldsymbol{p} - z\boldsymbol{\Delta}}{(\boldsymbol{p} - z\boldsymbol{\Delta}) + \epsilon^2} \right]^2. \tag{88}$$

Accomplishing the same procedure for the axial contribution, one gets:

$$\begin{aligned} z \frac{\mathrm{d}\sigma_T^f(q_f \to Gq_k)}{\mathrm{d}z\, \mathrm{d}^2\boldsymbol{p}\, \mathrm{d}^2\boldsymbol{\Delta}} \bigg|_A &= \frac{(C_f^G)^2 (g_{A,f}^G)^2}{2\pi^2}\, f(x, \boldsymbol{\Delta}) \Bigg\{ z^2 \big[(m_b + m_a) - z m_a \big]^2 \mathcal{E}_1(\boldsymbol{p}, \boldsymbol{\Delta}, \epsilon, z) \\ &\quad + \big[1 + (1-z)^2 \big] \mathcal{E}_2(\boldsymbol{p}, \boldsymbol{\Delta}, \epsilon, z) \Bigg\}. \end{aligned} \tag{89}$$

Likewise, for the longitudinal dipole-target cross-section, the vector contribution is:

$$\begin{aligned} z \frac{\mathrm{d}\sigma_L^f(q_f \to Gq_k)}{\mathrm{d}z\, \mathrm{d}^2\boldsymbol{p}\, \mathrm{d}^2\boldsymbol{\Delta}} \bigg|_V &= \frac{(C_f^G)^2 (g_{V,f}^G)^2}{(2\pi)^2}\, f(x, \boldsymbol{\Delta}) \Bigg\{ \frac{z^2 (m_b - m_a)^2}{M_G^2} \mathcal{E}_2(\boldsymbol{p}, \boldsymbol{\Delta}, \epsilon, z) \\ &\quad + \frac{\big[z^2 m_a (m_b - m_a) - z(m_b^2 - m_a^2) - 2(1-z) M_G^2 \big]^2}{M_G} \mathcal{E}_1(\boldsymbol{p}, \boldsymbol{\Delta}, \epsilon, z) \Bigg\}, \end{aligned} \tag{90}$$

and the axial contribution is

$$\begin{aligned} z \frac{\mathrm{d}\sigma_L^f(q_f \to Gq_k)}{\mathrm{d}z\, \mathrm{d}^2\boldsymbol{p}\, \mathrm{d}^2\boldsymbol{\Delta}} \bigg|_A &= \frac{(C_f^G)^2 (g_{A,f}^G)^2}{(2\pi)^2}\, f(x, \boldsymbol{\Delta}) \Bigg\{ \frac{z^2 (m_b + m_a)^2}{M_G^2} \mathcal{E}_2(\boldsymbol{p}, \boldsymbol{\Delta}, \epsilon, z) \\ &\quad + \frac{\big[z^2 m_a (m_b + m_a) + z(m_b^2 - m_a^2) + 2(1-z) M_G^2 \big]^2}{M_G} \mathcal{E}_1(\boldsymbol{p}, \boldsymbol{\Delta}, \epsilon, z) \Bigg\}. \end{aligned} \tag{91}$$

The expressions derived above constitute the central input for estimating associated jet + $W^\pm$ production at forward rapidities in hadronic collisions. Our results demonstrate that the differential cross-section is highly sensitive to the modeling of the unintegrated gluon distribution (UGD), which plays a key role in encoding the small x structure of the target. In particular, the UGD governs the transverse momentum imbalance between the jet and the gauge boson, thereby controlling the degree of momentum decorrelation observed in the final state. This highlights the potential of such processes as precision probes of gluon saturation and nonlinear QCD dynamics in the forward regime.

4.2.1   Associated Jet + photon production

For the photon production, the axial contribution vanishes, since $g_{A,f}^{\gamma^*} = 0$. Moreover, $g_{V,f}^{\gamma^*} = 1$, $C_{V,f}^{\gamma^*} = \sqrt{\alpha_{em}} e_f$ and $m_b = m_a = m_f$ once the emitting quark does not change its flavor. Thus, the differential cross-section for this final state is given by

$$
\left. \frac{d\sigma}{dz d^2 \boldsymbol{p} d^2 \boldsymbol{\Delta}} \right|_{qp \to \gamma^* X} = \left. \frac{\mathrm{d}\sigma_T}{dz d^2 \boldsymbol{p} d^2 \boldsymbol{\Delta}} \right|_V + \left. \frac{\mathrm{d}\sigma_L}{dz d^2 \boldsymbol{p} d^2 \boldsymbol{\Delta}} \right|_V,
$$

$$
\left. \frac{d\sigma}{dz d^2 \boldsymbol{p} d^2 \boldsymbol{\Delta}} \right|_{qp \to \gamma^* X} = \frac{\alpha_{em} e_f^2}{2\pi^2} f(x, \boldsymbol{\Delta}) \left\{ \frac{1 + (1-z)^2}{z} \mathcal{E}_2(\boldsymbol{p}, z\boldsymbol{\Delta}, \epsilon) + z^3 m_f^2 \mathcal{E}_1(\boldsymbol{p}, z\boldsymbol{\Delta}, \epsilon) \right\}
$$

$$
+ \frac{\alpha_{em} e_f^2}{4\pi^2} f(x, \boldsymbol{\Delta}) \left\{ \frac{4(1-z)^2 M_\gamma^2}{z} \mathcal{E}_1(\boldsymbol{p}, z\boldsymbol{\Delta}, \epsilon) \right\}
$$

$$
\left. \frac{d\sigma}{dz d^2 \boldsymbol{p} d^2 \boldsymbol{\Delta}} \right|_{qp \to \gamma^* X} = \frac{\alpha_{em} e_f^2}{2\pi^2} f(x, \boldsymbol{\Delta}) \left\{ \frac{1 + (1-z)^2}{z} \mathcal{E}_2(\boldsymbol{p}, z\boldsymbol{\Delta}, \epsilon) \right.
$$

$$
\left. + \left[z^3 m_f^2 + \frac{2(1-z)^2 M_\gamma^2}{z} \right] \mathcal{E}_1(\boldsymbol{p}, z\boldsymbol{\Delta}, \epsilon) \right\}, \tag{92}
$$

where $\epsilon^2 = (1-z)M_\gamma^2 + z^2 m_f^2$ in the general case of a virtual photon. In the massless quark case, one has

$$
\left. \frac{d\sigma}{dz d^2 \boldsymbol{p} d^2 \boldsymbol{\Delta}} \right|_{qp \to \gamma^* X}^{m_f = 0} = \frac{\alpha_{em} e_f^2}{2\pi^2} f(x, \boldsymbol{\Delta}) \left\{ \frac{1 + (1-z)^2}{z} \mathcal{E}_2(\boldsymbol{p}, z\boldsymbol{\Delta}, \epsilon) \right.
$$

$$
\left. + \frac{2(1-z)^2 M_\gamma^2}{z} \mathcal{E}_1(\boldsymbol{p}, z\boldsymbol{\Delta}, \epsilon) \right\}, \tag{93}
$$

which can be expressed as follows

$$
z \left. \frac{d\sigma}{dz d^2 \boldsymbol{p} d^2 \boldsymbol{\Delta}} \right|_{qp \to \gamma^* X}^{m_f = 0} = \frac{\alpha_{em} e_f^2}{(2\pi)^2} f(x, \boldsymbol{\Delta}) \left\{ \left[1 + (1-z)^2 \right] \right.
$$

$$
\times \frac{z^2 \boldsymbol{\Delta}^2}{\left((\boldsymbol{p} - z\boldsymbol{\Delta})^2 + (1-z)M_\gamma^2 \right) \left(\boldsymbol{p}^2 + (1-z)M_\gamma^2 \right)}
$$

$$
- z^2 (1-z) M_\gamma^2 \left[\frac{1}{\left((\boldsymbol{p} - z\boldsymbol{\Delta})^2 + (1-z)M_\gamma^2 \right)} \right.
$$

$$
\left. \left. - \frac{1}{\left(\boldsymbol{p}^2 + (1-z)M_\gamma^2 \right)} \right]^2 \right\}. \tag{94}
$$

Finally, for a real photon ($M_\gamma^2 = 0$) and massless quarks, we obtain

$$
z \left. \frac{d\sigma}{dz d^2 \boldsymbol{p} d^2 \boldsymbol{\Delta}} \right|_{qp \to \gamma X} = \frac{\alpha_{em} e_f^2}{(2\pi)^2} f(x, \boldsymbol{\Delta}) \left[1 + (1-z)^2 \right] \frac{z^2 \boldsymbol{\Delta}^2}{(\boldsymbol{p} - z\boldsymbol{\Delta})^2 \boldsymbol{p}^2}. \tag{95}
$$

In this case one needs to take care of the collinear pole in the final state $q \to q\gamma$ splitting at $\boldsymbol{p} = z\boldsymbol{\Delta}$, for example by imposing a photon isolation condition. The Eqs. (94) and (95) agree with those used in Refs.(Dominguez; Marquet; Xiao; Yuan, 2011; Stasto; Xiao; Zaslavsky, 2012; Basso; Goncalves; Nemchik; Pasechnik; Sumbera, 2016; Taels, 2024) to estimate the jet + photon production in hadronic collisions.

4.2.2 Associated Jet + Z^0 production

For the Z^0 production, the axial and vector contributions must be included, and the total differential cross-section will be given by

$$\frac{d\sigma}{dz d^2\boldsymbol{p} d^2\boldsymbol{\Delta}}\bigg|_{qp \to Z^0 X} = \frac{\mathrm{d}\sigma_T}{\mathrm{d}z\mathrm{d}^2\boldsymbol{p}\mathrm{d}^2\boldsymbol{\Delta}}\bigg|_V + \frac{\mathrm{d}\sigma_T}{\mathrm{d}z\mathrm{d}^2\boldsymbol{p}\mathrm{d}^2\boldsymbol{\Delta}}\bigg|_A$$
$$+ \frac{\mathrm{d}\sigma_L}{\mathrm{d}z\mathrm{d}^2\boldsymbol{p}\mathrm{d}^2\boldsymbol{\Delta}}\bigg|_V + \frac{\mathrm{d}\sigma_L}{\mathrm{d}z\mathrm{d}^2\boldsymbol{p}\mathrm{d}^2\boldsymbol{\Delta}}\bigg|_A. \tag{96}$$

Moreover, one has that $\mathcal{C}_f^Z = \frac{\sqrt{\alpha_{em}}}{\sin 2\theta_W}$ and $g_{V,A}^Z$ depends on the quark flavor. For up-type flavors ($f_u = u, c, t$) $g_{V,f_u}^Z = \frac{1}{2} - \frac{4}{3}\sin^2\theta_W$ and $g_{A,f_u}^Z = \frac{1}{2}$, while for down-type flavors ($f_d = d, s, b$) $g_{V,f_d}^Z = -\frac{1}{2} + \frac{2}{3}\sin^2\theta_W$ and $g_{A,f_d}^Z = -\frac{1}{2}$. Also, $m_b = m_a = m_f$, as this kind of process does not imply a change of quark flavor. Then, the parton level cross-sections for each contribution will be given by:

$$\frac{d\sigma_T^f}{dz d^2\boldsymbol{p} d^2\boldsymbol{\Delta}}\bigg|_V^{Z^0} = \frac{(C_f^Z)^2 (g_{V,f}^Z)^2}{2\pi^2} f(x, \boldsymbol{\Delta})\bigg\{\frac{1 + (1-z)^2}{z}\mathcal{E}_2(\boldsymbol{p}, z\boldsymbol{\Delta}, \epsilon)$$
$$+ z^3 m_f^2 \mathcal{E}_1(\boldsymbol{p}, z\boldsymbol{\Delta}, \epsilon)\bigg\} \tag{97}$$

$$\frac{d\sigma_T^f}{dz d^2\boldsymbol{p} d^2\boldsymbol{\Delta}}\bigg|_A^{Z^0} = \frac{(C_f^Z)^2 (g_{A,f}^Z)^2}{2\pi^2} f(x, \boldsymbol{\Delta})\bigg\{\frac{1 + (1-z)^2}{z}\mathcal{E}_2(\boldsymbol{p}, z\boldsymbol{\Delta}, \epsilon)$$
$$+ z(2-z) m_f^2 \mathcal{E}_1(\boldsymbol{p}, z\boldsymbol{\Delta}, \epsilon)\bigg\} \tag{98}$$

$$\frac{d\sigma_L^f}{dz d^2\boldsymbol{p} d^2\boldsymbol{\Delta}}\bigg|_V^{Z^0} = \frac{(C_f^Z)^2 (g_{V,f}^Z)^2}{(2\pi)^2} f(x, \boldsymbol{\Delta})\bigg\{4\frac{(1-z)^2}{z}M_Z^2 \mathcal{E}_1(\boldsymbol{p}, z\boldsymbol{\Delta}, \epsilon)\bigg\} \tag{99}$$

$$\frac{d\sigma_L^f}{dz d^2\boldsymbol{p} d^2\boldsymbol{\Delta}}\bigg|_A^{Z^0} = \frac{(C_f^Z)^2 (g_{A,f}^{Z^0})^2}{(2\pi)^2} f(x, \boldsymbol{\Delta})\bigg\{4\frac{z m_f^2}{M_Z^2}\mathcal{E}_2(\boldsymbol{p}, z\boldsymbol{\Delta}, \epsilon)$$
$$+ \frac{[4z^2 m_f^2 - 2(1-z)M_Z^2]^2}{zM_Z^2}\mathcal{E}_1(\boldsymbol{p}, z\boldsymbol{\Delta}, \epsilon)\bigg\}, \tag{100}$$

where $\epsilon^2 = (1-z)M_Z^2 + z^2 m_f^2$. In the massless quark case, the total cross-section can

be expressed as follows,

$$
\frac{d\sigma}{dz d^2\boldsymbol{p} d^2\boldsymbol{\Delta}}\bigg|_{qp \to Z^0 X}^{m_f=0} = \frac{(C_f^Z)^2}{(2\pi)^2}\left[(g_{V,f}^Z)^2 + (g_{A,f}^Z)^2\right] f(x, \boldsymbol{\Delta})
$$

$$
\times \quad \left\{ \frac{1+(1-z)^2}{z}\left[\frac{\boldsymbol{p} - z\boldsymbol{\Delta}}{[(\boldsymbol{p} - z\boldsymbol{\Delta})^2 + \bar{\epsilon}^2]} - \frac{\boldsymbol{p}}{(p^2 + \bar{\epsilon}^2)}\right]^2 \right.
$$

$$
+ \quad \left. 2\frac{(1-z)^2}{z}M_Z^2\left[\frac{1}{[(\boldsymbol{p} - z\boldsymbol{\Delta}) + \bar{\epsilon}^2]} - \frac{1}{(p^2 + \bar{\epsilon}^2)}\right]^2 \right\}, \quad (101)
$$

with $\bar{\epsilon}^2 = (1-z)M_Z^2$. Such an expression was used in Refs. (Basso; Goncalves; Nemchik; Pasechnik; Sumbera, 2016; Basso; Goncalves; Krelina; Nemchik; Pasechnik, 2016) to estimate the associated jet + Z^0 production at forward rapidities in hadronic collisions.

4.3 Summary

In this chapter, we have derived the parton-target cross-section for the isolated electroweak gauge boson and the associated jet plus electroweak gauge boson production.

We have discussed so far that the description of the particle production at forward rapidities in proton-proton and proton-nucleus collisions at high energies is still one of the main challenges of the strong interactions theory. In this kinematical region, new effects associated with the nonlinear effects in the QCD dynamics are expected to contribute and the usual treatment of the cross-section in terms of the collinear factorization formalism is predicted to breakdown. Over the last decades, several authors have discussed possible generalized factorization formalisms as well as improved the description of saturation effects in the hadronic wave functions. In general, the final formulas for the cross-sections associated with the production of two partons/hadrons involve new quantities, which are non-trivial to estimate. In this chapter, we addressed a simpler process, where one of the particles in the final state is an electroweak gauge boson G. In particular, two - particle production is predicted to be sensitive to the description of the dense target. In the general case, when two partons are produced, the presence of nonlinear effects implies a complex structure for the cross-section, that involves quantities that are not probed in the single particle production. Such aspects motivate the analysis of the associated jet plus electroweak gauge boson production which was performed in this chapter as well.

As we have demonstrated in Chap. 3, the differential cross-section for the associated production of the gauge boson with a quark can be fully expressed in terms of the squared light cone wave function (LCWF) for the $q_f \to G q_k$ transition, and the usual dipole-proton cross-section, which can be constrained by the HERA data. Moreover, we

have derived, for the first time, the generic expressions for the LCWF's. From this result, we were able to construct the parton-target cross-sections for the isolated electroweak gauge boson in section 4.1. In addition, we demonstrated that our results reduce to expressions previously used in the literature for the description of the real photon production and Drell - Yan process at forward rapidities in some particular limits. Finally, in the Appendix D, analytical expressions for the spectrum have been derived in the color transparency limit, which is a reasonable approximation of the linear regime of QCD dynamics together with a full description of the isolated electroweak gauge boson production within the impact parameter space. In section 4.2, we have extended the formalism presented so far for the associated jet + G production and derived the general formula for the differential cross-section at the partonic level, which is the main input to estimate the corresponding observable. In particular, we have presented, for the first time, the expressions associated with the jet + $W^{\pm}$ case and demonstrated that the general formula reproduces the approximated expressions previously used in the literature to estimate the jet + γ and jet + Z^0 production.

The results derived in this chapter are the main ingredients for the calculation of the pp and pA cross - sections, which can be compared with the current and forthcoming LHC data.

5 DRELL - YAN ANGULAR DISTRIBUTIONS AT FORWARD RAPIDITIES IN THE COLOR - DIPOLE S - MATRIX FRAME-WORK

The dilepton production in the hadronic interactions – the Drell - Yan process – is one of the main tools for studying the partonic structure of hadrons. In particular, the study of dilepton production at forward rapidities is considered a promising probe of quantum chromodynamics (QCD) at high energies. Over the last decades, several groups have estimated the transverse and rapidity differential distributions considering proton - proton (pp) and proton - nucleus (pA) collisions at the RHIC and LHC energies assuming different approaches for the description of the cross-section and distinct models for the treatment of the nonlinear effects, which are expected to modify the QCD dynamics at small x (Kopeliovich; Rezaeian; Pirner; Schmidt, 2007; Kopeliovich; Levin; Rezaeian; Schmidt, 2009; Santos; Silveira; Machado, 2020; Gelis; Jalilian-marian, 2002a; Jalilian-marian; Rezaeian, 2012; Ducloué; Lappi; Mäntysaari, 2018; Goncalves; Lima; Pasechnik; Šumbera, 2020; Lima; Giannini; Goncalves, 2024; Kopeliovich; Raufeisen; Tarasov, 2001; Raufeisen; Peng; Nayak, 2002; Kopeliovich; Raufeisen; Tarasov; Johnson, 2003; Betemps; Gay ducati, 2004; Betemps; Ducati; Machado; Raufeisen, 2003; Golec-biernat; Lewandowska; Stasto, 2010; Ducati; Griep; Machado, 2014; Schäfer; Szczurek, 2016; Ducloué, 2017; Gelis; Jalilian-marian, 2002b; Baier; Mueller; Schiff, 2004; Stasto; Xiao; Zaslavsky, 2012; Kang; Xiao, 2013; Basso; Goncalves; Krelina; Nemchik; Pasechnik, 2016; Basso; Goncalves; Nemchik; Pasechnik; Sumbera, 2016; Marquet; Wei; Xiao, 2020; Celiberto; Gordo gómez; Sabio vera, 2018; Marquet; Wei; Xiao, 2020). One of the largely used approaches is the hybrid factorization formalism, which is motivated by the fact that at forward rapidities the partons from the projectile scatter off a dense gluonic system in the target. In this formalism, the DY process is considered as an electroweak gauge boson bremsstrahlung off a fast projectile quark propagating through the low - x color field of the target, as illustrated in Fig. 13, and the cross-section is described in terms of a convolution of the standard quark distributions for the dilute projectile and the quark - target cross-section, which can include the

nonlinear QCD effects. This scenario was largely discussed throughout this thesis where in Chap. 3 and Chap. 4 — which are based on Refs. (Bandeira; Goncalves; Schäfer, 2024, 2025) — we have derived the general formulae for the inclusive electroweak gauge boson production at forward rapidities using the S - matrix framework proposed in Refs. (Nikolaev; Piller; Zakharov, 1995, 1996; Nikolaev; Schafer; Zakharov; Zoller, 2003; Nikolaev; Schafer, 2005; Nikolaev; Schafer; Zakharov; Zoller, 2005a; Nikolaev; Schafer; Zakharov, 2005a; Nikolaev; Schafer; Zakharov; Zoller, 2005b; Nikolaev; Schafer; Zakharov, 2005b).

A natural next step is to extend the results derived in the previous chapters for less inclusive observables, which provide additional information about the hadronic structure, as e.g., the angular distribution of the leptons pairs ($l_1 \bar{l}_2$). The important roles of the lepton angular distribution in understanding the mechanisms for W, Z and γ boson production in hadronic collisions were pointed out e.g. in Refs. (Mirkes, 1992; Mirkes; Ohnemus, 1994; Boer; Vogelsang, 2006). Differently from γ and Z boson production, where both l_1 and $\bar{l}_2 = \bar{l}_1$ decay products are detected, only the charged lepton from W boson decay is measured. It implies that distinct experimental uncertainties are encountered in the measurements of lepton angular distributions associated with the production of the different gauge bosons. Another important difference is that these distributions involve different couplings. In particular, W and Z boson productions involve different parity-violating couplings, which makes instructive to compare the corresponding lepton angular distributions. Such aspect has motivated the improvement of theoretical description of the DY process (See e.g. Refs. (Lyubovitskij; Zhevlakov; Anikin, 2024; Nefedov; Nikolaev; Saleev, 2013; Piloneta; Vladimirov, 2024)), as well as the measurement of the angular coefficients in pp collisions at high energies by the distinct LHC experimental collaborations (Aad et al., 2012, 2016; Khachatryan et al., 2015; Aaij et al., 2022).

In this chapter, we will focus on the calculation of the angular distributions of leptonic pairs ($l_1 \bar{l}_2$) at forward rapidities and LHC energies, expanding our work presented so far (Refs. (Bandeira; Goncalves; Schäfer, 2024, 2025)) and generalizing the results derived in Ref. (Schäfer; Szczurek, 2016) for the cases where the dilepton system is produced by a Z^0 or a $W^\pm$ gauge boson. Our goal is to derive all density matrix elements needed to estimate the angular coefficients using the CDSM. As we will demonstrate, the resulting expressions will be linearly dependent of the target unintegrated gluon distribution (UGD), which is sensitive to the description of the QCD dynamics, and are valid for pp and pA collisions. In our analysis, we will calculate the angular coefficients in pp collisions at $\sqrt{s} = 14$ TeV, assuming that the dileptons are produced in the rapidity range covered by the LHCb detector, and considering distinct models for the proton UGD. In particular, we will consider a model that takes into account nonlinear effects in the QCD dynamics and will compare with those derived disregarding these effects. The

Figure 13 – Drell - Yan process in the hybrid factorization.
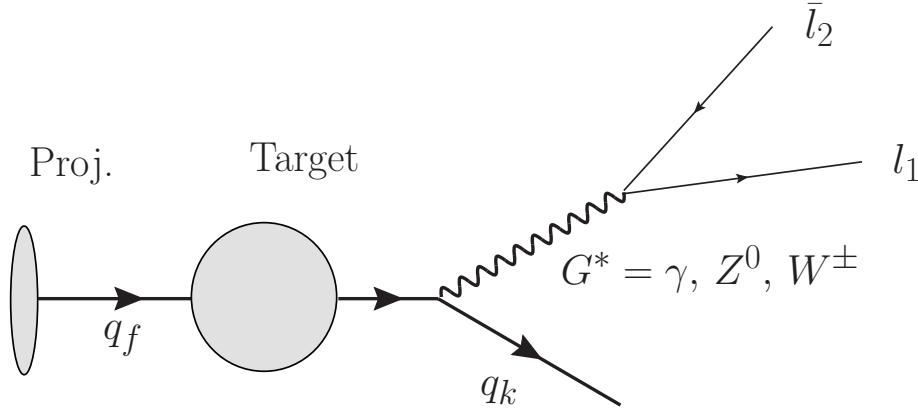
One of two diagrams for the Drell - Yan process in the hybrid factorization formalism. In the high energy limit, the gauge boson vertex can occur before or after interaction with the target fields.

results presented in this chapter are the basis of an article in preparation (Bandeira; Goncalves; Schäfer, 2025).

We organize this chapter as follows. In the next section, we derive the expressions for the gauge boson polarization density matrix elements (DME) in terms of the structure functions present in the decomposition of the hadronic tensor. In particular, we will demonstrate that distinctly from the case of virtual photons, where there are four parity conserving structure functions (Lam; Tung, 1978), for the case of electroweak gauge bosons $W^\pm, Z^0$, the lepton angular distributions give access to nine independent structure functions (Körner; Mirkes, 1991; Mirkes, 1992; Lyubovitskij; Vogelsang; Wunder; Zhevlakov, 2024). In section 5.2 we will present the derivation of the density matrix elements using the color - dipole S - matrix framework for the generic $q \to qG$ process, with $G = \gamma$, Z or a W boson. We will demonstrate that the results derived in Ref. (Schäfer; Szczurek, 2016) are recovered for $G = \gamma$. Moreover, the collinear limit of the Lam - Tung relation will be discussed. Our predictions for the distinct density matrix elements will be presented in section 5.3, considering the dilepton production at forward rapidities ($2.0 \le y \le 4.0$) in pp collisions at $\sqrt{s} = 14$ TeV. In order to estimate the impact of the non - linear effects on the density matrix elements, we will present the results associated with distinct models for the proton UGD.

5.1 Structure functions and the gauge boson polarization density matrix

The cross–section for the Drell–Yan process in pp collisions at the center-of-mass energy $\sqrt{s}$ can be expressed in terms of the leptonic $L^{\mu\nu}$ and hadronic tensors $W_{\mu\nu}$ as

follows

$$(2\pi)^4 \frac{d\sigma(pp \to \ell_1(l_1)\bar{\ell}_2(l_2) + X)}{d^4q} = \frac{1}{2s} \frac{W_{\mu\nu}L^{\mu\nu}}{(M^2 - M_G^2)^2 + \Gamma_G^2 M_G^2} \, d\Phi(q, l_1, l_2), \qquad (102)$$

where $q = l_1 + l_2$ is the four-momentum of the virtual gauge boson, $M^2 = q^2$ is the invariant mass of the lepton pair, M_G is the gauge boson mass, Γ_G is its total decay width and $d\Phi$ is the dilepton phase space. We have adopted the relativistic Breit–Wigner form as appropriate for a narrow resonance. As emphasized, e.g., in Ref. (Mirkes, 1992), the lepton tensor $L_{\mu\nu}$ acts as an analyzer of the gauge boson polarization. In contrast, $W_{\mu\nu}$ contains all the dynamical information on the gauge boson production.

As there is no standard notation for the relevant structure functions, in this work we will adopt the decomposition and notational conventions recently proposed in Ref.(Lyubovitskij; Vogelsang; Wunder; Zhevlakov, 2024) and write:

$$\begin{aligned}
W^{\mu\nu} = {} & (X^\mu X^\nu + Y^\mu Y^\nu) W_T + i (X^\mu Y^\nu - Y^\mu X^\nu) W_{T_p} + Z^\mu Z^\nu W_L \\
& + (Y^\mu Y^\nu - X^\mu X^\nu) W_{\Delta\Delta} - (X^\mu Y^\nu + Y^\mu X^\nu) W_{\Delta\Delta_p} \\
& - (X^\mu Z^\nu + Z^\mu X^\nu) W_\Delta - (Y^\mu Z^\nu + Z^\mu Y^\nu) W_{\Delta_p} \\
& + i (Z^\mu X^\nu - X^\mu Z^\nu) W_\nabla + i (Y^\mu Z^\nu - Z^\mu Y^\nu) W_{\nabla_p} .
\end{aligned} \qquad (103)$$

Here X^μ, Y^μ, Z^μ is an orthogonal basis of spacelike vectors, which fulfill $X^2 = Y^2 = Z^2 = -1$. Together with the timelike unit vector $T^\mu = q^\mu/M, T^2 = 1$, they form a right-handed, i.e., $Y^\mu = \epsilon^{\mu\nu\alpha\beta} T_\nu Z_\alpha X_\beta$, basis of Minkowski space. In a given rest frame of the gauge boson, they can be thought of having the canonical form $T^\mu = (1,0,0,0), X^\mu = (0,1,0,0), Y^\mu = (0,0,1,0), Z^\mu = (0,0,0,1)$. For useful covariant expressions of X^μ, Y^μ, Z^μ in terms of the four momenta of incoming hadrons and the gauge boson, which fix the orientation of axes with relation to these particle momenta, see e.g. (Boer; Vogelsang, 2006). In our discussion, we will adopt a convention where X^μ, Z^μ span the gauge–boson production plane, and Y^μ is the out-of plane direction. The frames such as Gottfried–Jackson (GJ) and Collins–Soper (CS) ones differ by a rotation in the production plane as shown in the Appendix E. Other frame choices are discussed, e.g., in (Richter-was; Was, 2017). Moreover, in eq. (103), the hadronic tensor $W_{\mu\nu}$ has being parametrized in terms of

1. Two transverse functions, the P-even W_T and the P- odd W_{T_p},

2. One longitudinal function, W_L which is P- even,

3. Two transverse-transverse interference (double-spin-flip) functions, the P-even $W_{\Delta\Delta}$ and the P-odd $W_{\Delta\Delta_p}$,

4. Four transverse-longitudinal interference (single-spin-flip) functions, the P-even

W_Δ, W_∇ and the P-odd W_{Δ_P}, W_{∇_P}.

On the other hand, the lepton tensor $L_{\mu\nu}$, for massless leptons coupled to gauge bosons with the respective vector and axial couplings g_V, g_A, reads

$$L_{\mu\nu} = 4(g_V^2 + g_A^2)\left(l_{1\mu}l_{2\nu} + l_{2\mu}l_{1\nu} - (l_1 \cdot l_2)g_{\mu\nu}\right) - 8g_V g_A i\epsilon_{\mu\nu\alpha\beta}l_1^\alpha l_2^\beta \ . \tag{104}$$

In a given rest frame of the lepton pair, we parameterize the four vectors of leptons as

$$l_{1\mu} = \frac{M}{2}(T_\mu + n_\mu), \quad l_{2\mu} = \frac{M}{2}(T_\mu - n_\mu) \ , \tag{105}$$

with

$$n_\mu = \sin\theta \cos\phi \, X_\mu + \sin\theta \sin\phi \, Y_\mu + \cos\theta \, Z_\mu. \tag{106}$$

Consequently, the lepton tensor can be expressed as follows

$$L_{\mu\nu} = 2M^2(g_V^2 + g_A^2)\,\mathcal{L}_{\mu\nu}, \tag{107}$$

with

$$\mathcal{L}_{\mu\nu} = -g_{\mu\nu} + T_\mu T_\nu - n_\mu n_\nu + i c_G \, \epsilon_{\mu\nu\alpha\beta} T^\alpha n^\beta \ , \tag{108}$$

where $c_G = 2g_V g_A/(g_V^2 + g_A^2)$. In the Standard Model $c_\gamma = 0, c_W = 1, c_Z \approx 0.08$.

In our analysis, we are interested in the lepton angular distributions, $dN/d\Omega$, which can be obtained in a straightforward manner from the differential cross-section for the DY process, given by

$$\frac{d\sigma}{d^4q d\Omega} = \frac{d\sigma}{d^4q}\frac{dN}{d\Omega} \ . \tag{109}$$

As a consequence, one has that

$$\frac{dN}{d\Omega} = \frac{3}{8\pi}\frac{W_{\mu\nu}\mathcal{L}^{\mu\nu}}{2W_T + W_L} \ . \tag{110}$$

Such a distribution can be expressed as follows

$$\begin{aligned}
\frac{dN}{d\Omega} &= \frac{3}{8\pi}\frac{1}{2W_T + W_L}\Bigg[g_T W_T + g_L W_L + g_\Delta W_\Delta + g_{\Delta\Delta} W_{\Delta\Delta} \\
&\quad + c_G g_{T_P} W_{T_P} + c_G g_{\nabla_P} W_{\nabla_P} + c_G g_\nabla W_\nabla + g_{\Delta\Delta_P} W_{\Delta\Delta_P} + g_{\Delta_P} W_{\Delta_P} \Bigg]
\end{aligned} \tag{111}$$

$$= \frac{3}{8\pi}\left[g_T\rho_T + g_L\rho_L + g_\Delta\rho_\Delta + g_{\Delta\Delta}\rho_{\Delta\Delta} \right.$$

$$\left. + c_G g_{T_P}\rho_{T_P} + c_G g_{\nabla_P}\rho_{\nabla_P} + c_G g_\nabla\rho_\nabla + g_{\Delta\Delta_P}\rho_{\Delta\Delta_P} + g_{\Delta_P}\rho_{\Delta_P} \right], \tag{112}$$

where $g_i = g_i(\theta, \phi)$ are the angular coefficients

$$g_T = 1 + \cos^2\theta\,, \qquad g_L = 1 - \cos^2\theta\,, \qquad g_{T_P} = 2\cos\theta\,,$$

$$g_{\Delta\Delta} = \sin^2\theta\cos 2\phi\,, \qquad g_\Delta = \sin 2\theta\cos\phi\,, \qquad g_{\nabla_P} = 2\sin\theta\cos\phi\,,$$

$$g_{\Delta\Delta_P} = \sin^2\theta\sin 2\phi\,, \qquad g_{\Delta_P} = \sin 2\theta\sin\phi\,, \qquad g_\nabla = 2\sin\theta\sin\phi\,, \tag{113}$$

with θ and ϕ being the polar and azimuthal lepton decay angles. Moreover, the angular coefficients

$$\rho_i \equiv \frac{W_i}{2W_T + W_L}\,, \quad i \in \{T, L, \Delta\Delta, \Delta\Delta_p, T_p, \Delta, \nabla, \Delta_p, \nabla_p\}, \tag{114}$$

are defined in terms of combinations of the gauge boson polarization DMEs, $\rho^{\lambda\lambda'}$, defined in a helicity basis as

$$\rho^{\lambda\lambda'} = \frac{W^{\mu\nu}\epsilon_\mu^{(\lambda)}\epsilon_\nu^{(\lambda')*}}{2W_T + W_L}\,, \tag{115}$$

with the gauge boson polarization vectors $\epsilon_\lambda^\mu(q)$ being given by

$$\epsilon_\pm^\mu(q) = \frac{\mp X^\mu - iY^\mu}{\sqrt{2}}\,, \quad \epsilon_0^\mu(q) = Z^\mu\,. \tag{116}$$

In particular, one has that

$$
\begin{aligned}
\rho_T &= \frac{1}{2}(\rho^{++} + \rho^{--}), \\
\rho_L &= \rho^{00}, \\
\rho_{\Delta\Delta} &= \frac{1}{2}(\rho^{-+} + \rho^{+-}), \\
\rho_{\Delta\Delta_P} &= \frac{i}{2}\left(\rho^{+-} - \rho^{-+}\right), \\
\rho_{T_P} &= \frac{1}{2}\left(\rho^{++} - \rho^{--}\right), \\
\rho_\Delta &= -\frac{1}{2\sqrt{2}}\left(\rho^{-0} + \rho^{0-} - \rho^{+0} - \rho^{0+}\right), \\
\rho_\nabla &= \frac{i}{2\sqrt{2}}\left(\rho^{-0} - \rho^{0-} + \rho^{0+} - \rho^{+0}\right), \\
\rho_{\Delta_P} &= \frac{i}{2\sqrt{2}}\left(-\rho^{0-} + \rho^{-0} - \rho^{0+} + \rho^{+0}\right), \\
\rho_{\nabla_P} &= -\frac{1}{2\sqrt{2}}\left(\rho^{0-} + \rho^{-0} + \rho^{0+} + \rho^{+0}\right).
\end{aligned}
\tag{117}
$$

For completeness, in Appendix F we present the relation between our representation for the angular distribution and other conventions used in the literature. Some aspects are important to be emphasized. First, the angular coefficients ρ_i depend on the invariant mass, transverse momentum, and rapidity of the lepton pair, being sensitive to the description of the QCD dynamics. Second, for the purely electromagnetic Drell-Yan process, only the four structure functions W_T, W_L, W_Δ and $W_{\Delta\Delta}$ contribute. Third, the parton model predicts that the quantity $A_{LT} = (2W_L - 4W_{\Delta\Delta})/(2W_T + W_L)$, denoted Lam - Tung relation (Lam; Tung, 1978), is equal to zero. Recent high-statistics measurements of the lepton angular distribution coefficients in Z boson production in pp collision at the LHC (Aad et al., 2016; Khachatryan et al., 2015; Aaij et al., 2022), over a broad range of the gauge boson transverse momentum, by the ATLAS, CMS and LHCb experiments revealed a clear violation of the Lam-Tung relation, in contrast with the experimental results at smaller center - of - mass energies. One possible physical explanation for this violation is that QCD radiative effects, which arise at next - to - leading order (or beyond), become important at LHC energies (Gauld; Gehrmann-de ridder; Gehrmann; Glover; Huss, 2017). Another possibility is that intrinsic transverse momenta of the initial partons (Peng; Chang; Mcclellan; Teryaev, 2016; Motyka; Sadzikowski; Stebel, 2017) and/or higher-twist contributions (Brandenburg; Brodsky; Khoze; Mueller, 1994; Eskola; Hoyer; Vanttinen; Vogt, 1994; Gelis; Jalilian-marian, 2007), usually neglected in the calculations based on the collinear factorization framework, may become relevant, and its contributions cannot be neglected in the description of the cross-sections. Such aspects motivate the analysis of the angular distributions using the hybrid factorization

formalism, which is expected to take into account of the contributions associated with the intrinsic momentum of the target, part of the NLO corrections as well the higher - twist contributions associated, e.g., with the nonlinear QCD effects.

5.2 Helicity density matrix elements from the $q \to Gq$ process in the color–dipole S–matrix framework

In this section we focus on the helicity density matrix for the gauge-boson production, which can be obtained from the different contractions $\epsilon_\mu^{(\lambda)} \epsilon_\nu^{(\lambda')*} W^{\mu\nu}$. In the following, we will further simplify the calculation by replacing the Breit-Wigner distribution of the dilepton mass by a delta function. We therefore do not discuss the dependence on lepton invariant mass, nor do we include the $Z^0 - \gamma$ interference. We start from the cross-section for inclusive gauge–boson production which can be expressed through the hadronic tensor as

$$\frac{d\sigma(pp \to G(x_F, \boldsymbol{q})X)}{dx_F d^2\boldsymbol{q}} = \frac{1}{32\pi^3 s x_F}(2W_T + W_L). \tag{118}$$

We are interested in the forward rapidity region of one of the protons which has, say, a large light cone plus-momentum, and the gauge boson carries a fraction x_F thereof. By $\boldsymbol{q}$ we denote the transverse momentum of the gauge boson in the pp center-of-mass frame. Now the polarization density matrix elements in the helicity basis are related to the hadronic tensor via

$$\rho^{\lambda\lambda'} \frac{d\sigma(pp \to G(x_F, \boldsymbol{q})X)}{dx_F d^2\boldsymbol{q}} = \frac{1}{32\pi^3 s x_F} \epsilon_\mu^{(\lambda)} \epsilon_\nu^{(\lambda')*} W^{\mu\nu} . \tag{119}$$

As we have demonstrated in this thesis (Chap. 3), the gauge boson production at forward rapidities can be described using the hybrid factorization formula, which implies that

$$\begin{aligned}
\rho_{\lambda\lambda'} \frac{d\sigma(pp \to G(x_F, \boldsymbol{q})X)}{\mathrm{d}x_F \mathrm{d}^2\boldsymbol{q}} &= \sum_f \int \mathrm{d}x_1 \mathrm{d}z\, \delta(x_F - zx_1) \left[q_f(x_1, \mu^2) + \overline{q}_f(x_1, \mu^2) \right] \\
&\times \hat{\rho}_{\lambda\lambda'} \frac{\mathrm{d}\hat{\sigma}(qp \to G(z, \boldsymbol{q})X)}{\mathrm{d}z \mathrm{d}^2\boldsymbol{q}} ,
\end{aligned} \tag{120}$$

where $q_f(x_1, \mu^2)$ are the projectile parton distributions with a momentum fraction x_1 at a factorization scale $\mu^2 \approx \boldsymbol{q}^2 + M_G^2$, z is the fraction of the quark's longitudinal momentum carried by the gauge boson. Moreover, the partonic density matrix is given in the

color–dipole S–matrix approach by

$$\hat{\rho}^{\lambda\lambda'} \frac{\mathrm{d}\sigma(qp \to GX)}{\mathrm{d}z\mathrm{d}^2\boldsymbol{q}} = \frac{1}{2(2\pi)^2} \overline{\sum_{\eta\eta'}} \int \mathrm{d}^2\boldsymbol{r}\mathrm{d}^2\boldsymbol{r}' e^{-i\boldsymbol{q}(\boldsymbol{r}-\boldsymbol{r}')} \Psi_{\eta\eta'}^{(\lambda)}(z,\boldsymbol{r}) \Psi_{\eta\eta'}^{(\lambda')\dagger}(z,\boldsymbol{r}')$$
$$\times \Big[\sigma(x,z\boldsymbol{r}) + \sigma(x,z\boldsymbol{r}') - \sigma(x,z(\boldsymbol{r}-\boldsymbol{r}')) \Big], \tag{121}$$

where $\Psi_{\eta\eta'}^{(\lambda)}$ is the light front wave function (LFWF) for the $q_\eta \to Gq'_{\eta'}$ transition in the impact parameter space, with $\eta, \eta', \lambda, \lambda'$ denoting the helicities of particles, and $\sigma(x,\boldsymbol{r})$ is the color dipole–proton cross–section (Nikolaev; Zakharov, 1991), which is determined by the QCD dynamics. For an early discussion of Drell–Yan lepton angular distributions in the color-dipole approach, see (Brodsky; Hebecker; Quack, 1997).

In what follows, we will use the results for the LFWF obtained in Chap. 3 in order to derive the elements of the partonic density matrix. As demonstrated in that chapter, the calculation can be performed in two equivalent representations, the impact parameter and momentum space representations, which are related by a Fourier transform. Here we will perform our study in the momentum space representation. In order to do that, we will use in Eq. (121) the relation between the dipole - proton cross–section and the unintegrated gluon distribution, $f(x,\boldsymbol{k})$, given by

$$\sigma(x,\boldsymbol{r}) = \frac{1}{2} \int \mathrm{d}^2\boldsymbol{k} f(x,\boldsymbol{k}) \left(1 - e^{-i\boldsymbol{k}\boldsymbol{r}}\right) \left(1 - e^{i\boldsymbol{k}\boldsymbol{r}}\right). \tag{122}$$

Inserting this expression into eq.(121), we obtain the following representation, now fully in momentum space:

$$\hat{\rho}^{\lambda\lambda'} \frac{d\sigma(qp \to GX)}{dz d^2\boldsymbol{q}} = \frac{1}{2(2\pi)^2} \overline{\sum_{\eta\eta'}} \int d^2\boldsymbol{k} f(x_2,\boldsymbol{k})$$
$$\times \left(\Psi_{\eta'\eta}^{(\lambda)}(z,\boldsymbol{q}) - \Psi_{\eta'\eta}^{(\lambda)}(z,\boldsymbol{q}-z\boldsymbol{k}) \right) \left(\Psi_{\eta'\eta}^{(\lambda')}(z,\boldsymbol{q}) - \Psi_{\eta'\eta}^{(\lambda')}(z,\boldsymbol{q}-z\boldsymbol{k}) \right)^\dagger$$
$$= \frac{1}{2(2\pi)^2} \int d^2\boldsymbol{k} f(x_2,\boldsymbol{k}) I^{(\lambda,\lambda')}(z,\boldsymbol{q},z\boldsymbol{k}). \tag{123}$$

Here, the argument of the unintegrated gluon distribution is caculated from the transverse mass of the $q + G$–system:

$$x_1 x_2 s = M_{qG}^2 + \boldsymbol{k}^2 = \frac{M_G^2 + \boldsymbol{q}^2}{z} + \frac{m_f^2 + (\boldsymbol{k}-\boldsymbol{q})^2}{1-z}. \tag{124}$$

As demonstrated in the previous chapters, the LFWF in the momentum space are

defined as[1]

$$\Psi_V^{\pm}(z, \boldsymbol{k}) = \frac{C_f^G g_{V,f}^G \sqrt{z}}{\boldsymbol{k}^2 + \epsilon^2} \chi_{\eta'}^\dagger \left\{ \frac{2-z}{z} \left(\boldsymbol{k} \cdot \boldsymbol{e}^*(\pm) \right) \mathbb{1} + i \left(\boldsymbol{k} \times \boldsymbol{e}^*(\pm) \right)_{\hat{z}} \sigma_3 \right.$$
$$\left. - \Gamma_V \left(\boldsymbol{\sigma} \cdot \boldsymbol{e}^*(\pm) \right) \sigma_3 \right\} \chi_\eta \tag{125}$$

$$\Psi_V^0(z, \boldsymbol{k}) = \frac{C_f^G g_{V,f}^G}{\sqrt{z} M [\boldsymbol{k}^2 + \epsilon^2]} \chi_{\eta'}^\dagger \left\{ \Lambda_V \mathbb{1} + z(m_b - m_a) \left(\boldsymbol{\sigma} \cdot \boldsymbol{k} \right) \sigma_3 \right\} \chi_\eta \tag{126}$$

$$\Psi_A^{\pm}(z, \boldsymbol{k}) = \frac{C_f^G g_{A,f}^G \sqrt{z}}{\boldsymbol{k}^2 + \epsilon^2} \chi_{\eta'}^\dagger \left\{ \frac{2-z}{z} \left(\boldsymbol{k} \cdot \boldsymbol{e}^*(\pm) \right) \sigma_3 + i \left(\boldsymbol{k} \times \boldsymbol{e}^*(\pm) \right)_{\hat{z}} \mathbb{1} \right.$$
$$\left. - \Gamma_A \left(\boldsymbol{\sigma} \cdot \boldsymbol{e}^*(\pm) \right) \right\} \chi_\eta \tag{127}$$

$$\Psi_A^0(z, \boldsymbol{k}) = \frac{C_f^G g_{A,f}^G}{\sqrt{z} M [\boldsymbol{k}^2 + \epsilon^2]} \chi_{\eta'}^\dagger \left\{ -\Lambda_A \sigma_3 - z(m_b + m_a) \left(\boldsymbol{\sigma} \cdot \boldsymbol{k} \right) \mathbb{1} \right\} \chi_\eta \tag{128}$$

where

$$\Gamma_V \equiv m_b - (1-z)m_a, \quad \Gamma_A \equiv m_b + (1-z)m_a$$
$$\Lambda_V \equiv z^2 m_a \left(m_b - m_a \right) - z \left(m_b^2 - m_a^2 \right) - 2(1-z)M^2$$
$$\Lambda_A \equiv z^2 m_a \left(m_b + m_a \right) + z \left(m_b^2 - m_a^2 \right) + 2(1-z)M^2,$$

It is useful to introduce the shorthand notations

$$\Phi_0 = \frac{1}{\boldsymbol{q}^2 + \epsilon^2} - \frac{1}{(\boldsymbol{q} - z\boldsymbol{k})^2 + \epsilon^2}, \quad \boldsymbol{\Phi} = \frac{\boldsymbol{q}}{\boldsymbol{q}^2 + \epsilon^2} - \frac{\boldsymbol{q} - z\boldsymbol{k}}{(\boldsymbol{q} - z\boldsymbol{k})^2 + \epsilon^2}, \tag{129}$$

so that the combinations of relevant wave functions for the density matrix in momentum space take the form

$$\Psi_{\eta'\eta}^{(\lambda)}(z, \boldsymbol{q}) - \Psi_{\eta'\eta}^{(\lambda)}(z, \boldsymbol{q} - z\boldsymbol{k}) = \chi_{\eta'}^\dagger \mathcal{O}^{(\lambda)} \chi_\eta, \tag{130}$$

with

$$\mathcal{O}^{(\pm)} = C_f^G \sqrt{z} \quad \left\{ \frac{2-z}{z} \left(\boldsymbol{\Phi} \cdot \boldsymbol{e}^*(\pm) \right) \left(g_{V,f}^G \mathbb{1} + g_{A,f}^G \sigma_3 \right) + i(\boldsymbol{\Phi} \times \boldsymbol{e}^*(\pm)) \cdot \boldsymbol{e}_z \left(g_{V,f}^G \sigma_3 + g_{A,f}^G \mathbb{1} \right) \right.$$
$$\left. - \Phi_0 \left(\boldsymbol{\sigma} \cdot \boldsymbol{e}^*(\pm) \right) \left(g_{V,f}^G \Gamma_V \sigma_3 + g_{A,f}^G \Gamma_A \mathbb{1} \right) \right\}, \tag{131}$$

and

$$\mathcal{O}^{(0)} = \frac{C_f^G}{\sqrt{z} M} \left\{ \Phi_0 \left(g_{V,f}^G \Lambda_V \mathbb{1} - g_{A,f}^G \Lambda_A \sigma_3 \right) + z(\boldsymbol{\sigma} \cdot \boldsymbol{\Phi}) \left(g_{V,f}^G (m_b - m_a) \sigma_3 - g_{A,f}^G (m_b + m_a) \mathbb{1} \right) \right\}. \tag{132}$$

---

[1]Note that we only redefined some terms in order to make the calculations less complicated. However, are the same expressions seen in Chap. 3.

Therefore, the relevant integrands of Eq.(123) can be written as

$$I^{(\lambda,\lambda')}(z, \boldsymbol{q}, z\boldsymbol{k}) = \frac{1}{2}\text{Tr}[\mathcal{O}^{(\lambda)}\mathcal{O}^{(\lambda')\dagger}]. \tag{133}$$

The traces are readily evaluated using

$$\text{Tr}(\mathbb{1}) = 2, \quad \text{Tr}(\sigma_i) = 0, \quad \text{Tr}(\sigma_i\sigma_j) = 2\delta_{ij}, \quad \text{Tr}(\sigma_l\sigma_j\sigma_k) = 2i\,\varepsilon_{ljk}. \tag{134}$$

Consequently, for the transverse polarizations of gauge bosons, one has:

$$\begin{aligned}
I^{(\pm,\pm)}(z, \boldsymbol{q}, z\boldsymbol{k}) &= |C_f^G|^2\Big\{\Big((g_{V,f}^G)^2 + (g_{A,f}^G)^2\Big)\frac{1 + (1-z)^2}{z}\boldsymbol{\Phi}^2 \pm 2g_{V,f}^G g_{A,f}^G(2-z)\boldsymbol{\Phi}^2 \\
&\quad + \Big((g_{V,f}^G)^2\Gamma_V^2 + (g_{A,f}^G)^2\Gamma_A^2 \pm 2g_{V,f}^G g_{A,f}^G\Gamma_V\Gamma_A\Big)z\Phi_0^2\Big\}
\end{aligned} \tag{135}$$

$$\begin{aligned}
I^{(\pm,\mp)}(z, \boldsymbol{q}, z\boldsymbol{k}) &= |C_f^G|^2\Big((g_{V,f}^G)^2 + (g_{A,f}^G)^2\Big)2\frac{1-z}{z}\Big(\Phi_y^2 - \Phi_x^2\Big) \\
&= |C_f^G|^2\Big((g_{V,f}^G)^2 + (g_{A,f}^G)^2\Big)2\frac{1-z}{z}\Big\{\boldsymbol{\Phi}^2 - 2\Big(\frac{\boldsymbol{q}\cdot\boldsymbol{\Phi}}{|\boldsymbol{q}|}\Big)^2\Big\},
\end{aligned} \tag{136}$$

while for the longitudinally polarized bosons results

$$\begin{aligned}
I^{(0,0)}(z, \boldsymbol{q}, z\boldsymbol{k}) &= \frac{|C_f^G|^2}{zM^2}\Big\{\Big((g_{V,f}^G)^2\Lambda_V^2 + (g_{A,f}^G)^2\Lambda_A^2\Big)\Phi_0^2 \\
&\quad + z^2\Big((g_{V,f}^G)^2(m_b - m_a)^2 + (g_{A,f}^G)^2(m_b + m_a)^2\Big)\boldsymbol{\Phi}^2\Big\}.
\end{aligned} \tag{137}$$

Finally, the interference contributions are given by

$$\begin{aligned}
I^{(\pm,0)}(z, \boldsymbol{q}, z\boldsymbol{k}) &= \frac{|C_f^G|^2}{M\sqrt{2}}\Big\{\mp\frac{2-z}{z^2}\Big((g_{V,f}^G)^2\Lambda_V - (g_{A,f}^G)^2\Lambda_A\Big) - \frac{g_{V,f}^G g_{A,f}^G}{z}(\Lambda_V - \Lambda_A) \\
&\quad \pm (g_{V,f}^G)^2\Gamma_V(m_b - m_a) \mp (g_{A,f}^G)^2\Gamma_A(m_b + m_a) \\
&\quad + g_{V,f}^G g_{A,f}^G\Big(\Gamma_A(m_b - m_a) - \Gamma_V(m_b + m_a)\Big)\Big\}z\Phi_0\frac{\boldsymbol{q}\cdot\boldsymbol{\Phi}}{|\boldsymbol{q}|}
\end{aligned} \tag{138}$$

$$I^{(0,\pm)}(z, \boldsymbol{q}, z\boldsymbol{k}) = \Big(I^{(\pm,0)}(z, \boldsymbol{q}, z\boldsymbol{k})\Big)^* = I^{(\pm,0)}(z, \boldsymbol{q}, z\boldsymbol{k}). \tag{139}$$

The above expressions can be used to estimate the different elements of polarization density matrix, $\rho^{\lambda\lambda'}$. Moreover, these quantities allow us to derive the angular coefficients defined in eq. (117). In particular, ρ_T and $\rho_{\Delta\Delta}$, which are the parity conserving transverse structure functions, will be proportional to

$$I_T(z, \boldsymbol{q}, z\boldsymbol{k}) = |C_f^G|^2\Big\{\Big((g_{V,f}^G)^2 + (g_{A,f}^G)^2\Big)\frac{1 + (1-z)^2}{z}\boldsymbol{\Phi}^2 + \Big((g_{V,f}^G)^2\Gamma_V^2 + (g_{A,f}^G)^2\Gamma_A^2\Big)z\Phi_0^2\Big\} \tag{140}$$

and

$$I_{\Delta\Delta}(z, \boldsymbol{q}, z\boldsymbol{k}) = |C_f^G|^2 \left((g_{V,f}^G)^2 + (g_{A,f}^G)^2\right) 2 \frac{1-z}{z} \left\{ \boldsymbol{\Phi}^2 - 2\left(\frac{\boldsymbol{q}\cdot\boldsymbol{\Phi}}{|\boldsymbol{q}|}\right)^2 \right\}, \qquad (141)$$

respectively. There is only one nonvanishing parity odd transverse combination, namely

$$\rho_{T_p} \propto I_{T_p}(z, \boldsymbol{q}, z\boldsymbol{k}) = |C_f^G|^2 \, 2g_{V,f}^G g_{A,f}^G \left\{ (2-z)\boldsymbol{\Phi}^2 + z\Phi_0^2 \right\}, \qquad (142)$$

while $\rho_{\Delta\Delta_p} = 0$ since $I_{\Delta\Delta_p} = 0$. For the longitudinal polarizations we have

$$\rho_L \propto I_L(z, \boldsymbol{q}, z\boldsymbol{k}) = I^{(0,0)}(z, \boldsymbol{q}, z\boldsymbol{k}). \qquad (143)$$

As far as the longitudinal-transverse interference structure functions are concerned, the identities of eq. (139) immediately yield the vanishing of

$$\rho_{\nabla} = \rho_{\Delta_p} = 0 \text{ since } I_{\nabla} = I_{\Delta_p} = 0. \qquad (144)$$

In addition, we obtain one nonvanishing parity even LT-interference structure function ρ_{Δ}, with the kernel

$$\begin{aligned} I_{\Delta}(z, \boldsymbol{q}, z\boldsymbol{k}) &= \frac{|C_f^G|^2}{M} \Big\{ \frac{2-z}{z} \left((g_{A,f}^G)^2 \Lambda_A - (g_{V,f}^G)^2 \Lambda_V \right) \\ &\quad + z\left((g_{V,f}^G)^2 \Gamma_V (m_b - m_a) - (g_{A,f}^G)^2 \Gamma_A (m_b + m_a) \right) \Big\} \Phi_0 \frac{\boldsymbol{q}\cdot\boldsymbol{\Phi}}{|\boldsymbol{q}|}, \quad (145) \end{aligned}$$

and a parity odd ρ_{∇_p} proportional to

$$I_{\nabla_p}(z, \boldsymbol{q}, z\boldsymbol{k}) = \frac{|C_f^G|^2}{M} \, g_{V,f}^G g_{A,f}^G \left\{ \Lambda_V - \Lambda_A + z\left((m_b - m_a)\Gamma_A - (m_b + m_a)\Gamma_V \right) \right\} \Phi_0 \frac{\boldsymbol{q}\cdot\boldsymbol{\Phi}}{|\boldsymbol{q}|}. \tag{146}$$

For the case of virtual photons, our results are in agreement with the results of (Schäfer; Szczurek, 2016). Notice that for massless quarks $\Gamma_{V,A} \to 0$, and the parity–conserving structure functions of electroweak gauge bosons become proportional to the ones for virtual photons. For finite quark masses, this is evidently not the case, due to the non-conservation of the axial current. Substantial simplifications occur in the limit of massless quarks, which is relevant for the practical applications. For example it is instructive to analyze in the massless quark limit the integration kernel relevant for the Lam–Tung relation which reads

$$\begin{aligned} I_{\text{Lam-Tung}}(z, \boldsymbol{q}, z\boldsymbol{k}) &= I_L(z, \boldsymbol{q}, z\boldsymbol{k}) - 2I_{\Delta\Delta}(z, \boldsymbol{q}, z\boldsymbol{k}) \\ &= |C_f^G|^2 \left((g_{V,f}^G)^2 + (g_{A,f}^G)^2 \right) \frac{4(1-z)}{z} \end{aligned}$$

$$\times \quad \left\{ (1-z)M^2\Phi_0^2 - \mathbf{\Phi}^2 + 2\frac{(\mathbf{q}\cdot\mathbf{\Phi})^2}{\mathbf{q}^2} \right\}. \tag{147}$$

Expanding in the limit of $\mathbf{k}^2 \ll \mathbf{q}^2 + \epsilon^2 \equiv \mu^2$, i.e.

$$I_{\text{Lam-Tung}}(z, \mathbf{q}, z\mathbf{k}) = I_0 + \frac{1}{2}z^2\frac{\mathbf{k}^2}{\mu^2}I_2 + \dots, \tag{148}$$

one immediately finds that not only is $I_0 = 0$ (see eq. (129)), but also $I_2 = 0$. Now, we have

$$\int d^2\mathbf{k}\,\mathbf{k}^2 f(x, \mathbf{k}) \to xg(x, \mu^2), \tag{149}$$

where $g(x)$ is the collinear gluon distribution of the target, so that in the collinear limit, the Lam-Tung structure function vanishes. In our case a finite contribution violating the Lam–Tung relation comes from the large–$\mathbf{k}$ tail of the unintegrated gluon distribution, as in the approach of (Motyka; Sadzikowski; Stebel, 2017).

5.3 Results

In this section, we will present our predictions for the transverse momentum dependence of the six nonvanishing angular coefficients ρ_i, with $i = T, L, \Delta, \Delta\Delta, T_p$ and ∇_p. We will consider pp collisions at the LHC energy of $\sqrt{s} = 14$ TeV and focus on dileptons produced at forward rapidities ($2.0 \le y \le 4.0$), where the hybrid factorization assumed in our calculations is expected to be valid. The results derived in the previous section indicate that the structure functions W_i are linearly proportional to the target unintegrated gluon distribution, $f(x, \mathbf{k})$. Together with the collinear parton distributions of quarks and antiquarks, this quantity is the main input in our calculations and is determined by the QCD dynamics.

5.3.1 Input: Unintegrated gluon distribution and collinear quarks and antiquarks

At forward rapidities, the collinear distributions $q(x, \mu^2)$ and $\bar{q}(x, \mu^2)$ in eq. (120) are probed at large values of x, where the parton distribution functions obtained by the distinct groups that perform the global analysis are similar. In what follows, we use the CT14LL parameterization of the CTEQ collaboration (Dulat; Hou; Gao; Guzzi; Huston; Nadolsky; Pumplin; Schmidt; Stump; Yuan, 2016) for the collinear distributions $q(x, \mu^2)$ and $\bar{q}(x, \mu^2)$ in eq. (120). As the angular coefficients are given in terms of ratios of structure functions, the impact of next - to - leading order corrections to the PDFs on our results is expected to be small.

On the other hand, as the small - x region is probed in the proton target, we will consider three distinct models for the proton UGD: two based on a linear QCD dynamics

Figure 14 – Unintegrated gluon distribution behavior.
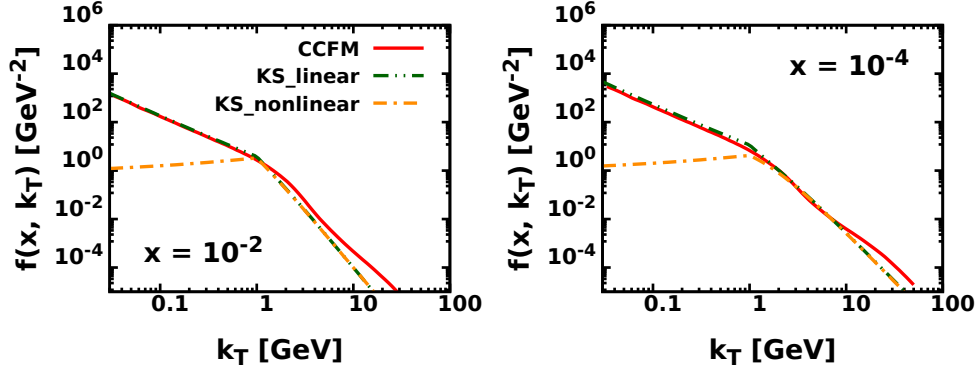
Comparison between the distinct models for the unintegrated gluon distribution considered in our analysis, derived considering two values of the Bjorken - x variable: $x = 10^{-2}$ (left panel) and $x = 10^{-4}$ (right panel).

(CCFM and KS-linear), proposed in Refs. (Hautmann; Jung, 2014; Kutak; Sapeta, 2012), and one based on a non - linear QCD dynamics (KS-nonlinear). In particular, the KS-nonlinear UGD is based on the solution of the Balitsky - Kovchegov (BK) equation, with the free parameters adjusted using the ep HERA data, while the KS-linear UGD has been obtained neglecting the non - linear term in the BK equation. As a consequence, the comparison between the predictions derived using these two models allow us to estimate how sensitive is the quantity to non - linear effects in the QCD dynamics. For completeness, we also present the predictions associated with the CCFM, which also is able to describe the HERA data at small values of Bjorken - x variable, but are based on distinct assumptions. In Fig. 14 we present a comparison between these distinct UGD's for two different values of x. One has that the UDG's differ on the predicted transverse momentum dependence. At small k_T, one has that the CCFM and KS-linear models are similar, but become distinct with the increasing of the transverse momentum. In both models, one has that $f(x, \boldsymbol{k})$ increases for $k_T \to 0$. In contrast, the KS-nonlinear model predict that $f(x, \boldsymbol{k}) \to 0$ when $k_T \to 0$. Another important aspect is that the value of k_T where the KS-nonlinear and KS-linear UGD's become identical is dependent of x, increasing for smaller values of x. Such result is expected, since the transition line between the non - linear and linear regimes of QCD dynamics is determined by the saturation scale Q_s, which is dependent of x (For a more detailed discussion see, e.g., Ref. (Golec-biernat; Wusthoff, 1998, 1999; Bandeira; Goncalves, 2023)).

5.3.2 Helicity density matrix elements

In order to present our predictions for the angular coefficients, we must to specify the choice of the coordinate system in the gauge boson rest, with respect to which the momentum of one of the two decay products is expressed in spherical coordinates.

Figure 15 – Density matrix elements plot for Z^0 decay at GJ frame.
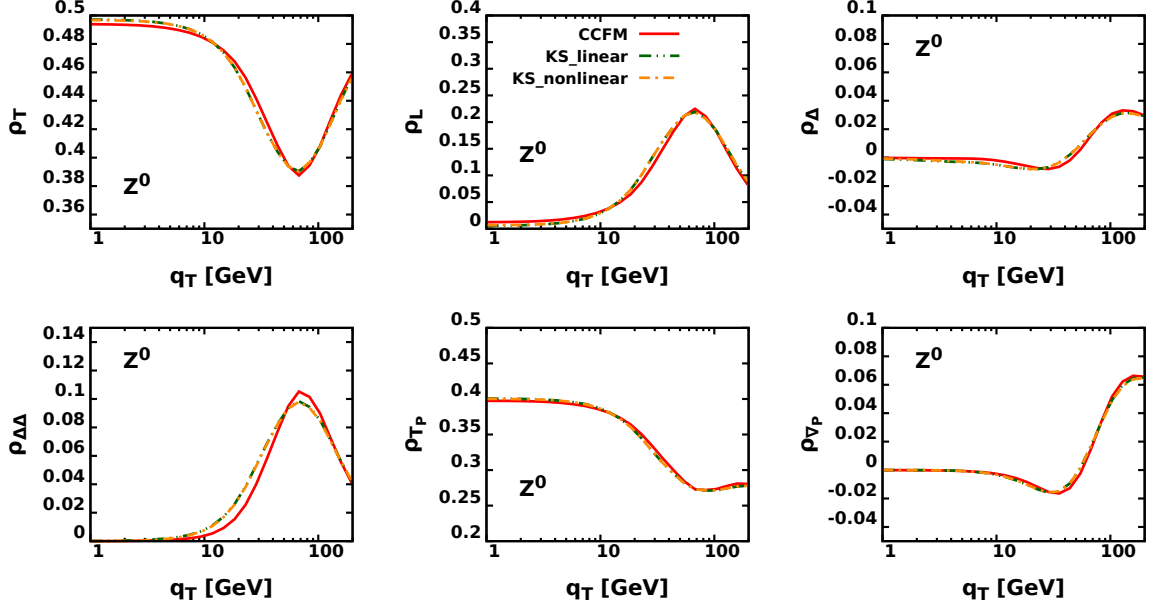
Transverse momentum dependence of the DY angular coefficients $\rho_{i=T, L, \Delta, \Delta\Delta, T_P, \nabla_P}$ for the Z^0 gauge boson decay, derived in the GJ frame and considering the dilepton production at forward rapidities $(2 \leq y \leq 4)$.

Such choice is arbitrary, which implies that distinct coordinate systems are often used in different studies in the literature (See discussion in Ref. (Faccioli; Lourenco, 2023)). Two of the more used frames are the Gottfried - Jackson (GJ) and Collins - Soper (CS) frames, which differ in the way the momenta of the colliding hadrons are used as reference directions. While in the GJ frame the polarization axis z is the direction of one of the two colliding hadrons, in the CS frame such a polarization axis has the direction of the bisector of the angle formed by the direction of the incoming hadrons in the gauge boson rest frame. In what follows, we will present our results considering the GJ frame. For completeness, in Appendix E the transformation matrix connecting the description of the structure function W_i's in the GJ and CS frames is presented.

In Figs. 15 and 16 we present our predictions for the six nonvanishing dilepton angular coefficients ρ_i's, associated with the Z^0 and W decay, respectively, derived considering the different models for the proton UGD's. As the angular coefficients are defined by the ratio between structure functions, $\rho_i = W_i/(2W_T + W_L)$, we can anticipate that these quantities will not be strongly sensitive to the modelling of $f(x, \boldsymbol{k})$. However, as the integrands are distinct for different i's, with the main contribution for the transverse momentum integrations coming from different $\boldsymbol{k}$ regions, we can expect that the magnitude and transverse momentum dependence of some of the ρ_i's will be dependent on $f(x, \boldsymbol{k})$. Such expectations are confirmed by the results presented in Figs. 15 and 16. We have that the more sensitive angular coefficients

Figure 16 – Density matrix elements plot for W^+ decay at GJ frame.
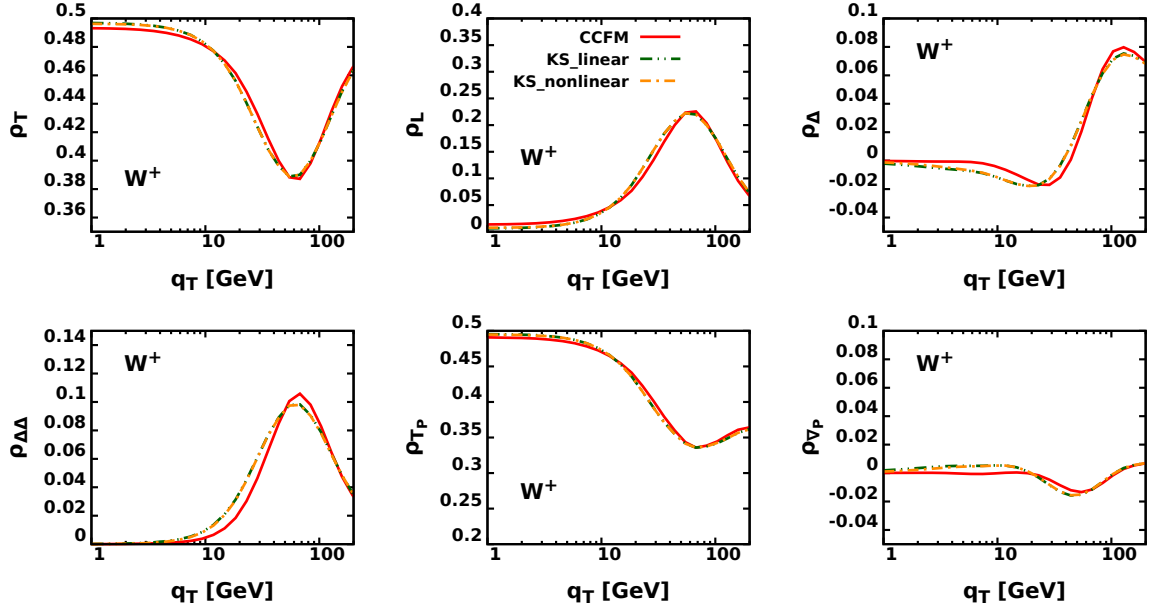
Transverse momentum dependence of the DY angular coefficients $\rho_{i=T, L, \Delta, \Delta\Delta, T_P, \nabla_P}$ for the W^+ gauge boson decay, derived in the GJ frame and considering the dilepton production at forward rapidities $(2 \leq y \leq 4)$.

to the description of $f(x, \boldsymbol{k})$ are $\rho_{\Delta\Delta}$ and ρ_Δ. In addition, our results also indicate that the angular coefficients associated with the Z^0 and W^+ decay are, in general, similar, differing mainly in the predictions for ρ_Δ, ρ_{T_P} and ρ_{∇_P}.

5.3.3 Lam-Tung relation

Finally, in Fig. 17 we present our predictions for the transverse momentum dependence of the Lam - Tung relation, defined by $A_{LT} = (2W_L - 4W_{\Delta\Delta})/(2W_T + W_L)$. As discussed in the previous section, the parton model predicts $A_{LT} = 0$. We present our predictions associated with the Z^0 (left panel) and W^+ (right panel) decays, which were estimated considering the GJ frame and the gauge boson production at forward rapidities $(2.0 \leq y \leq 4.0)$. Clearly, we predict $A_{LT} \neq 0$ in the kinematical range considered, with the the results for both gauge bosons being similar. Moreover, one has that the CCFM UGD predicts a peak at smaller values of p_T in comparison with the predictions from the other UGD's. In addition, we have that the KS-linear and KS-nonlinear predictions are almost identical, which indicates that the nonlinear effects have a small impact on the Lam-Tung relation.

Figure 17 – Transverse momentum dependence of the Lam-Tung relation.
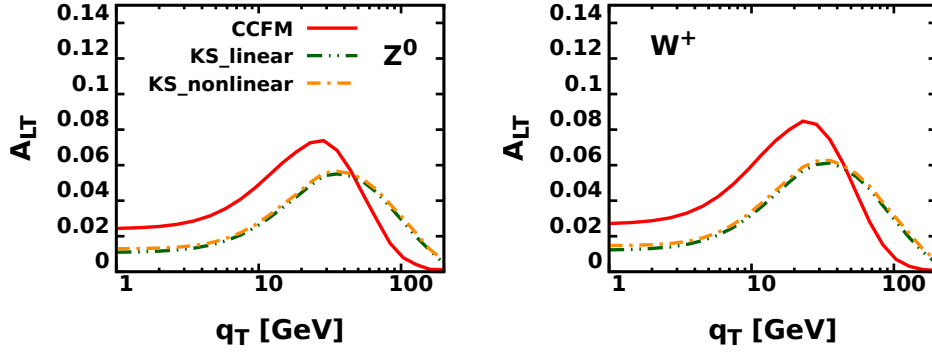
Transverse momentum dependence of the Lam-Tung relation, $A_{LT} = (2W_L - 4W_{\Delta\Delta})/(2W_T + W_L)$, considering the Z^0 (left panel) and W^+ (right panel) decays, derived in the GJ frame and considering the gauge boson production at forward rapidities ($2.0 \leq y \leq 4.0$).

5.4 Summary

In this chapter, we have seen Drell–Yan angular coefficients associated with Z and W decays at forward rapidities using the framework constructed in the previous chapters of this thesis.

Over the last years, the measurement, and the description of the Drell–Yan angular coefficients has been a subject of intense experimental and theoretical activity. Such studies were strongly motivated by the possibility to use these quantities to improve our understanding of the particle production mechanism. In this chapter, we have focused on forward rapidities, where new dynamical effects are expected to modify the description of the gauge boson production, implying the breakdown of the standard collinear factorization formalism. In particular, we have considered the color dipole S matrix framework, which was used discussed in this thesis and extended by us to the electroweak gauge boson production, and derived, for the first time, the corresponding DY angular coefficients associated with the Z and W decays. We have demonstrated that our formalism implies that the angular distribution is fully characterized by six non-vanishing angular coefficients. Moreover, we have presented results for the transverse momentum dependence of the distinct angular coefficients considering pp collisions at $\sqrt{s} = 14$ TeV and that the dileptons are produced in the rapidity range $2 \leq y \leq 4$. Three distinct models for the proton UGD have been considered, which has allowed to estimate the sensitivity of the coefficients on the description of the QCD dynamics. Our results indicate that the predictions associated with the Z and W decays are similar and that the impact of the nonlinear QCD effects is small.

A final comment is in order. In this chapter, we have established the formalism needed to estimate the DY angular coefficients using the color–dipole S–matrix frame-

work. Although we have presented predictions for the transverse momentum dependence of these coefficients, a comparison with the data was not performed since the experimental cuts assumed by the LHC collaborations were not considered. Moreover, the magnitude of the next–to–leading order corrections for our predictions is still an open question (For recent advances on this topic see, e.g., Ref. (Taels, 2024)). Both aspects deserve more detailed analysis, which we intend to perform in forthcoming studies.

6 CONCLUSIONS

Understanding the internal structure of the proton in the high–energy regime remains one of the central challenges in Quantum Chromodynamics (QCD). As discussed in the introduction, at small values of Bjorken–x, the proton wave function becomes densely populated with gluons, leading to a nonlinear regime where saturation effects and high–density QCD dynamics become relevant. Forward rapidity processes in hadronic collisions provide a unique opportunity to probe this regime, offering complementary information to that obtained from deep inelastic scattering (DIS) experiments, such as those performed at HERA.

At high energies, QCD processes like pp collisions cannot be fully described from first principles and are typically approached using perturbative QCD combined with factorization schemes. The collinear factorization framework, commonly applied in hadronic scattering, assumes a symmetric momentum configuration and becomes inadequate at forward rapidities, where interactions occur between large x and small x partons. In this asymmetric regime, the small x component of the hadron develops a dense gluon system, making nonlinear QCD effects significant and leading to the breakdown of collinear factorization. To address this, alternative approaches such as the hybrid factorization scheme have been developed to properly account for both perturbative and non-perturbative dynamics in the forward region.

In this thesis, we addressed this challenge by performing a comprehensive study of electroweak gauge boson production at forward rapidities within the hybrid factorization framework, as formulated in the Color Dipole S–Matrix (CDSM) formalism (Nikolaev; Schafer; Zakharov; Zoller, 2003; Nikolaev; Schafer, 2005; Nikolaev; Schafer; Zakharov; Zoller, 2005a; Nikolaev; Schafer; Zakharov, 2005a; Nikolaev; Schafer; Zakharov; Zoller, 2005b; Nikolaev; Schafer; Zakharov, 2005b). This approach is particularly suited for describing asymmetric collisions between a dilute projectile — characterized by large x partons — and a dense target populated by small x gluons, capturing both perturbative and nonlinear QCD dynamics.

In Chap. 3, we extended the CDSM formalism to cover the electroweak gauge boson. As seen, the differential cross-section to describe such process depends on proton's

inner dynamics description — dipole cross-section for the impact parameter space or the unintegrated gluon distribution for the momentum space — and the Light Front Wave Function of an electroweak gauge boson radiated from a quark generalized for any electroweak gauge boson, along the chapter we have derived, for the first time, the LFWF expressions for the production of any electroweak gauge boson radiated off a quark. From this result, we were able to construct the general formulae for the inclusive electroweak gauge boson production at forward rapidities using the CDSM framework and demonstrated that it reduces to those used in the literature to estimate the real photon and Z^0 production in the appropriate limits and representations, in Chap. 4. Also, the cross-section for the $W^\pm$ production in the hybrid factorization formalism was derived for the first time. Furthermore, in Chap. 5 we extended our previous result to less inclusive observables, which provides additional information about the hadronic structure, such as the angular distribution of lepton pairs ($l_1\bar{l}_2$). We have demonstrated that our formalism implies that the angular distribution is fully characterized by six nonvanishing angular coefficients. Moreover, we have presented results for the transverse momentum dependence of the distinct angular coefficients considering pp collisions at $\sqrt{s} = 14$ TeV and that the dileptons are produced in the rapidity range $2 \leq y \leq 4$. Three distinct models for the proton UGD have been considered, which has allowed to estimate the sensitivity of the coefficients on the description of the QCD dynamics. Our results indicate that the predictions associated with the Z and W decays are similar and that impact of the nonlinear QCD effects is small.

Throughout this work, we derived general expressions for inclusive electroweak gauge boson production — including real photons, Z^0, and, for the first time, $W^\pm$ bosons — within this formalism. Additionally, we extended the application of the CDSM framework to the study of angular distributions in the Drell–Yan process. These results provide a robust theoretical foundation for investigating the interplay between QCD dynamics and electroweak processes in the forward region.

The developments presented in this thesis represent a step forward in the theoretical understanding of proton structure at small x and establish new tools for interpreting current and future data from hadron colliders, particularly in the kinematic regions where saturation effects are expected to manifest.

Building upon the general formalism derived, we demonstrated that, in appropriate limits, our expressions reduce to the well-established results in the literature for real photon and Z^0 production, serving as a consistency check of the framework. The derivation of the cross-section for $W^\pm$ production within the hybrid factorization represents a novel contribution, expanding the applicability of the CDSM approach to processes involving charged electroweak currents in the forward region — a gap in the literature addressed here for the first time.

Furthermore, we extended our formalism to the angular distributions of dilepton

pairs resulting from electroweak gauge boson decays, which is a less inclusive observable. In particular, we provided a systematic description of the relevant density matrix elements within the CDSM framework, including their dependence on the proton's partonic structure at small-x. This allowed us to compute angular coefficients, offering a deeper insight into the connection between QCD dynamics and the final-state angular distributions in forward processes.

Finally, we emphasize that the formalism developed in this thesis lays the groundwork for future theoretical and phenomenological studies, which are part of a series of already published papers (Bandeira; Goncalves; Schäfer, 2025, 2024) and one in preparation. These include the analysis of less inclusive observables, correlations between jets and vector bosons, and applications to proton–nucleus and nucleus–nucleus collisions. Numerical implementations of our results, along with comparisons to experimental data, are natural next steps, especially within the forward physics programs of the LHC and RHIC. These results are not only theoretically relevant but also timely, considering the growing experimental efforts focused on forward physics at the LHC and the future Forward Physics Facility (FPF) (Feng et al., 2023). The theoretical framework developed here can directly support the interpretation of forthcoming data, particularly in processes involving electroweak bosons accompanied by hadronic activity in the forward region. Moreover, we plan to apply the formalism developed here to phenomenological studies, particularly in light of available experimental data such as $W^{\pm}$ production measured by the LHCb Collaboration. Similarly, an extension of this framework to nuclear targets is envisioned, paving the way for phenomenological analyses in pA and AA collisions.

REFERENCES

AAD, G. et al. Measurement of the polarisation of W bosons produced with large transverse momentum in pp collisions at $\sqrt{s} = 7$ TeV with the ATLAS experiment. **Eur. Phys. J. C**, [S.l.], v. 72, p. 2001, 2012.

AAD, G. et al. Measurement of the angular coefficients in Z-boson events using electron and muon pairs from data taken at $\sqrt{s} = 8$ TeV with the ATLAS detector. **JHEP**, [S.l.], v. 08, p. 159, 2016.

AAIJ, R. et al. First Measurement of the Z→μ+μ- Angular Coefficients in the Forward Region of pp Collisions at s=13 TeV. **Phys. Rev. Lett.**, [S.l.], v. 129, n. 9, p. 091801, 2022.

ADLOFF, C. et al. Measurement and QCD analysis of neutral and charged current cross-sections at HERA. **Eur. Phys. J. C**, [S.l.], v. 30, p. 1–32, 2003.

ALBACETE, J. L.; ARMESTO, N.; MILHANO, J. G.; QUIROGA-ARIAS, P.; SALGADO, C. A. AAMQS: A non-linear QCD analysis of new HERA data at small-x including heavy quarks. **Eur. Phys. J. C**, [S.l.], v. 71, p. 1705, 2011.

ALBACETE, J. L.; ARMESTO, N.; MILHANO, J. G.; SALGADO, C. A. Non-linear QCD meets data: A Global analysis of lepton-proton scattering with running coupling BK evolution. **Phys. Rev. D**, [S.l.], v. 80, p. 034031, 2009.

ALBACETE, J. L.; MARQUET, C. Azimuthal correlations of forward di-hadrons in d+Au collisions at RHIC in the Color Glass Condensate. **Phys. Rev. Lett.**, [S.l.], v. 105, p. 162301, 2010.

ALTARELLI, G.; PARISI, G. Asymptotic Freedom in Parton Language. **Nucl. Phys. B**, [S.l.], v. 126, p. 298–318, 1977.

BAIER, R.; MUELLER, A. H.; SCHIFF, D. Saturation and shadowing in high-energy proton nucleus dilepton production. **Nucl. Phys. A**, [S.l.], v. 741, p. 358–380, 2004.

BALITSKY, I. Operator expansion for high-energy scattering. **Nucl. Phys. B**, [S.l.], v. 463, p. 99–160, 1996.

BALITSKY, I. Factorization for high-energy scattering. **Phys. Rev. Lett.**, [S.l.], v. 81, p. 2024–2027, 1998.

BALITSKY, I. Factorization and high-energy effective action. **Phys. Rev. D**, [S.l.], v. 60, p. 014020, 1999.

BALITSKY, I. Effective field theory for the small x evolution. **Phys. Lett. B**, [S.l.], v. 518, p. 235–242, 2001.

BALITSKY, I. I.; BELITSKY, A. V. Nonlinear evolution in high density QCD. **Nucl. Phys. B**, [S.l.], v. 629, p. 290–322, 2002.

BANDEIRA, Y. B. **Descrição da dinâmica das interações fortes a altas energias além da ordem dominante no regime de saturação**. 2021. Pelotas: [s.n.], 2021. Available in: Dissertacao_YAN.pdf.

BANDEIRA, Y. B.; GONCALVES, V. P. Higher twists effects in DIS on nuclei at the EIC and LHeC: a phenomenological analysis. **Eur. Phys. J. A**, [S.l.], v. 59, n. 2, p. 19, 2023.

BANDEIRA, Y. B.; GONCALVES, V. P.; SCHÄFER, W. Production of electroweak gauge bosons at forward rapidities in the color-dipole S-matrix framework. **JHEP**, [S.l.], v. 07, p. 171, 2024.

BANDEIRA, Y. B.; GONCALVES, V. P.; SCHÄFER, W. Associated jet+electroweak gauge boson production in hadronic collisions at forward rapidities in the color-dipole S-matrix framework. **Phys. Rev. D**, [S.l.], v. 111, n. 7, p. 074041, 2025.

BANDEIRA, Y. B.; GONCALVES, V. P.; SCHÄFER, W. Dilepton angular distributions in the color-dipole S-matrix framework. , [S.l.], 7 2025.

BASSO, E.; GONCALVES, V. P.; KRELINA, M.; NEMCHIK, J.; PASECHNIK, R. Nuclear effects in Drell-Yan pair production in high-energy pA collisions. **Phys. Rev. D**, [S.l.], v. 93, n. 9, p. 094027, 2016.

BASSO, E.; GONCALVES, V. P.; NEMCHIK, J.; PASECHNIK, R.; SUMBERA, M. Drell-Yan phenomenology in the color dipole picture revisited. **Phys. Rev. D**, [S.l.], v. 93, n. 3, p. 034023, 2016.

BETEMPS, M. A.; DUCATI, M. B. G.; MACHADO, M. V. T.; RAUFEISEN, J. Investigating the Drell-Yan transverse momentum distribution in the color dipole approach. **Phys. Rev. D**, [S.l.], v. 67, p. 114008, 2003.

BETEMPS, M. A.; GAY DUCATI, M. B. Dilepton low p(T) suppression as an evidence of the Color Glass Condensate. **Phys. Rev. D**, [S.l.], v. 70, p. 116005, 2004.

BETHKE, S. The 2009 World Average of alpha(s). **Eur. Phys. J. C**, [S.l.], v. 64, p. 689–703, 2009.

BOER, D.; VOGELSANG, W. Drell-Yan lepton angular distribution at small transverse momentum. **Phys. Rev. D**, [S.l.], v. 74, p. 014004, 2006.

BRANDENBURG, A.; BRODSKY, S. J.; KHOZE, V. V.; MUELLER, D. Angular distributions in the Drell-Yan process: A Closer look at higher twist effects. **Phys. Rev. Lett.**, [S.l.], v. 73, p. 939–942, 1994.

BRODSKY, S. J.; HEBECKER, A.; QUACK, E. The Drell-Yan process and factorization in impact parameter space. **Phys. Rev. D**, [S.l.], v. 55, p. 2584–2590, 1997.

BRODSKY, S. J.; PAULI, H.-C.; PINSKY, S. S. Quantum chromodynamics and other field theories on the light cone. **Phys. Rept.**, [S.l.], v. 301, p. 299–486, 1998.

CELIBERTO, F. G.; GORDO GÓMEZ, D.; SABIO VERA, A. Forward Drell–Yan production at the LHC in the BFKL formalism with collinear corrections. **Phys. Lett. B**, [S.l.], v. 786, p. 201–206, 2018.

CHEKANOV, S. et al. A ZEUS next-to-leading-order QCD analysis of data on deep inelastic scattering. **Phys. Rev. D**, [S.l.], v. 67, p. 012007, 2003.

COLLINS, J. **Foundations of Perturbative QCD**. [S.l.]: Cambridge University Press, 2023. (Cambridge Monographs on Particle Physics, Nuclear Physics and Cosmology).

D'ENTERRIA, D. et al. The strong coupling constant: state of the art and the decade ahead. **J. Phys. G**, [S.l.], v. 51, n. 9, p. 090501, 2024.

DOKSHITZER, Y. L. Calculation of the Structure Functions for Deep Inelastic Scattering and e+ e- Annihilation by Perturbation Theory in Quantum Chromodynamics. **Sov. Phys. JETP**, [S.l.], v. 46, p. 641–653, 1977.

DOMINGUEZ, F.; MARQUET, C.; STASTO, A. M.; XIAO, B.-W. Universality of multiparticle production in QCD at high energies. **Phys. Rev. D**, [S.l.], v. 87, p. 034007, 2013.

DOMINGUEZ, F.; MARQUET, C.; XIAO, B.-W.; YUAN, F. Universality of Unintegrated Gluon Distributions at small x. **Phys. Rev. D**, [S.l.], v. 83, p. 105005, 2011.

DUCATI, M. B. G.; GRIEP, M. T.; MACHADO, M. V. T. Study on the low mass Drell-Yan production at the CERN LHC within the dipole formalism. **Phys. Rev. D**, [S.l.], v. 89, n. 3, p. 034022, 2014.

DUCLOUÉ, B. Nuclear modification of forward Drell-Yan production at the LHC. **Phys. Rev. D**, [S.l.], v. 96, n. 9, p. 094014, 2017.

DUCLOUÉ, B.; LAPPI, T.; MÄNTYSAARI, H. Isolated photon production in proton-nucleus collisions at forward rapidity. **Phys. Rev. D**, [S.l.], v. 97, n. 5, p. 054023, 2018.

DULAT, S.; HOU, T.-J.; GAO, J.; GUZZI, M.; HUSTON, J.; NADOLSKY, P.; PUMPLIN, J.; SCHMIDT, C.; STUMP, D.; YUAN, C. P. New parton distribution functions from a global analysis of quantum chromodynamics. **Phys. Rev. D**, [S.l.], v. 93, n. 3, p. 033006, 2016.

ESKOLA, K. J.; HOYER, P.; VANTTINEN, M.; VOGT, R. Higher twist effects in the Drell-Yan angular distribution. **Phys. Lett. B**, [S.l.], v. 333, p. 526–530, 1994.

FACCIOLI, P.; LOURENCO, C. **Particle Polarization in High Energy Physics**: An Introduction and Case Studies on Vector Particle Production at the LHC. [S.l.]: Springer International Publishing, 2023.

FACCIOLI, P.; LOURENCO, C.; SEIXAS, J. Rotation-invariant relations in vector meson decays into fermion pairs. **Phys. Rev. Lett.**, [S.l.], v. 105, p. 061601, 2010.

FACCIOLI, P.; LOURENCO, C.; SEIXAS, J.; WOHRI, H. K. Rotation-invariant observables in parity-violating decays of vector particles to fermion pairs. **Phys. Rev. D**, [S.l.], v. 82, p. 096002, 2010.

FACCIOLI, P.; LOURENCO, C.; SEIXAS, J.; WOHRI, H. K. Model-independent constraints on the shape parameters of dilepton angular distributions. **Phys. Rev. D**, [S.l.], v. 83, p. 056008, 2011.

FENG, J. L. et al. The Forward Physics Facility at the High-Luminosity LHC. **J. Phys. G**, [S.l.], v. 50, n. 3, p. 030501, 2023.

FUJII, H.; GELIS, F.; VENUGOPALAN, R. Quantitative study of the violation of k-perpendicular-factorization in hadroproduction of quarks at collider energies. **Phys. Rev. Lett.**, [S.l.], v. 95, p. 162002, 2005.

GAULD, R.; GEHRMANN-DE RIDDER, A.; GEHRMANN, T.; GLOVER, E. W. N.; HUSS, A. Precise predictions for the angular coefficients in Z-boson production at the LHC. **JHEP**, [S.l.], v. 11, p. 003, 2017.

GELIS, F.; IANCU, E.; JALILIAN-MARIAN, J.; VENUGOPALAN, R. The Color Glass Condensate. **Ann. Rev. Nucl. Part. Sci.**, [S.l.], v. 60, p. 463–489, 2010.

GELIS, F.; JALILIAN-MARIAN, J. Photon production in high-energy proton nucleus collisions. **Phys. Rev. D**, [S.l.], v. 66, p. 014021, 2002.

GELIS, F.; JALILIAN-MARIAN, J. Dilepton production from the color glass condensate. **Phys. Rev. D**, [S.l.], v. 66, p. 094014, 2002.

GELIS, F.; JALILIAN-MARIAN, J. Drell-Yan production and Lam-Tung relation in the color glass condensate formalism. **Phys. Rev. D**, [S.l.], v. 76, p. 074015, 2007.

GOLEC-BIERNAT, K. J.; WUSTHOFF, M. Saturation effects in deep inelastic scattering at low Q**2 and its implications on diffraction. **Phys. Rev. D**, [S.l.], v. 59, p. 014017, 1998.

GOLEC-BIERNAT, K. J.; WUSTHOFF, M. Saturation in diffractive deep inelastic scattering. **Phys. Rev. D**, [S.l.], v. 60, p. 114023, 1999.

GOLEC-BIERNAT, K.; LEWANDOWSKA, E.; STASTO, A. M. Drell-Yan process at forward rapidity at the LHC. **Phys. Rev. D**, [S.l.], v. 82, p. 094010, 2010.

GONCALVES, V. P.; LIMA, Y.; PASECHNIK, R.; ŠUMBERA, M. Isolated photon production and pion-photon correlations in high-energy pp and pA collisions. **Phys. Rev. D**, [S.l.], v. 101, n. 9, p. 094019, 2020.

GREINER, W.; REINHARDT, J. **Quantum electrodynamics**. Heidelberg, GER: Springer Berlin, 2008.

GRIBOV, V. N.; LIPATOV, L. N. Deep inelastic electron scattering in perturbation theory. **Phys. Lett. B**, [S.l.], v. 37, p. 78–80, 1971.

GRIFFITHS, D. **Introduction to elementary particles**. Berlin, GER: Wiley-VCH, 2008.

HAUTMANN, F.; JUNG, H. Transverse momentum dependent gluon density from DIS precision data. **Nucl. Phys. B**, [S.l.], v. 883, p. 1–19, 2014.

IANCU, E.; ITAKURA, K.; MUNIER, S. Saturation and BFKL dynamics in the HERA data at small x. **Phys. Lett. B**, [S.l.], v. 590, p. 199–208, 2004.

JALILIAN-MARIAN, J.; KOVCHEGOV, Y. V. Saturation physics and deuteron-Gold collisions at RHIC. **Prog. Part. Nucl. Phys.**, [S.l.], v. 56, p. 104–231, 2006.

JALILIAN-MARIAN, J.; REZAEIAN, A. H. Prompt photon production and photon-hadron correlations at RHIC and the LHC from the Color Glass Condensate. **Phys. Rev. D**, [S.l.], v. 86, p. 034016, 2012.

KANG, Z.-B.; XIAO, B.-W. Sivers asymmetry of Drell-Yan production in small-x regime. **Phys. Rev. D**, [S.l.], v. 87, n. 3, p. 034038, 2013.

KHACHATRYAN, V. et al. Angular coefficients of Z bosons produced in pp collisions at $\sqrt{s}$ = 8 TeV and decaying to $\mu^+\mu^-$ as a function of transverse momentum and rapidity. **Phys. Lett. B**, [S.l.], v. 750, p. 154–175, 2015.

KOGUT, J. B.; SOPER, D. E. Quantum Electrodynamics in the Infinite Momentum Frame. **Phys. Rev. D**, [S.l.], v. 1, p. 2901–2913, 1970.

KOPELIOVICH, B. Z.; LEVIN, E.; REZAEIAN, A. H.; SCHMIDT, I. Direct photons at forward rapidities in high-energy pp collisions. **Phys. Lett. B**, [S.l.], v. 675, p. 190–195, 2009.

KOPELIOVICH, B. Z.; RAUFEISEN, J.; TARASOV, A. V. The Color dipole picture of the Drell-Yan process. **Phys. Lett. B**, [S.l.], v. 503, p. 91–98, 2001.

KOPELIOVICH, B. Z.; RAUFEISEN, J.; TARASOV, A. V.; JOHNSON, M. B. Nuclear effects in the Drell-Yan process at very high-energies. **Phys. Rev. C**, [S.l.], v. 67, p. 014903, 2003.

KOPELIOVICH, B. Z.; REZAEIAN, A. H.; PIRNER, H. J.; SCHMIDT, I. Direct photons and dileptons via color dipoles. **Phys. Lett. B**, [S.l.], v. 653, p. 210–215, 2007.

KÖRNER, J. G.; MIRKES, E. Polarization density matrix of high q(T) gauge bosons in high-energy proton - anti-proton collisions. **Nucl. Phys. B Proc. Suppl.**, [S.l.], v. 23, p. 9–13, 1991.

KOTKO, P.; KUTAK, K.; MARQUET, C.; PETRESKA, E.; SAPETA, S.; HAMEREN, A. van. Improved TMD factorization for forward dijet production in dilute-dense hadronic collisions. **JHEP**, [S.l.], v. 09, p. 106, 2015.

KOVCHEGOV, Y. V. Small x F(2) structure function of a nucleus including multiple pomeron exchanges. **Phys. Rev. D**, [S.l.], v. 60, p. 034008, 1999.

KOVCHEGOV, Y. V. Unitarization of the BFKL pomeron on a nucleus. **Phys. Rev. D**, [S.l.], v. 61, p. 074018, 2000.

KOVCHEGOV, Y. V.; LEVIN, E. **Quantum Chromodynamics at High Energy**. [S.l.]: Oxford University Press, 2013. v. 33.

KOWALSKI, H.; MOTYKA, L.; WATT, G. Exclusive diffractive processes at HERA within the dipole picture. **Phys. Rev. D**, [S.l.], v. 74, p. 074016, 2006.

KOWALSKI, H.; TEANEY, D. An Impact parameter dipole saturation model. **Phys. Rev. D**, [S.l.], v. 68, p. 114005, 2003.

KUTAK, K.; SAPETA, S. Gluon saturation in dijet production in p-Pb collisions at Large Hadron Collider. **Phys. Rev. D**, [S.l.], v. 86, p. 094043, 2012.

LAM, C. S.; TUNG, W.-K. A Systematic Approach to Inclusive Lepton Pair Production in Hadronic Collisions. **Phys. Rev. D**, [S.l.], v. 18, p. 2447, 1978.

LEPAGE, G. P.; BRODSKY, S. J. Exclusive Processes in Perturbative Quantum Chromodynamics. **Phys. Rev. D**, [S.l.], v. 22, p. 2157, 1980.

LIMA, Y. N.; GIANNINI, A. V.; GONCALVES, V. P. Isolated photon production in pp collisions at forward rapidities and high multiplicity events. **Eur. Phys. J. A**, [S.l.], v. 60, n. 3, p. 54, 2024.

LYUBOVITSKIJ, V. E.; VOGELSANG, W.; WUNDER, F.; ZHEVLAKOV, A. S. Perturbative T-odd asymmetries in the Drell-Yan process revisited. **Phys. Rev. D**, [S.l.], v. 109, n. 11, p. 114023, 2024.

LYUBOVITSKIJ, V. E.; ZHEVLAKOV, A. S.; ANIKIN, I. A. Transverse momentum dependence of the T-even hadronic structure functions in the Drell-Yan process. **Phys. Rev. D**, [S.l.], v. 110, n. 7, p. 074028, 2024.

MARQUET, C. Forward inclusive dijet production and azimuthal correlations in p(A) collisions. **Nucl. Phys. A**, [S.l.], v. 796, p. 41–60, 2007.

MARQUET, C.; WEI, S.-Y.; XIAO, B.-W. Probing parton saturation with forward Z^0-boson production at small transverse momentum in p+p and p+A collisions. **Phys. Lett. B**, [S.l.], v. 802, p. 135253, 2020.

MIRKES, E. Angular decay distribution of leptons from W bosons at NLO in hadronic collisions. **Nucl. Phys. B**, [S.l.], v. 387, p. 3–85, 1992.

MIRKES, E.; OHNEMUS, J. W and Z polarization effects in hadronic collisions. **Phys. Rev. D**, [S.l.], v. 50, p. 5692–5703, 1994.

MORREALE, A.; SALAZAR, F. Mining for Gluon Saturation at Colliders. **Universe**, [S.l.], v. 7, n. 8, p. 312, 2021.

MOTYKA, L.; SADZIKOWSKI, M.; STEBEL, T. Lam-Tung relation breaking in Z^0 hadroproduction as a probe of parton transverse momentum. **Phys. Rev. D**, [S.l.], v. 95, n. 11, p. 114025, 2017.

MUTA, T. **Foundations of Quantum Chromodynamics**. [S.l.]: World Scientific, 2010.

NEFEDOV, M. A.; NIKOLAEV, N. N.; SALEEV, V. A. Drell-Yan lepton pair production at high energies in the Parton Reggeization Approach. **Phys. Rev. D**, [S.l.], v. 87, n. 1, p. 014022, 2013.

NEWMAN, P. Deep inelastic lepton nucleon scattering at HERA. **Int. J. Mod. Phys. A**, [S.l.], v. 19, p. 1061–1073, 2004.

NIKOLAEV, N. N.; PILLER, G.; ZAKHAROV, B. G. Quantum coherence in heavy flavor production on nuclei. **J. Exp. Theor. Phys.**, [S.l.], v. 81, p. 851–859, 1995.

NIKOLAEV, N. N.; PILLER, G.; ZAKHAROV, B. G. Inclusive heavy flavor production from nuclei. **Z. Phys. A**, [S.l.], v. 354, p. 99–105, 1996.

NIKOLAEV, N. N.; SCHAFER, W. Breaking of k perpendicular-factorization for single jet production off nuclei. **Phys. Rev. D**, [S.l.], v. 71, p. 014023, 2005.

NIKOLAEV, N. N.; SCHAFER, W.; ZAKHAROV, B. G. Nonlinear k(perpendicular)-factorization for gluon-gluon dijets produced off nuclear targets. **Phys. Rev. D**, [S.l.], v. 72, p. 114018, 2005.

NIKOLAEV, N. N.; SCHAFER, W.; ZAKHAROV, B. G. Nonuniversality aspects of nonlinear k-perpendicular-factorization for hard dijets. **Phys. Rev. Lett.**, [S.l.], v. 95, p. 221803, 2005.

NIKOLAEV, N. N.; SCHAFER, W.; ZAKHAROV, B. G.; ZOLLER, V. R. Nonlinear k-perpendicular factorization for forward dijets in DIS off nuclei in the saturation regime. **J. Exp. Theor. Phys.**, [S.l.], v. 97, p. 441–465, 2003.

NIKOLAEV, N. N.; SCHAFER, W.; ZAKHAROV, B. G.; ZOLLER, V. R. Nonlinear k-perpendicular-factorization for quark-gluon dijet production off nuclei. **Phys. Rev. D**, [S.l.], v. 72, p. 034033, 2005.

NIKOLAEV, N. N.; SCHAFER, W.; ZAKHAROV, B. G.; ZOLLER, V. R. Nonlinear K(T) factorization: A new paradigm for hard QCD processes in a nuclear environment. **JETP Lett.**, [S.l.], v. 82, p. 325–334, 2005.

NIKOLAEV, N. N.; ZAKHAROV, B. G. Color transparency and scaling properties of nuclear shadowing in deep inelastic scattering. **Z. Phys. C**, [S.l.], v. 49, p. 607–618, 1991.

PENG, J.-C.; CHANG, W.-C.; MCCLELLAN, R. E.; TERYAEV, O. Interpretation of Angular Distributions of Z-boson Production at Colliders. **Phys. Lett. B**, [S.l.], v. 758, p. 384–388, 2016.

PILONETA, S.; VLADIMIROV, A. Angular distributions of Drell-Yan leptons in the TMD factorization approach. **JHEP**, [S.l.], v. 12, p. 059, 2024.

PUMPLIN, J.; STUMP, D. R.; HUSTON, J.; LAI, H. L.; NADOLSKY, P. M.; TUNG, W. K. New generation of parton distributions with uncertainties from global QCD analysis. **JHEP**, [S.l.], v. 07, p. 012, 2002.

RAUFEISEN, J.; PENG, J.-C.; NAYAK, G. C. Parton model versus color dipole formulation of the Drell-Yan process. **Phys. Rev. D**, [S.l.], v. 66, p. 034024, 2002.

REZAEIAN, A. H.; SIDDIKOV, M.; KLUNDERT, M. Van de; VENUGOPALAN, R. Analysis of combined HERA data in the Impact-Parameter dependent Saturation model. **Phys. Rev. D**, [S.l.], v. 87, n. 3, p. 034002, 2013.

RICHTER-WAS, E.; WAS, Z. W production at LHC: lepton angular distributions and reference frames for probing hard QCD. **Eur. Phys. J. C**, [S.l.], v. 77, n. 2, p. 111, 2017.

SANTOS, G. Sampaio dos; SILVEIRA, G. Gil da; MACHADO, M. V. T. The color dipole picture for prompt photon production in pp and pPb collisions at the CERN-LHC. **Eur. Phys. J. C**, [S.l.], v. 80, n. 9, p. 812, 2020.

SCHÄFER, W.; SZCZUREK, A. Low mass Drell-Yan production of lepton pairs at forward directions at the LHC: a hybrid approach. **Phys. Rev. D**, [S.l.], v. 93, n. 7, p. 074014, 2016.

STASTO, A.; WEI, S.-Y.; XIAO, B.-W.; YUAN, F. On the Dihadron Angular Correlations in Forward pA collisions. **Phys. Lett. B**, [S.l.], v. 784, p. 301–306, 2018.

STASTO, A.; XIAO, B.-W.; YUAN, F. Back-to-Back Correlations of Di-hadrons in dAu Collisions at RHIC. **Phys. Lett. B**, [S.l.], v. 716, p. 430–434, 2012.

STASTO, A.; XIAO, B.-W.; ZASLAVSKY, D. Drell-Yan Lepton-Pair-Jet Correlation in pA collisions. **Phys. Rev. D**, [S.l.], v. 86, p. 014009, 2012.

TAELS, P. Forward production of a Drell-Yan pair and a jet at small x at next-to-leading order. **JHEP**, [S.l.], v. 01, p. 005, 2024.

THOMSON, M. **Modern particle physics**. New York: Cambridge University Press, 2013.

TRICOLI, A.; SCHÖNHERR, M.; AZZURRI, P. Vector Bosons and Jets in Proton Collisions. **Rev. Mod. Phys.**, [S.l.], v. 93, n. 2, p. 025007, 2021.

WATT, G.; KOWALSKI, H. Impact parameter dependent colour glass condensate dipole model. **Phys. Rev. D**, [S.l.], v. 78, p. 014016, 2008.

WEIGERT, H. Evolution at small x(bj): The Color glass condensate. **Prog. Part. Nucl. Phys.**, [S.l.], v. 55, p. 461–565, 2005.

ZYLA, P. A. et al. Review of Particle Physics. **PTEP**, [S.l.], v. 2020, n. 8, p. 083C01, 2020.

Appendix

APPENDIX A – Conventions

This appendix outlines the general conventions adopted throughout this thesis. In particular, we provide a compact comparison between the *instant form* and the *light–front form* of relativistic dynamics, as shown in Fig. 18, which highlights the key differences in their respective variable definitions and symmetry properties.

Given the central role of light-front quantization in the framework adopted in this work — especially in describing high–energy scattering processes and light-cone wave functions— we present the conventions used in both the instant and light–front forms. The light–front formalism offers significant advantages in the study of relativistic systems, including a more intuitive treatment of parton dynamics and boost invariance along the longitudinal direction.

For a comprehensive review of the light–front approach and its applications in quantum field theory and high-energy physics, we refer the reader to Refs. (Brodsky; Hebecker; Quack, 1997; Kovchegov; Levin, 2013). For an introductory discussion in Brazilian Portuguese, see Ref. (Bandeira, 2021).

A.1 Instant form

A.1.1 Lorentz vectors

We write contravariant position four–vectors, x^μ in the instant form as

$$x^\mu = \left(x^0, x^1, x^2, x^3\right) = \left(x^0, \vec{x}_\perp, x^3\right) = \left(x^0, \vec{x}\right). \tag{150}$$

Moreover, the covariant four-vector, x_μ is given by

$$x_\mu = (x_0, x_1, x_2, x_3) = (t, -x, -y, -z) = g_{\mu\nu}x^\nu \tag{151}$$

Figure 18 – Dirac's two dynamical forms

The instant form

$$\widetilde{x}^0 = ct$$
$$\widetilde{x}^1 = x$$
$$\widetilde{x}^2 = y$$
$$\widetilde{x}^3 = z$$

$$\widetilde{g}_{\mu\nu} = \begin{pmatrix} 1 & 0 & 0 & 0 \\ 0 & -1 & 0 & 0 \\ 0 & 0 & -1 & 0 \\ 0 & 0 & 0 & -1 \end{pmatrix}$$

The front form

$$\widetilde{x}^0 = ct + z$$
$$\widetilde{x}^1 = x$$
$$\widetilde{x}^2 = y$$
$$\widetilde{x}^3 = ct - z$$

$$\widetilde{g}_{\mu\nu} = \begin{pmatrix} 0 & 0 & 0 & \frac{1}{2} \\ 0 & -1 & 0 & 0 \\ 0 & 0 & -1 & 0 \\ \frac{1}{2} & 0 & 0 & 0 \end{pmatrix}$$
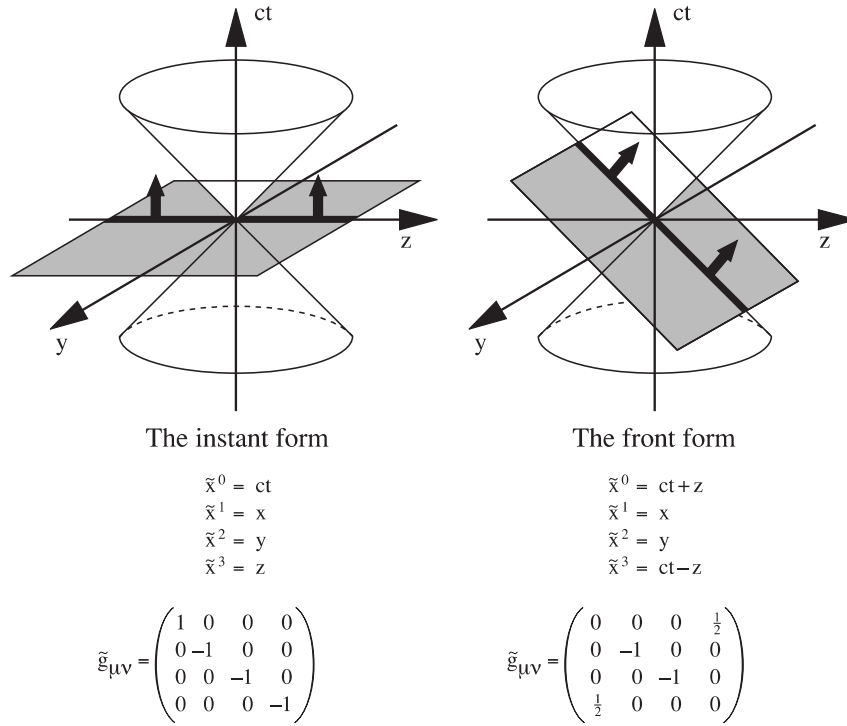
Source: adapted from (Brodsky; Pauli; Pinsky, 1998).

and obtained from the contravariant vector by the metric tensor

$$g_{\mu\nu} = \begin{pmatrix} 1 & 0 & 0 & 0 \\ 0 & -1 & 0 & 0 \\ 0 & 0 & -1 & 0 \\ 0 & 0 & 0 & -1 \end{pmatrix}. \tag{152}$$

The scalar products are

$$x \cdot p = x^\mu p_\mu = x^0 p_0 + x^1 p_1 + x^2 p_2 + x^3 p_3 = tE - \vec{x} \cdot \vec{p}, \tag{153}$$

with the four–momentum $p^\mu = (p_0, p_1, p_2, p_3) = (E, \vec{p})$. The metric tensor $g_{\mu\nu}$ raises the indices.

A.1.2 Dirac matrices

Up to unitary transformations, the 4×4 Dirac matrices γ^μ are defined by

$$\gamma^\mu \gamma^\nu + \gamma^\nu \gamma^\mu = 2g^{\mu\nu}, \tag{154}$$

where γ^0 is hermitean and γ^k anti–hermitean. Useful combinations are $\beta = \gamma^0$ and $\alpha = \gamma^0\gamma^k$, as well as

$$\sigma^{\mu\nu} = \frac{i}{2}\left(\gamma^\mu\gamma^\nu - \gamma^\nu\gamma^\mu\right), \quad \gamma_5 = i\gamma^0\gamma^1\gamma^2\gamma^3. \tag{155}$$

The γ's matrices are usually expressed in terms of the 2×2 Pauli matrices

$$I = \begin{pmatrix} 1 & 0 \\ 0 & 1 \end{pmatrix}, \quad \sigma^1 = \begin{pmatrix} 0 & 1 \\ 1 & 0 \end{pmatrix}, \quad \sigma^2 = \begin{pmatrix} 0 & -i \\ i & 0 \end{pmatrix}, \quad \sigma^3 = \begin{pmatrix} 1 & 0 \\ 0 & -1 \end{pmatrix}, \tag{156}$$

moreover, there are different representations for those σ's matrices which forms the Dirac matrices. In what follows, we'll see the Dirac and chiral representations.

Dirac representation: In this representation, the matrices are (Brodsky; Pauli; Pinsky, 1998)

$$
\begin{aligned}
\gamma^0 &= \begin{pmatrix} I & 0 \\ 0 & -I \end{pmatrix}, \gamma^k = \begin{pmatrix} 0 & \sigma^k \\ -\sigma^k & 0 \end{pmatrix}, \\
\gamma_5 &= \begin{pmatrix} 0 & I \\ I & 0 \end{pmatrix}, \alpha^k = \begin{pmatrix} 0 & \sigma^k \\ \sigma^k & 0 \end{pmatrix}, \sigma^{ij} = \begin{pmatrix} \sigma^k & 0 \\ 0 & \sigma^k \end{pmatrix}.
\end{aligned}
\tag{157}
$$

Chiral representation: In this representation the matrices are (Brodsky; Pauli; Pinsky, 1998)

$$
\begin{aligned}
\gamma^0 &= \begin{pmatrix} 0 & I \\ I & 0 \end{pmatrix}, \gamma^k = \begin{pmatrix} 0 & \sigma^k \\ -\sigma^k & 0 \end{pmatrix}, \\
\gamma_5 &= \begin{pmatrix} I & 0 \\ 0 & -I \end{pmatrix}, \alpha^k = \begin{pmatrix} \sigma^k & 0 \\ 0 & -\sigma^k \end{pmatrix}, \sigma^{ij} = \begin{pmatrix} \sigma^k & 0 \\ 0 & \sigma^k \end{pmatrix}.
\end{aligned}
\tag{158}
$$

A.2   Dirac spinors

The spinors $u(p,\lambda)$ and $v(p,\lambda)$ are solutions of the Dirac equation

$$(\not{p} - m)\gamma^\mu u(p,\lambda) = 0, \quad -(\not{p} + m)\gamma^\mu v(p,\lambda) = 0, \tag{159}$$

where $\not a = a_\mu \gamma^\mu$. They are orthonormal and complete:

$$\overline{u}(p,\lambda)u(p,\lambda') = -\overline{v}(p,\lambda)v(p,\lambda') = 2m\delta_{\lambda\Lambda'} \,, \tag{160}$$

$$\sum_\lambda u(p,\lambda)\overline{u}(p,\lambda) = \not p + m \,, \quad \sum_\lambda v(p,\lambda)\overline{v}(p,\lambda) = \not p - m \,. \tag{161}$$

Some useful relations are the Gordon decomposition of the currents:

$$\overline{u}(p,\lambda)\gamma^\mu u(p,\lambda') = \overline{v}(p,\lambda)\gamma^\mu v(p,\lambda') = \frac{1}{2m}\overline{u}(p,\lambda)\left((p+q)^\mu + i\sigma^{\mu\nu}(p-q)_\nu\right)u(q,\lambda') \,, \tag{162}$$

and

$$\gamma^\mu \not a \gamma_\mu = -2a \,, \tag{163}$$

$$\gamma^\mu \not a \not b \gamma_\mu = 4ab \,, \tag{164}$$

$$\gamma^\mu \not a \not b \not c \gamma_\mu = \not c \not b \not a \,, \tag{165}$$

with $\lambda = \pm 1$, the spin projection is $s = \lambda/2$.

A.3 Polarization vectors

The two polarization 4–vectors $\epsilon_\mu(p,\lambda)$ are labeled by the spin projectors $\lambda = \pm 1$. Moreover, as solutions of the free Maxwell equations they are orthonormal and complete, i.e.,

$$\epsilon^\mu(p,\lambda)\epsilon^*(p,\lambda') = -\delta_{\lambda\Lambda'} \,, \quad p^\mu\epsilon_\mu(p,\lambda) = 0 \,. \tag{166}$$

The polarization sum is

$$\sum_\lambda \epsilon_\lambda(p,\lambda)\epsilon^*_\nu(p,\lambda) = -g_{\mu\nu} + \frac{\eta_\mu p_\nu + \eta_\nu p_\mu}{p^\kappa \eta_\kappa} \,, \tag{167}$$

with the null vector as $\eta^\mu \eta_\mu = 0$.

A.4 Light front form

In the light–front formalism, a redefinition of coordinates is performed by rotating the time and one spatial direction to construct a new set of light–cone coordinates. However, multiple conventions exist for carrying out this transformation from instant–form to light–front variables. These different conventions lead to distinct prescriptions for key quantities such as Dirac spinors and polarization vectors. In what follows, we present the two most widely used conventions: the Kogut–Soper (KS) convention (Kogut; Soper, 1970) and the Lepage–Brodsky (LB) convention (Lepage; Brodsky, 1980).

A.4.1 The Lepage–Brodsky convention (LB)

A.4.1.1 Lorentz vectors

In the light front approach, the contravariant 4–vectors of position x^μ are written as

$$x^\mu = (x^+, x^-, x^1, x^2) = (x^+, x^-, \boldsymbol{x})\,, \tag{168}$$

The time–like and space–like components are related to the instant form by the following transformations:

$$x^+ = x^0 + x^3 \quad \text{and} \quad x^- = x^0 - x^3, \tag{169}$$

and referred to as the '*light–cone time*' and '*light–cone position*', respectively. The covariant vectors are obtained by the contraction with the metric tensor, $x_\mu = g_{\mu\nu} x^\nu$, which is given by

$$g^{\mu\nu} = \begin{pmatrix} 0 & 2 & 0 & 0 \\ 2 & 0 & 0 & 0 \\ 0 & 0 & -1 & 0 \\ 0 & 0 & 0 & -1 \end{pmatrix} \quad \text{and} \quad g_{\mu\nu} = \begin{pmatrix} 0 & \frac{1}{2} & 0 & 0 \\ \frac{1}{2} & 0 & 0 & 0 \\ 0 & 0 & -1 & 0 \\ 0 & 0 & 0 & -1 \end{pmatrix}. \tag{170}$$

The scalar products are

$$x \cdot p = x^\mu p_\mu = x^+ p^+ + x^- p_- + x^1 p_1 x^2 p_2 = \frac{1}{2}(x^+ p^- + x^- p^+) - \boldsymbol{x} \cdot \boldsymbol{p}, \tag{171}$$

and all other 4-vectors including γ^μ are treated correspondingly.

A.4.1.2 Dirac matrices

As well as the coordinates, we can construct the $+$ and $-$ γ-matrices via

$$\gamma^+ = \gamma^0 + \gamma^3 \quad \text{and} \quad \gamma^- = \gamma^0 - \gamma^3, \tag{172}$$

where we use the Dirac representation of the γ–matrices, particularly

$$\gamma^+ \gamma^+ = \gamma^- \gamma^- = 0\,. \tag{173}$$

Other useful products are

$$\gamma^+ \gamma^- \gamma^+ = 4\gamma^+ \quad \text{and} \quad \gamma^+ \gamma^- \gamma^- = 4\gamma^-\,. \tag{174}$$

A.4.1.3 Dirac spinors

Lepage and Brodsky use a particularly simple spinor representation defined as

$$u_\lambda(q) = \frac{1}{\sqrt{q^+}} \left(q^+ I_4 + \beta m + \vec{\alpha} \cdot \vec{q} \right) \chi_\lambda \begin{cases} \chi(\uparrow) \text{ for } \lambda = +1 \\ \chi(\downarrow) \text{ for } \lambda = -1 \end{cases} \tag{175}$$

$$v_\lambda(q) = \frac{1}{\sqrt{q^+}} \left(q^+ I_4 - \beta m + \vec{\alpha} \cdot \vec{q} \right) \chi_\lambda \begin{cases} \chi(\downarrow) \text{ for } \lambda = +1 \\ \chi(\uparrow) \text{ for } \lambda = -1 \end{cases} \tag{176}$$

where

$$\chi(\uparrow) = \frac{1}{\sqrt{2}} \begin{pmatrix} 1 \\ 0 \\ 1 \\ 0 \end{pmatrix} ; \ \chi(\downarrow) = \frac{1}{\sqrt{2}} \begin{pmatrix} 0 \\ 1 \\ 0 \\ -1 \end{pmatrix} .$$

A.4.1.4 Polarization vectors

The null vector is

$$\eta^\mu = (0, 2, \mathbf{0}) , \tag{177}$$

the transversal polarization vector are $\vec{\epsilon}(+1) = -1/\sqrt{2}(1, i)$ and $\vec{\epsilon}(-1) = 1/\sqrt{2}(1, -i)$, which collectively is

$$\vec{\epsilon}(\pm 1) = \frac{-1}{\sqrt{2}}(\pm 1\hat{x} + i\hat{y}) , \tag{178}$$

with $\hat{x}$ and $\hat{y}$ as unit vectors in p_{x-} and p_{y-} direction, respectively. In the light-cone gauge, $\epsilon^+(p, \lambda) = 0$, then the polarization vector is

$$\epsilon^\mu(p, \lambda) = \left(0, \frac{2\vec{\epsilon}(\lambda) \cdot \boldsymbol{p}}{p^+}, \vec{\epsilon}(\lambda) \right) , \tag{179}$$

for $\lambda = +1 =\uparrow$ and $\lambda = -1 =\downarrow$.

A.4.2   The Kogut–Soper convention (KS)

A.4.2.1   Lorentz vectors

In the Kogut and Soper convention, they have used the following coordinates transformations to define the light cone time and light cone position,

$$x^+ = \frac{1}{\sqrt{2}} \left(x^0 + x^3 \right) \quad \text{and} \quad x^- = x^0 - x^3 \,. \tag{180}$$

The covariant vectors are obtained by the contraction with the metric tensor, $x_\mu = g_{\mu\nu} x^\nu$, which is given by

$$g^{\mu\nu} = g_{\mu\nu} = \begin{pmatrix} 0 & 1 & 0 & 0 \\ 1 & 0 & 0 & 0 \\ 0 & 0 & -1 & 0 \\ 0 & 0 & 0 & -1 \end{pmatrix} , \tag{181}$$

and the scalar products are (the same values to all other four–vectors including the gamma matrices, γ^μ)

$$x^\mu p_\mu = x^+ p^- + x^- p^+ - \boldsymbol{x} \cdot \boldsymbol{p} \,. \tag{182}$$

A.4.2.2   Dirac matrices

The $+$ and $-$ gamma matrices are build following the same transformation as for the coordinates, so

$$\gamma^\pm = \frac{1}{\sqrt{2}} (\gamma^0 \pm \gamma^3) \,, \tag{183}$$

using the chiral representation for the γ's matrices. Particularly,

$$\gamma^+ \gamma^+ = \gamma^- \gamma^- = 0 \,, \tag{184}$$

and the alternate products are

$$\gamma^+ \gamma^- \gamma^+ = 2\gamma^+ \quad \text{and} \quad \gamma^- \gamma^+ \gamma^- = 2\gamma^- \,. \tag{185}$$

A.4.2.3   Dirac spinors

In this convention, Kogut and Soper use a spinor representation defined as

$$
u(k,\uparrow) = \frac{1}{\sqrt{\sqrt{2}k^+}}
\begin{pmatrix} \sqrt{2}k^+ \\ k_x + ik_y \\ m \\ 0 \end{pmatrix} \,, \quad
u(k,\downarrow) = \frac{1}{\sqrt{\sqrt{2}k^+}}
\begin{pmatrix} 0 \\ m \\ -k_x + ik_y \\ \sqrt{2}k^+ \end{pmatrix} \,,
$$

$$
v(k,\uparrow) = \frac{1}{\sqrt{\sqrt{2}k^+}}
\begin{pmatrix} 0 \\ -m \\ -k_x + ik_y \\ \sqrt{2}k^+ \end{pmatrix} \,, \quad
v(k,\downarrow) = \frac{1}{\sqrt{\sqrt{2}k^+}}
\begin{pmatrix} \sqrt{2}k^+ \\ k_x + ik_y \\ -m \\ 0 \end{pmatrix} \,.
\tag{186}
$$

A.4.2.4   Polarization vectors

Following the ref. (Brodsky; Pauli; Pinsky, 1998), the null vector is

$$
\eta^\mu = (0, 1, \mathbf{0}) \,,
\tag{187}
$$

and the polarization vector which corresponds to linear polarization $\lambda = 1$ and $\lambda = 2$ are

$$
\begin{aligned}
\epsilon^\mu(p, \lambda = 1) &= \left(0, \frac{p_x}{p^+}, 1, 0 \right) \,, \\
\epsilon^\mu(p, \lambda = 1) &= \left(0, \frac{p_y}{p^+}, 0, 1 \right) \,.
\end{aligned}
\tag{188}
$$

APPENDIX B – Spinors and matrix elements

B.1   Modified Lepage–Brodsky spinors

The LFWF calculations present in the section 3.3 were done using the Lepage-Brodsky spinors which are given by [1]

$$u_\lambda(q) = \frac{1}{\sqrt{\sqrt{2}q^+}} \left(\sqrt{2}q^+ I_4 + \beta m + \vec{\alpha} \cdot \vec{q} \right) \chi_\lambda \begin{cases} \chi(\uparrow) \text{ for } \lambda = +1 \\ \chi(\downarrow) \text{ for } \lambda = -1 \end{cases} \tag{189}$$

$$v_\lambda(q) = \frac{1}{\sqrt{\sqrt{2}q^+}} \left(\sqrt{2}q^+ I_4 - \beta m + \vec{\alpha} \cdot \vec{q} \right) \chi_\lambda \begin{cases} \chi(\downarrow) \text{ for } \lambda = +1 \\ \chi(\uparrow) \text{ for } \lambda = -1 \end{cases} \tag{190}$$

where

$$\chi(\uparrow) = \frac{1}{\sqrt{2}} \begin{pmatrix} 1 \\ 0 \\ 1 \\ 0 \end{pmatrix} \ ; \ \chi(\downarrow) = \frac{1}{\sqrt{2}} \begin{pmatrix} 0 \\ 1 \\ 0 \\ -1 \end{pmatrix}.$$

For convenience, let's remember the explicit expressions for all these spinors in the Dirac representation of γ matrices:

$$\beta = \gamma^0 = \begin{pmatrix} I & 0 \\ 0 & -I \end{pmatrix} \quad \gamma^k = \begin{pmatrix} 0 & \sigma^k \\ -\sigma^k & 0 \end{pmatrix} \quad \alpha^k = \begin{pmatrix} 0 & \sigma^k \\ \sigma^k & 0 \end{pmatrix} \quad \gamma^5 = \begin{pmatrix} 0 & I \\ I & 0 \end{pmatrix}. \tag{191}$$

---

[1] The $\sqrt{2}$ is because we are using the Kogut-Soper convention for the coordinates

moreover, also for convenience, we can rewrite the spinor as a 2×2 matrix defined as

$$u_\lambda(q) = \frac{1}{\sqrt{2}\sqrt{\sqrt{2}q^+}} \begin{pmatrix} \sqrt{2}q^+ + m_q & \boldsymbol{\sigma} \cdot \boldsymbol{q} \\ \\ \boldsymbol{\sigma} \cdot \boldsymbol{q} & \sqrt{2}q^+ - m_q \end{pmatrix} \begin{pmatrix} \chi_\lambda \\ \\ \lambda\chi_\lambda \end{pmatrix} \tag{192}$$

$$v_\lambda(q) = \frac{1}{\sqrt{2}\sqrt{\sqrt{2}q^+}} \begin{pmatrix} \sqrt{2}q^+ - m_q & \boldsymbol{\sigma} \cdot \boldsymbol{q} \\ \\ \boldsymbol{\sigma} \cdot \boldsymbol{q} & \sqrt{2}q^+ + m_q \end{pmatrix} \begin{pmatrix} \chi_{-\lambda} \\ \\ -\lambda\chi_{-\lambda} \end{pmatrix} \tag{193}$$

where we redefine χ_λ as

$$\chi_{\lambda=+1} = \begin{pmatrix} 1 \\ \\ 0 \end{pmatrix} ; \;\; \chi_{\lambda=-1} = \begin{pmatrix} 0 \\ \\ 1 \end{pmatrix}. \tag{194}$$

In what follows, we'll perform two simpler vertex calculations to teach the method to perform these kinds of calculations. To obtain j^μ and j_A^μ as presented in the section 3.3, it just follows the steps that will be present straightforwardly.

B.1.1 The identity vertex

Let's start with an easy vertex calculation

$$\overline{u}_{\lambda'}(p)\mathbb{1}u_\lambda(q) \tag{195}$$

which we can rewrite as a matrices product like (using that in LC-QFT $\boldsymbol{q} = 0$)

$$\overline{u}_{\lambda'}(p)\mathbb{1}u_\lambda(q) = \left[\frac{1}{\sqrt{2}\sqrt{\sqrt{2}p^+}} \begin{pmatrix} \sqrt{2}p'^+ + m_p & \boldsymbol{\sigma} \cdot \boldsymbol{p} \\ \\ \boldsymbol{\sigma} \cdot \boldsymbol{p} & \sqrt{2}p'^+ - m_p \end{pmatrix} \begin{pmatrix} \chi_{\lambda'} \\ \\ \lambda'\chi_{\lambda'} \end{pmatrix} \right]^\dagger \gamma_0 \mathbb{1}$$

$$\times \frac{1}{\sqrt{2}\sqrt{\sqrt{2}q^+}} \begin{pmatrix} \sqrt{2}q^+ + m_q & 0 \\ \\ 0 & \sqrt{2}q^+ - m_q \end{pmatrix} \begin{pmatrix} \chi_\lambda \\ \\ \lambda\chi_\lambda \end{pmatrix}$$

$$\overline{u}_{\lambda'}(p)\mathbb{1}u_\lambda(q) = \frac{1}{2\sqrt{2}\sqrt{p^+q^+}} \begin{pmatrix} \chi_{\lambda'}^\dagger & \lambda'\chi_{\lambda'}^\dagger \end{pmatrix} \hat{\mathcal{I}} \begin{pmatrix} \chi_\lambda \\ \\ \lambda\chi_\lambda \end{pmatrix}$$

where

$$
\hat{\mathcal{I}} = \begin{pmatrix} \sqrt{2}p^+ + m_p & \boldsymbol{\sigma}\cdot\boldsymbol{p} \\ \\ \boldsymbol{\sigma}\cdot\boldsymbol{p} & \sqrt{2}p^+ - m_p \end{pmatrix} \gamma_0 \mathbb{1} \begin{pmatrix} \sqrt{2}q^+ + m_q & 0 \\ \\ 0 & \sqrt{2}q^+ - m_q \end{pmatrix}
$$

$$
\hat{\mathcal{I}} = \begin{pmatrix} \sqrt{2}p'^+ + m_p & \boldsymbol{\sigma}\cdot\boldsymbol{p} \\ \\ \boldsymbol{\sigma}\cdot\boldsymbol{p} & \sqrt{2}p^+ - m_p \end{pmatrix} \begin{pmatrix} I & 0 \\ 0 & -I \end{pmatrix} \begin{pmatrix} I & 0 \\ 0 & I \end{pmatrix} \begin{pmatrix} \sqrt{2}q^+ + m_q & 0 \\ \\ 0 & \sqrt{2}q^+ - m_q \end{pmatrix}
$$

$$
\hat{\mathcal{I}} = \begin{pmatrix} \sqrt{2}p^+ + m_p & \boldsymbol{\sigma}\cdot\boldsymbol{p} \\ \\ \boldsymbol{\sigma}\cdot\boldsymbol{p} & \sqrt{2}p^+ - m_p \end{pmatrix} \begin{pmatrix} I & 0 \\ 0 & -I \end{pmatrix} \begin{pmatrix} \sqrt{2}q^+ + m_q & 0 \\ \\ 0 & \sqrt{2}q^+ - m_q \end{pmatrix}
$$

$$
\hat{\mathcal{I}} = \begin{pmatrix} \sqrt{2}p^+ + m_p & \boldsymbol{\sigma}\cdot\boldsymbol{p} \\ \\ \boldsymbol{\sigma}\cdot\boldsymbol{p} & \sqrt{2}p^+ - m_p \end{pmatrix} \begin{pmatrix} \sqrt{2}q^+ + m_q & 0 \\ \\ 0 & -(\sqrt{2}q^+ - m_q) \end{pmatrix}
$$

$$
\hat{\mathcal{I}} = \begin{pmatrix} (\sqrt{2}p^+ + m_p)(\sqrt{2}q^+ + m_q) & -(\sqrt{2}q^+ - m_q)\boldsymbol{\sigma}\cdot\boldsymbol{p} \\ \\ (\sqrt{2}q^+ + m_q)\boldsymbol{\sigma}\cdot\boldsymbol{p} & -(\sqrt{2}p^+ - m_p)(\sqrt{2}q^+ - m_q) \end{pmatrix}
$$

returning to the vertex expression

$$
\bar{u}_{\lambda'}(p)\mathbb{1}u_\lambda(p) = \frac{1}{2\sqrt{2}p^+q^+} \begin{pmatrix} \chi^\dagger_{\lambda'} & \lambda'\chi^\dagger_{\lambda'} \end{pmatrix}
$$

$$
\times \begin{pmatrix} (\sqrt{2}p^+ + m_p)(\sqrt{2}q^+ + m_q) & -(\sqrt{2}q^+ - m_q)\boldsymbol{\sigma}\cdot\boldsymbol{p} \\ \\ (\sqrt{2}q^+ + m_q)\boldsymbol{\sigma}\cdot\boldsymbol{p} & -(\sqrt{2}p^+ - m_p)(\sqrt{2}q^+ - m_q) \end{pmatrix} \begin{pmatrix} \chi_\lambda \\ \\ \lambda\chi_\lambda \end{pmatrix}
$$

as

$$
\begin{pmatrix} A & B \end{pmatrix} \begin{pmatrix} 1 & 2 \\ \\ 3 & 4 \end{pmatrix} \begin{pmatrix} C \\ \\ D \end{pmatrix} = A1C + B3C + A2D + B4D,
$$

we have that

$$
\bar{u}_{\lambda'}(p)\mathbb{1}u_\lambda(p) = \frac{1}{2\sqrt{2}\sqrt{p^+q^+}} \Big\{ \chi^\dagger_{\lambda'}(\sqrt{2}p^+ + m_p)(\sqrt{2}q^+ + m_q)\chi_\lambda + \lambda'\chi^\dagger_{\lambda'}(\sqrt{2}q^+ + m_q)\boldsymbol{\sigma}\cdot\boldsymbol{p}\chi_\lambda
$$

$$-\lambda\chi_{\lambda'}^{\dagger}(\sqrt{2}q^{+}-m_q)\boldsymbol{\sigma}\cdot\boldsymbol{p}\chi_{\lambda}-\lambda'\lambda\chi_{\lambda'}^{\dagger}(\sqrt{2}p^{+}-m_p)(\sqrt{2}q^{+}-m_q)\chi_{\lambda}\Big\}$$

$$\overline{u}_{\lambda'}(p)\mathbb{1}u_{\lambda}(p)=\frac{1}{2\sqrt{2}\sqrt{p^{+}q^{+}}}\Big\{\chi_{\lambda'}^{\dagger}(\sqrt{2}p^{+}+m_p)(\sqrt{2}q^{+}+m_q)\chi_{\lambda}+\lambda'\chi_{\lambda'}^{\dagger}(\sqrt{2}q^{+}+m_q)\boldsymbol{\sigma}\cdot\boldsymbol{p}\chi_{\lambda}$$

$$-\lambda\chi_{\lambda'}^{\dagger}(\sqrt{2}q^{+}-m_q)\boldsymbol{\sigma}\cdot\boldsymbol{p}\chi_{\lambda}-\lambda'\lambda\chi_{\lambda'}^{\dagger}(\sqrt{2}p^{+}-m_p)(\sqrt{2}q^{+}-m_q)\chi_{\lambda}\Big\}$$

as $\chi_{\lambda'}^{\dagger}\chi_{\lambda}=\delta_{\lambda'\lambda}$ this implies that $\lambda\lambda'$ in the 4th term will be equals to one. Therefore,

$$\overline{u}_{\lambda'}(p)\mathbb{1}u_{\lambda}(p)=\frac{1}{2\sqrt{2}\sqrt{p^{+}q^{+}}}\Big\{\delta_{\lambda'\lambda}\Big[(\sqrt{2}p^{+}+m_p)(\sqrt{2}q^{+}+m_q)-(\sqrt{2}p^{+}-m_p)(\sqrt{2}q^{+}-m_q)\Big]$$

$$-\lambda\chi_{\lambda'}^{\dagger}(\sqrt{2}q^{+}-m_q)\boldsymbol{\sigma}\cdot\boldsymbol{p}\chi_{\lambda}+\lambda'\chi_{\lambda'}^{\dagger}(\sqrt{2}q^{+}+m_q)\boldsymbol{\sigma}\cdot\boldsymbol{p}\chi_{\lambda}\Big\}$$

$$\overline{u}_{\lambda'}(p)\mathbb{1}u_{\lambda}(p)=\frac{1}{2\sqrt{2}\sqrt{p^{+}q^{+}}}\Big\{\delta_{\lambda'\lambda}\Big[\cancel{2p^{\pm}q^{+}}+\sqrt{2}p^{+}m_q+\sqrt{2}q^{+}m_p+\cancel{m_p m_q}$$

$$-\cancel{2p^{\pm}q^{+}}+\sqrt{2}p^{+}m_q+\sqrt{2}q^{+}m_p-\cancel{m_p m_q}\Big]$$

$$\sqrt{2}q^{+}\chi_{\lambda'}^{\dagger}\boldsymbol{\sigma}\cdot\boldsymbol{p}\chi_{\lambda}(\lambda'-\lambda)+m_q\chi_{\lambda'}^{\dagger}\boldsymbol{\sigma}\cdot\boldsymbol{p}\chi_{\lambda}(\lambda'+\lambda)\Big\}$$

is easy to see, just by inserting the definition of χ_{λ} and modifying λ values, that the product $\chi_{\lambda'}^{\dagger}\boldsymbol{\sigma}\cdot\boldsymbol{p}\chi_{\lambda}$ will be non-zero only when $\lambda'\neq\lambda$. Thus, the sum $\lambda'+\lambda$ will be equal zero for this case. Remaining us with,

$$\overline{u}_{\lambda'}(p)\mathbb{1}u_{\lambda}(p)=\frac{1}{2\sqrt{2}\sqrt{p^{+}q^{+}}}\Big[2\sqrt{2}\delta_{\lambda'\lambda}\big[p^{+}m_q+q^{+}m_p\big]-\lambda2\sqrt{2}q^{+}\chi_{\lambda'}^{\dagger}\boldsymbol{\sigma}\cdot\boldsymbol{p}\chi_{\lambda}\Big]$$

$$\overline{u}_{\lambda'}(p)\mathbb{1}u_{\lambda}(p)=\sqrt{p^{+}q^{+}}\Big[\delta_{\lambda'\lambda}\Big(\frac{m_q}{q^{+}}+\frac{m_p}{p^{+}}\Big)-\lambda\frac{\chi_{\lambda'}^{\dagger}\boldsymbol{\sigma}\cdot\boldsymbol{p}\chi_{\lambda}}{p^{+}}\Big]$$

$$\overline{u}_{\lambda'}(p)\mathbb{1}u_{\lambda}(p)=\sqrt{p^{+}q^{+}}\Big[\delta_{\lambda'\lambda}\Big(\frac{m_q}{q^{+}}+\frac{m_p}{p^{+}}\Big)+\frac{p(\lambda)}{p^{+}}\Big],$$

where $p(\lambda)=-\lambda p_x-ip_y$.

B.1.2 The γ_5 vertex

The next vertex to be evaluated is

$$\overline{u}_{\lambda'}(p)\gamma_5 u_{\lambda}(q), \tag{196}$$

which we will evaluate using the B-L spinors as in the last subsection. Hence, using the γ_5 definition shown in eq.(191),

$$\overline{u}_{\lambda'}(p)\gamma_5 u_{\lambda}(q)=\frac{1}{2\sqrt{2}\sqrt{p^{+}q^{+}}}\begin{pmatrix}\chi_{\lambda'}^{\dagger}, & \lambda'\chi_{\lambda'}^{\dagger}\end{pmatrix}\hat{\mathcal{Q}}\begin{pmatrix}\chi_{\lambda}\\ \lambda\chi_{\lambda}\end{pmatrix} \tag{197}$$

where the operator is defined as

$$\hat{\mathcal{Q}} = \begin{pmatrix} \sqrt{2}p^+ + m_p & \boldsymbol{\sigma} \cdot \boldsymbol{p} \\ \\ \boldsymbol{\sigma} \cdot \boldsymbol{p} & \sqrt{2}p^+ - m_p \end{pmatrix} \gamma_0 \gamma_5 \begin{pmatrix} \sqrt{2}q^+ + m_q & 0 \\ \\ 0 & \sqrt{2}q^+ - m_q \end{pmatrix}$$

$$\hat{\mathcal{Q}} = \begin{pmatrix} \sqrt{2}p^+ + m_p & \boldsymbol{\sigma} \cdot \boldsymbol{p} \\ \\ \boldsymbol{\sigma} \cdot \boldsymbol{p} & \sqrt{2}p^+ - m_p \end{pmatrix} \begin{pmatrix} I & 0 \\ 0 & -I \end{pmatrix} \begin{pmatrix} 0 & I \\ I & 0 \end{pmatrix} \begin{pmatrix} \sqrt{2}q^+ + m_q & 0 \\ \\ 0 & \sqrt{2}q^+ - m_q \end{pmatrix}$$

$$\hat{\mathcal{Q}} = \begin{pmatrix} \sqrt{2}p^+ + m_p & -\boldsymbol{\sigma} \cdot \boldsymbol{p} \\ \\ \boldsymbol{\sigma} \cdot \boldsymbol{p} & -(\sqrt{2}p^+ - m_p) \end{pmatrix} \begin{pmatrix} 0 & \sqrt{2}q^+ - m_q \\ \\ \sqrt{2}q^+ + m_q & 0 \end{pmatrix}$$

$$\hat{\mathcal{Q}} = \begin{pmatrix} -\boldsymbol{\sigma} \cdot \boldsymbol{p}(\sqrt{2}q^+ + m_q) & (\sqrt{2}p^+ + m_p)(\sqrt{2}q^+ - m_q) \\ \\ -(\sqrt{2}p^+ - m_p)(\sqrt{2}q^+ + m_q) & \boldsymbol{\sigma} \cdot \boldsymbol{p}(\sqrt{2}q^+ - m_q) \end{pmatrix}$$

returning the result for the operator into eq.(197),

$$\bar{u}_{\lambda'}(p)\gamma_5 u_\lambda(q) = \frac{1}{2\sqrt{2}\sqrt{p^+q^+}} \begin{pmatrix} \chi_{\lambda'}^\dagger, & \lambda'\chi_{\lambda'}^\dagger \end{pmatrix}$$

$$\times \begin{pmatrix} -\boldsymbol{\sigma} \cdot \boldsymbol{p}(\sqrt{2}q^+ + m_q) & (\sqrt{2}p^+ + m_p)(\sqrt{2}q^+ - m_q) \\ \\ -(\sqrt{2}p^+ - m_p)(\sqrt{2}q^+ + m_q) & \boldsymbol{\sigma} \cdot \boldsymbol{p}(\sqrt{2}q^+ - m_q) \end{pmatrix} \begin{pmatrix} \chi_\lambda \\ \lambda\chi_\lambda \end{pmatrix},$$

we get

$$\bar{u}_{\lambda'}(p)\gamma_5 u_\lambda(q) = \frac{1}{2\sqrt{2}\sqrt{p^+q^+}} \Big\{ -(\sqrt{2}q^+ + m_q)\chi_{\lambda'}^\dagger \boldsymbol{\sigma} \cdot \boldsymbol{p}\chi_\lambda$$
$$-\lambda'(\sqrt{2}p^+ - m_p)(\sqrt{2}q^+ + m_q)\chi_{\lambda'}^\dagger \chi_\lambda$$
$$+\lambda(\sqrt{2}p^+ + m_p)(\sqrt{2}q^+ - m_q)\chi_{\lambda'}^\dagger \chi_\lambda$$
$$+\lambda'\lambda(\sqrt{2}q^+ - m_q)\chi_{\lambda'}^\dagger \boldsymbol{\sigma} \cdot \boldsymbol{p}\chi_\lambda \Big\},$$

we have seen that $\chi_{\lambda'}^\dagger \chi_\lambda = \delta_{\lambda\lambda'}$ and $\chi_{\lambda'}^\dagger \boldsymbol{\sigma} \cdot \boldsymbol{p}\chi_\lambda$ is non-zero when $\lambda' \neq \lambda$ which implies that $\lambda'\lambda = -1$ in the 4th term. So,

$$\bar{u}_{\lambda'}(p)\gamma_5 u_\lambda(q) = \frac{1}{2\sqrt{2}\sqrt{p^+q^+}} \Big\{ \lambda\delta_{\lambda'\lambda} \Big[(\sqrt{2}p^+ + m_p)(\sqrt{2}q^+ - m_q) - (\sqrt{2}p^+ - m_p)(\sqrt{2}q^+ + m_q) \Big]$$

$$-\chi^\dagger_{\lambda'}\boldsymbol{\sigma}\cdot\boldsymbol{p}\chi_\lambda\left[(\sqrt{2}q^+ + \cancel{m_q}) + (\sqrt{2}q^+ - \cancel{m_q})\right]\Big\}$$

$$\bar{u}_{\lambda'}(p)\gamma_5 u_\lambda(q) = \frac{1}{2\sqrt{2}\sqrt{p^+q^+}}\Big\{\lambda\delta_{\lambda'\lambda}\left[\cancel{2p^+q^+} - \sqrt{2}p^+m_q + \sqrt{2}q^+m_p - \cancel{m_p m_q} - \cancel{2p^+q^+}\right.$$

$$\left. - \sqrt{2}p^+m_q + \sqrt{2}q^+m_q + \cancel{m_p m_q}\right] - 2\sqrt{2}q^+\chi^\dagger_{\lambda'}\boldsymbol{\sigma}\cdot\boldsymbol{p}\chi_\lambda\Big\}$$

$$\bar{u}_{\lambda'}(p)\gamma_5 u_\lambda(q) = \frac{1}{2\sqrt{2}\sqrt{p^+q^+}}\Big\{2\sqrt{2}\lambda\delta_{\lambda'\lambda}\left(q^+m_p - p^+m_q\right) - 2\sqrt{2}q^+\chi^\dagger_{\lambda'}\boldsymbol{\sigma}\cdot\boldsymbol{p}\chi_\lambda\Big\}$$

$$\bar{u}_{\lambda'}(p)\gamma_5 u_\lambda(q) = \sqrt{p^+q^+}\chi^\dagger_{\lambda'}\left\{\lambda\left(\frac{m_p}{p^+} - \frac{m_q}{q^+}\right)\mathbb{1} - \frac{\boldsymbol{\sigma}\cdot\boldsymbol{p}}{p^+}\right\}\chi_\lambda.$$

To connect with the momentum labels presented in section 3.3, one must do $p_b \leftrightarrow p$ and $p_a \leftrightarrow q$. Here we have used a simpler notation.

B.2 Spinor matrix elements

Here we collect the spinor matrix elements relevant for the calculation of LCWFs. We use the spinors of Lepage and Brodsky (Lepage; Brodsky, 1980), adjusted for the fact, that we define LF components as $p^\pm = (p^0 \pm p^3)/\sqrt{2}$. Notice that in general the spinors for initial and final state quark can belong to different masses.

$$\bar{u}(p_b, \lambda', m_b)\mathbb{1}u_\lambda(p_a, \lambda, m_a) = \sqrt{p_b^+ p_a^+}\,\chi^\dagger_{\lambda'}\left\{\left(\frac{m_a}{p_a^+} + \frac{m_b}{p_b^+}\right)\mathbb{1} - \frac{\boldsymbol{\sigma}\cdot\boldsymbol{p}_b}{p_b^+}(\boldsymbol{\sigma}\cdot\boldsymbol{n})\right\}\chi_\lambda$$

$$\bar{u}(p_b, \lambda', m_b)\gamma_5 u(p_a, \lambda, m_a) = \sqrt{p_a^+ p_b^+}\chi^\dagger_{\lambda'}\left\{\left(\frac{m_b}{p_b^+} - \frac{m_a}{p_a^+}\right)(\boldsymbol{\sigma}\cdot\boldsymbol{n}) - \frac{\boldsymbol{\sigma}\cdot\boldsymbol{p}_b}{p_b^+}\right\}\chi_\lambda \quad (198)$$

For completeness, we give all components of the vector and axial vector bilinears, although the LF minus component does not appear in the gauge adopted in this paper. For $j = [j^+, j^-, \boldsymbol{j}]$, we obtain for the vector and axial vector bilinear

$$j_\mu^V = \bar{u}(p_b, \lambda', m_b)\gamma_\mu u(p_a, \lambda, m_a)\,,\; j_\mu^A = \bar{u}(p_b, \lambda', m_b)\gamma_\mu\gamma_5 u(p_a, \lambda, m_a)\,, \quad (199)$$

are given, respectively, by

$$j_{\lambda'\lambda}^{V+} = 2\sqrt{p_b^+ p_a^+}\,\chi^\dagger_{\lambda'}\mathbb{1}\chi_\lambda$$

$$j_{\lambda'\lambda}^{V-} = \sqrt{p_b^+ p_a^+}\,\chi^\dagger_{\lambda'}\left\{\frac{m_a m_b}{p_a^+ p_b^+}\mathbb{1} - \frac{m_a}{p_a^+ p_b^+}(\boldsymbol{\sigma}\cdot\boldsymbol{p}_b)(\boldsymbol{\sigma}\cdot\boldsymbol{n})\right\}\chi_\lambda$$

$$\boldsymbol{j}_{\lambda'\lambda}^{V}\cdot\boldsymbol{a} = \sqrt{p_a^+ p_b^+}\,\chi^\dagger_{\lambda'}\left\{\left(\frac{\boldsymbol{p}_b\cdot\boldsymbol{a}}{p_b^+} + i\frac{[\boldsymbol{p}_b, \boldsymbol{a}]}{p_b^+}(\boldsymbol{\sigma}\cdot\boldsymbol{n})\right)\mathbb{1} + \frac{p_a^+ m_b - p_b^+ m_a}{p_a^+ p_b^+}(\boldsymbol{\sigma}\cdot\boldsymbol{a})(\boldsymbol{\sigma}\cdot\boldsymbol{n})\right\}\chi_\lambda\,,$$

$$(200)$$

and

$$j_{\lambda'\lambda}^{A+} = 2\sqrt{p_a^+ p_b^+}\,\chi^\dagger_{\lambda'}(\boldsymbol{\sigma}\cdot\boldsymbol{n})\chi_\lambda$$

$$j^{A-}_{\lambda'\lambda} = \sqrt{p_a^+ p_b^+}\, \chi_{\lambda'}^\dagger \left\{ -\frac{m_a m_b}{p_a^+ p_b^+}(\boldsymbol{\sigma}\cdot\boldsymbol{n}) + \frac{m_a}{p_a^+ p_b^+}\,\boldsymbol{\sigma}\cdot\boldsymbol{p}_b \right\}\chi_\lambda$$

$$\boldsymbol{j}^A_{\lambda'\lambda}\cdot\boldsymbol{a} = \sqrt{p_a^+ p_b^+}\, \chi_{\lambda'}^\dagger \left\{ \left(\frac{\boldsymbol{p}_b\cdot\boldsymbol{a}}{p_b^+}(\boldsymbol{\sigma}\cdot\boldsymbol{n}) + i\frac{[\boldsymbol{p}_b,\boldsymbol{a}]}{p_b^+} \right)\mathbb{1} + \frac{p_a^+ m_b + p_b^+ m_a}{p_a^+ p_b^+}\,\boldsymbol{\sigma}\cdot\boldsymbol{a} \right\}\chi_\lambda .$$

$$(201)$$

Above, vectors $\boldsymbol{p}_b$ is the transverse momentum of quark b, $\boldsymbol{a}$ is an arbitrary transverse vector, and $\boldsymbol{n} = (0,0,1)$. Pauli spinors χ_λ are eigenstates of $\boldsymbol{\sigma}\cdot\boldsymbol{n}$:

$$(\boldsymbol{\sigma}\cdot\boldsymbol{n})\chi_\lambda = \lambda\,\chi_\lambda, \quad \lambda = \pm 1, \tag{202}$$

so that $\lambda/2$ is the quark helicity.

APPENDIX C – Useful functions and integrals

C.1 Bessel Functions

$$J_0(pr) = \frac{1}{2\pi} \int d\phi\, e^{i\boldsymbol{p}\cdot\boldsymbol{r}} = \frac{1}{2\pi} \int d\phi\, e^{ipr\cos\phi}. \tag{203}$$

$$J_1(pr) = \frac{1}{2\pi i} \int d\phi\, e^{ipr\cos\phi} \cos\phi. \tag{204}$$

$$K_0(\varepsilon r) = \frac{1}{2\pi} \int d^2\boldsymbol{l}\, e^{i\boldsymbol{l}\cdot\boldsymbol{r}} \frac{1}{(l^2+\epsilon^2)} \tag{205}$$

$$K_1(\varepsilon r) = -\frac{1}{\epsilon}\frac{d}{dr}K_0(\epsilon r) = \frac{1}{2\pi i\epsilon} \int d^2\boldsymbol{l}\, e^{i\boldsymbol{l}\cdot\boldsymbol{r}} \frac{\boldsymbol{l}}{(l^2+\epsilon^2)} \cdot \frac{\boldsymbol{r}}{r} \tag{206}$$

Consequently:

$$\frac{\boldsymbol{r}}{r}K_1(\varepsilon r) = \frac{1}{2\pi i\epsilon} \int d^2\boldsymbol{l}\, e^{i\boldsymbol{l}\cdot\boldsymbol{r}} \frac{\boldsymbol{l}}{(l^2+\epsilon^2)} \tag{207}$$

Moreover, we can also write:

$$K_1(\varepsilon r) = -\frac{1}{r}\frac{d}{d\epsilon}K_0(\epsilon r) = \frac{\epsilon}{\pi r} \int d^2\boldsymbol{l}\, e^{i\boldsymbol{l}\cdot\boldsymbol{r}} \frac{1}{(l^2+\epsilon^2)^2} \tag{208}$$

C.2 Useful integrals for the calculations in the impact parameter space

$$\int d^2\boldsymbol{r}\, d^2\boldsymbol{r}'\, \exp[i\boldsymbol{p}\cdot(\boldsymbol{r}-\boldsymbol{r}')]K_0(\epsilon r)K_0(\epsilon r')\sigma_{q\bar{q}}(zr) = \frac{(2\pi)^2}{(p^2+\epsilon^2)}\int dr\, r\, J_0(pr)K_0(\epsilon r)\sigma(zr)$$

$$= \frac{(2\pi)^2}{(p^2+\epsilon^2)}I_1(z,p) \tag{209}$$

$$\int d^2\boldsymbol{r}d^2\boldsymbol{r'}\exp[i\boldsymbol{p}\cdot(\boldsymbol{r}-\boldsymbol{r'})]\mathrm{K}_0(\epsilon r)\mathrm{K}_0(\epsilon r')\sigma_{q\bar{q}}(z|\boldsymbol{r}-\boldsymbol{r'}|) = \frac{2\pi^2}{\epsilon}\int drr^2\mathrm{J}_0(pr)\mathrm{K}_1(\epsilon r)\sigma(z\boldsymbol{r})$$

$$= \frac{2\pi^2}{\epsilon}I_2(z,p) \qquad (210)$$

$$\int d^2\boldsymbol{r}d^2\boldsymbol{r'}\exp[i\boldsymbol{p}\cdot(\boldsymbol{r}-\boldsymbol{r'})]\frac{\boldsymbol{r}\cdot\boldsymbol{r'}}{rr'}\mathrm{K}_1(\epsilon r)\mathrm{K}_1(\epsilon r')\sigma_{q\bar{q}}(z\boldsymbol{r}) = \frac{(2\pi)^2}{\epsilon}\frac{p}{(p^2+\epsilon^2)}$$

$$\times\int drr\mathrm{J}_1(pr)\mathrm{K}_1(\epsilon r)\sigma_{q\bar{q}}(z\boldsymbol{r})$$

$$\int d^2\boldsymbol{r}d^2\boldsymbol{r'}\exp[i\boldsymbol{p}\cdot(\boldsymbol{r}-\boldsymbol{r'})]\frac{\boldsymbol{r}\cdot\boldsymbol{r'}}{rr'}\mathrm{K}_1(\epsilon r)\mathrm{K}_1(\epsilon r')\sigma_{q\bar{q}}(z\boldsymbol{r}) = \frac{(2\pi)^2}{\epsilon}\frac{p}{(p^2+\epsilon^2)}I_3(z,p)$$

$$(211)$$

$$\int d^2\boldsymbol{r}d^2\boldsymbol{r'}\exp[i\boldsymbol{p}\cdot(\boldsymbol{r}-\boldsymbol{r'})]\frac{\boldsymbol{r}\cdot\boldsymbol{r'}}{rr'}\mathrm{K}_1(\epsilon r)\mathrm{K}_1(\epsilon r')\sigma_{q\bar{q}}(z|\boldsymbol{r}-\boldsymbol{r'}|) = \frac{(2\pi)^2}{\epsilon^2}I_1(z,p) - \frac{2\pi^2}{\epsilon}I_2(z,p)$$

$$(212)$$

C.3 Useful integrals for the calculations in the transverse momentum space

$$\int d^2\boldsymbol{r}d^2\boldsymbol{r'}\exp[i\boldsymbol{p}\cdot(\boldsymbol{r}-\boldsymbol{r'})]\mathrm{K}_0(\epsilon r)\mathrm{K}_0(\epsilon r') = (2\pi)^2\frac{1}{(p^2+\epsilon^2)^2} \qquad (213)$$

$$\int d^2\boldsymbol{r}d^2\boldsymbol{r'}\exp[i\boldsymbol{p}\cdot(\boldsymbol{r}-\boldsymbol{r'})]\mathrm{K}_0(\epsilon r)\mathrm{K}_0(\epsilon r')e^{iz\boldsymbol{k}\cdot\boldsymbol{r}} = (2\pi)^2\frac{1}{[(\boldsymbol{p}-z\boldsymbol{k})^2+\epsilon^2]}\frac{1}{(p^2+\epsilon^2)} \qquad (214)$$

$$\int d^2\boldsymbol{r}d^2\boldsymbol{r'}\exp[i\boldsymbol{p}\cdot(\boldsymbol{r}-\boldsymbol{r'})]\mathrm{K}_0(\epsilon r)\mathrm{K}_0(\epsilon r')e^{iz\boldsymbol{k}\cdot(\boldsymbol{r}-\boldsymbol{r'})} = (2\pi)^2\frac{1}{[(\boldsymbol{p}-z\boldsymbol{k})^2+\epsilon^2]^2} \qquad (215)$$

$$\int d^2\boldsymbol{r}d^2\boldsymbol{r'}\exp[i\boldsymbol{p}\cdot(\boldsymbol{r}-\boldsymbol{r'})]\frac{\boldsymbol{r}\cdot\boldsymbol{r'}}{rr'}\mathrm{K}_1(\epsilon r)\mathrm{K}_1(\epsilon r') = \frac{(2\pi)^2}{\epsilon^2}\frac{p^2}{(p^2+\epsilon^2)^2} \qquad (216)$$

$$\int d^2\boldsymbol{r}d^2\boldsymbol{r}' \exp[i\boldsymbol{p}\cdot(\boldsymbol{r}-\boldsymbol{r}')]\frac{\boldsymbol{r}\cdot\boldsymbol{r}'}{rr'}\mathrm{K}_1(\epsilon r)\mathrm{K}_1(\epsilon r')e^{iz\boldsymbol{k}\cdot\boldsymbol{r}} = \frac{(2\pi)^2}{\epsilon^2}\frac{\boldsymbol{p}\cdot(\boldsymbol{p}-z\boldsymbol{k})}{(p^2+\epsilon^2)[(\boldsymbol{p}-z\boldsymbol{k})^2+\epsilon^2]}$$

(217)

$$\int d^2\boldsymbol{r}d^2\boldsymbol{r}' \exp[i\boldsymbol{p}\cdot(\boldsymbol{r}-\boldsymbol{r}')]\frac{\boldsymbol{r}\cdot\boldsymbol{r}'}{rr'}\mathrm{K}_1(\epsilon r)\mathrm{K}_1(\epsilon r')e^{iz\boldsymbol{k}\cdot(\boldsymbol{r}-\boldsymbol{r}')} = \frac{(2\pi)^2}{\epsilon^2}\frac{(\boldsymbol{p}-z\boldsymbol{k})^2}{[(\boldsymbol{p}-z\boldsymbol{k})^2+\epsilon^2]^2}$$

(218)

APPENDIX D – Isolated electroweak gauge boson production in the impact momentum space

In this appendix, we'll derive in detail the electroweak gauge boson production cross section at the parton level in the impact parameter representation for a transverse polarization and vector contribution. The other three cross-sections can be derived similarly, therefore we'll present only their results.

From what we have seen at chapter 3, the main formulae which describe the parton-target cross-section for the transverse polarization is

$$
\begin{aligned}
\frac{d\sigma_T^f}{dz d^2\boldsymbol{p}} &= \frac{1}{2(2\pi)^2} \int d^2\boldsymbol{r}\mathrm{d}^2\boldsymbol{r}' e^{i\boldsymbol{p}\cdot(\boldsymbol{r}-\boldsymbol{r}')} \rho_V^T(z,\boldsymbol{r},\boldsymbol{r}') \\
&\times \left[\sigma_{q\bar{q}}(z\boldsymbol{r},x) + \sigma_{q\bar{q}}(z\boldsymbol{r}',x) - \sigma_{q\bar{q}}(z|\boldsymbol{r}-\boldsymbol{r}'|,x) \right] \\
&+ \frac{1}{2(2\pi)^2} \int d^2\boldsymbol{r}\mathrm{d}^2\boldsymbol{r}' e^{i\boldsymbol{p}\cdot(\boldsymbol{r}-\boldsymbol{r}')} \rho_A^T(z,\boldsymbol{r},\boldsymbol{r}') \\
&\times \left[\sigma_{q\bar{q}}(z\boldsymbol{r},x) + \sigma_{q\bar{q}}(z\boldsymbol{r}',x) - \sigma_{q\bar{q}}(z|\boldsymbol{r}-\boldsymbol{r}'|,x) \right] .
\end{aligned}
\tag{219}
$$

Substituting the expression for $\rho_V^T(z,\boldsymbol{r},\boldsymbol{r}')$, one has that the vector contribution can be expressed by:

$$
\begin{aligned}
\frac{d\sigma_T^f}{dz d^2\boldsymbol{p}}\Big|_V &= \frac{1}{2(2\pi)^2} \frac{(\mathcal{C}_f^G)^2 (g_{v,f}^G)^2}{2\pi^2} z[(m_b - m_a) + z m_a]^2 \\
&\times \int d^2\boldsymbol{r}\mathrm{d}^2\boldsymbol{r}' e^{i\boldsymbol{p}\cdot(\boldsymbol{r}-\boldsymbol{r}')} \mathrm{K}_0(\epsilon r)\mathrm{K}_0(\epsilon r') \\
&\times \left[\sigma_{q\bar{q}}(z\boldsymbol{r},x) + \sigma_{q\bar{q}}(z\boldsymbol{r}',x) - \sigma_{q\bar{q}}(z|\boldsymbol{r}-\boldsymbol{r}'|,x) \right] \\
&+ \frac{1}{2(2\pi)^2} \frac{(\mathcal{C}_f^G)^2 (g_{v,f}^G)^2}{2\pi^2} \frac{[1 + (1-z)^2]}{z} \epsilon^2 \\
&\times \int d^2\boldsymbol{r}\mathrm{d}^2\boldsymbol{r}' e^{i\boldsymbol{p}\cdot(\boldsymbol{r}-\boldsymbol{r}')} \frac{\boldsymbol{r}\cdot\boldsymbol{r}'}{rr'}\mathrm{K}_1(\epsilon r)\mathrm{K}_1(\epsilon r') \\
&\times \left[\sigma_{q\bar{q}}(z\boldsymbol{r},x) + \sigma_{q\bar{q}}(z\boldsymbol{r}',x) - \sigma_{q\bar{q}}(z|\boldsymbol{r}-\boldsymbol{r}'|,x) \right] .
\end{aligned}
\tag{220}
$$

From eq. (220), we can identify as the sum of three integrals terms, T_1, T_2 and T_3, which are:

$$T_1 = \frac{(\mathcal{C}_f^G)^2 (g_{f,V}^G)^2}{(2\pi)^4} \int \mathrm{d}^2\boldsymbol{r} \int \mathrm{d}^2\boldsymbol{r}' e^{i\boldsymbol{p}\cdot(\boldsymbol{r}-\boldsymbol{r}')} \left\{ \frac{1+(1-z)^2}{z} \frac{\boldsymbol{r}\cdot\boldsymbol{r}'}{rr'} \epsilon^2 \mathrm{K}_1(\epsilon r) \mathrm{K}_1(\epsilon r') \right.$$

$$\left. +z\left[(m_b - m_a) + zm_a\right]^2 \mathrm{K}_0(\epsilon r)\mathrm{K}_0(\epsilon r') \right\} \sigma_{q\bar{q}}(z\boldsymbol{r}, x) \tag{221}$$

$$T_2 = \frac{(\mathcal{C}_f^G)^2 (g_{f,V}^G)^2}{(2\pi)^4} \int \mathrm{d}^2\boldsymbol{r} \int \mathrm{d}^2\boldsymbol{r}' e^{i\boldsymbol{p}\cdot(\boldsymbol{r}-\boldsymbol{r}')} \left\{ \frac{1+(1-z)^2}{z} \frac{\boldsymbol{r}\cdot\boldsymbol{r}'}{rr'} \epsilon^2 \mathrm{K}_1(\epsilon r) \mathrm{K}_1(\epsilon r') \right.$$

$$\left. +z\left[(m_b - m_a) + zm_a\right]^2 \mathrm{K}_0(\epsilon r)\mathrm{K}_0(\epsilon r') \right\} \sigma_{q\bar{q}}(z\boldsymbol{r}', x) \tag{222}$$

$$T_3 = -\frac{(\mathcal{C}_f^G)^2 (g_{f,V}^G)^2}{(2\pi)^4} \int \mathrm{d}^2\boldsymbol{r} \int \mathrm{d}^2\boldsymbol{r}' e^{i\boldsymbol{p}\cdot(\boldsymbol{r}-\boldsymbol{r}')} \left\{ \frac{1+(1-z)^2}{z} \frac{\boldsymbol{r}\cdot\boldsymbol{r}'}{rr'} \epsilon^2 \mathrm{K}_1(\epsilon r) \mathrm{K}_1(\epsilon r') \right.$$

$$\left. +z\left[(m_b - m_a) + zm_a\right]^2 \mathrm{K}_0(\epsilon r)\mathrm{K}_0(\epsilon r') \right\} \sigma_{q\bar{q}}(z|\boldsymbol{r} - \boldsymbol{r}'|, x) \tag{223}$$

Therefore, let's approach each term at a time. Beginning with T_1,

$$T_1 = \frac{(\mathcal{C}_f^G)^2 (g_{f,V}^G)^2}{(2\pi)^4} \int \mathrm{d}^2\boldsymbol{r} \int \mathrm{d}^2\boldsymbol{r}' e^{i\boldsymbol{p}\cdot(\boldsymbol{r}-\boldsymbol{r}')} \left\{ \frac{1+(1-z)^2}{z} \frac{\boldsymbol{r}\cdot\boldsymbol{r}'}{rr'} \epsilon^2 \mathrm{K}_1(\epsilon r) \mathrm{K}_1(\epsilon r') \right.$$

$$\left. +z\left[(m_b - m_a) + zm_a\right]^2 \mathrm{K}_0(\epsilon r)\mathrm{K}_0(\epsilon r') \right\} \sigma_{q\bar{q}}(z\boldsymbol{r}, x)$$

$$T_1 = \frac{(\mathcal{C}_f^G)^2 (g_{f,V}^G)^2}{(2\pi)^4} \left\{ \frac{1+(1-z)^2}{z} \epsilon^2 \Gamma_1 + z\left[(m_b - m_a) + zm_a\right]^2 \Gamma_2 \right\} \tag{224}$$

where, is easy to see that it was divided into two integrals as:

$$\Gamma_1 = \int \mathrm{d}^2\boldsymbol{r}\,\mathrm{d}^2\boldsymbol{r}' e^{i\boldsymbol{p}\cdot(\boldsymbol{r}-\boldsymbol{r}')} \frac{\boldsymbol{r}\cdot\boldsymbol{r}'}{rr'} \mathrm{K}_1(\epsilon r)\mathrm{K}_1(\epsilon r')\sigma_{q\bar{q}}(z\boldsymbol{r}, x)$$

$$\Gamma_2 = \int \mathrm{d}^2\boldsymbol{r}\,\mathrm{d}^2\boldsymbol{r}' e^{i\boldsymbol{p}\cdot(\boldsymbol{r}-\boldsymbol{r}')} \mathrm{K}_0(\epsilon r)\mathrm{K}_0(\epsilon r')\sigma_{q\bar{q}}(z\boldsymbol{r}, x).$$

before we start the evaluation of these integrals, it's recommended to take a look in the Appendix C where we show the Bessel Functions into their respective integral form. All those integral forms will be important in what follows, in this first case we'll show them along the text but in the other cases will be done straightforwardly. Thus, as the modified Bessel Function of the second kind at zeroth order in its integral is

$$\mathrm{K}_0(\epsilon r) = \frac{1}{2\pi} \int \mathrm{d}^2\boldsymbol{l} \, \frac{e^{i\boldsymbol{l}\cdot\boldsymbol{r}}}{l^2 + \epsilon^2},$$

and we can extract the integral form of the next order by a differential over ϵ or r. Therefore, doing the derivative over r,

$$\mathrm{K}_1(\epsilon r) = -\frac{1}{\epsilon}\frac{\mathrm{d}}{\mathrm{d}r}\mathrm{K}_0(\epsilon r) = \frac{1}{2\pi i\epsilon} \int \mathrm{d}^2\boldsymbol{l} \, e^{i\boldsymbol{l}\cdot\boldsymbol{r}} \frac{\boldsymbol{l}}{l^2 + \epsilon^2} \cdot \frac{\boldsymbol{r}}{r},$$

which implies in

$$\frac{\boldsymbol{r}}{r} \cdot \mathrm{K}_1(\epsilon r) = \frac{1}{2\pi i \epsilon} \int \mathrm{d}^2 l e^{i \boldsymbol{l} \cdot \boldsymbol{r}} \frac{\boldsymbol{l}}{l^2 + \epsilon^2}.$$

Moreover, we can also represent $\mathrm{K}_1(\epsilon r)$ by the differential over ϵ:

$$\mathrm{K}_1(\epsilon r) = -\frac{1}{r}\frac{\mathrm{d}}{\mathrm{d}\epsilon}\mathrm{K}_0(\epsilon r) = \frac{\epsilon}{\pi r} \int \mathrm{d}^2 l \frac{e^{i\boldsymbol{l}\cdot\boldsymbol{r}}}{\left(l^2 + \epsilon^2\right)^2}.$$

Using the integral form to $\frac{\boldsymbol{r'}}{r'}\mathrm{K}_1\left(\epsilon r'\right)$, we have that

$$\Gamma_1 = \int \mathrm{d}^2 \boldsymbol{r} \mathrm{d}^2 \boldsymbol{r'} e^{i\boldsymbol{p}\cdot(\boldsymbol{r}-\boldsymbol{r'})}\frac{\boldsymbol{r}}{r}\mathrm{K}_1(\epsilon r)\frac{1}{2\pi i \epsilon} \int \mathrm{d}^2 l e^{i\boldsymbol{l}\cdot\boldsymbol{r'}}\frac{\boldsymbol{l}}{l^2 + \epsilon^2}\sigma_{q\bar{q}}(z\boldsymbol{r}, x)$$

$$\Gamma_1 = \frac{1}{2\pi i \epsilon} \int \mathrm{d}^2 \boldsymbol{r} \mathrm{d}^2 l e^{i\boldsymbol{p}\cdot\boldsymbol{r}}\frac{\boldsymbol{r}\cdot\boldsymbol{l}}{r\left(l^2 + \epsilon^2\right)}\mathrm{K}_1(\epsilon r)\sigma_{q\bar{q}}(z\boldsymbol{r}, x) \int \mathrm{d}^2 \boldsymbol{r'} e^{i\boldsymbol{r'}\cdot(\boldsymbol{l}-\boldsymbol{p})}$$

identifying the integral over $\boldsymbol{r'}$ as a Delta function over 2D space:

$$\frac{1}{(2\pi)^2} \int \mathrm{d}^2 \boldsymbol{x} e^{i\boldsymbol{x}\cdot(\boldsymbol{k}-\boldsymbol{q})} = \delta^{(2)}\left(\boldsymbol{k} - \boldsymbol{q}\right),$$

then,

$$\Gamma_1 = \frac{1}{2\pi i \epsilon} \int \mathrm{d}^2 \boldsymbol{r} \mathrm{d}^2 l e^{i\boldsymbol{p}\cdot\boldsymbol{r}}\frac{\boldsymbol{r}\cdot\boldsymbol{l}}{r\left(l^2 + \epsilon^2\right)}\mathrm{K}_1(\epsilon r)\sigma_{q\bar{q}}(z\boldsymbol{r}, x)(2\pi)^2\delta^{(2)}\left(\boldsymbol{l} - \boldsymbol{p}\right)$$

$$\Gamma_1 = \frac{2\pi}{i\epsilon\left(p^2 + \epsilon^2\right)} \int \mathrm{d}^2 \boldsymbol{r} e^{i\boldsymbol{p}\cdot\boldsymbol{r}}\frac{\boldsymbol{r}\cdot\boldsymbol{p}}{r}\mathrm{K}_1(\epsilon r)\sigma_{q\bar{q}}(z\boldsymbol{r}, x)$$

as $\boldsymbol{r}\cdot\boldsymbol{p} = rp\cos\phi$

$$\Gamma_1 = \frac{2\pi p}{i\epsilon\left(p^2 + \epsilon^2\right)} \int \mathrm{d}\phi \mathrm{d}r \, r e^{i\boldsymbol{p}\cdot\boldsymbol{r}}\cos\phi\sigma_{q\bar{q}}(z\boldsymbol{r}, x),$$

in addition to the Bessel Function of the second kind, is important look at the Bessel Function of the first kind in its integral form which at zeroth order is

$$\mathrm{J}_0(pr) = \frac{1}{2\pi} \int \mathrm{d}\phi e^{i\boldsymbol{p}\cdot\boldsymbol{r}} = \frac{1}{2\pi} \int \mathrm{d}\phi \, e^{ipr\cos\phi},$$

once more, the next order is obtained by a differential over p or r, which give us

$$\mathrm{J}_1(pr) = -\frac{1}{r}\frac{\mathrm{d}}{\mathrm{d}p}\mathrm{J}_0(pr) = \frac{1}{2\pi i} \int \mathrm{d}\phi \, e^{ipr\cos\phi}\cos\phi$$

$$\mathrm{J}_1(pr) = -\frac{1}{p}\frac{\mathrm{d}}{\mathrm{d}r}\mathrm{J}_0(pr) = \frac{1}{2\pi i} \int \mathrm{d}\phi \, e^{ipr\cos\phi}\cos\phi$$

now, using this representation we obtain

$$\Gamma_1 = \frac{2\pi p}{i\epsilon \left(p^2 + \epsilon^2\right)} \int \mathrm{d}r \, r \left(2\pi i\right) \mathrm{J}_1(pr) \mathrm{K}_1(\epsilon r) \sigma_{q\bar{q}}(z\boldsymbol{r}, x)$$

$$\Gamma_1 = \frac{(2\pi)^2}{\epsilon} \frac{p}{\left(p^2 + \epsilon^2\right)} \int \mathrm{d}r \, r J_1(pr) \mathrm{K}_1(\epsilon r) \sigma_{q\bar{q}}(z\boldsymbol{r}, x)$$

$$\Gamma_1 = \frac{(2\pi)^2}{\epsilon} \frac{p}{\left(p^2 + \epsilon^2\right)} I_3(z, p),$$

where we have defined

$$I_3(z, p) = \int \mathrm{d}r \, r J_1(pr) \mathrm{K}_1(\epsilon r) \sigma_{q\bar{q}}(z\boldsymbol{r}, x). \tag{225}$$

Now, let's evaluate Γ_2, in what follows the use of the Bessel Functions integral form as well as the Delta Dirac function definition will be done in a direct manner. So,

$$\Gamma_2 = \int \mathrm{d}^2\boldsymbol{r}\mathrm{d}^2\boldsymbol{r}' e^{i\boldsymbol{p}\cdot(\boldsymbol{r}-\boldsymbol{r}')} \mathrm{K}_0(\epsilon r) \frac{1}{2\pi} \int \mathrm{d}^2\boldsymbol{l} \, \frac{e^{i\boldsymbol{l}\cdot\boldsymbol{r}'}}{l^2 + \epsilon^2} \sigma_{q\bar{q}}(z\boldsymbol{r}, x).$$

$$\Gamma_2 = \frac{1}{2\pi} \int \mathrm{d}^2\boldsymbol{r}\mathrm{d}^2\boldsymbol{l} \, e^{i\boldsymbol{p}\cdot\boldsymbol{r}} \mathrm{K}_0(\epsilon r) \sigma_{q\bar{q}}(z\boldsymbol{r}, x) \frac{1}{l^2 + \epsilon^2} \int \mathrm{d}^2\boldsymbol{r} \, e^{i\boldsymbol{r}'\cdot(\boldsymbol{l}-\boldsymbol{p})}$$

$$\Gamma_2 = \frac{1}{2\pi} \int \mathrm{d}^2\boldsymbol{r}\mathrm{d}^2\boldsymbol{l} \, e^{i\boldsymbol{p}\cdot\boldsymbol{r}} \mathrm{K}_0(\epsilon r) \sigma_{q\bar{q}}(z\boldsymbol{r}, x) \frac{1}{l^2 + \epsilon^2} \left(2\pi\right)^2 \delta^{(2)} \left(\boldsymbol{l} - \boldsymbol{p}\right)$$

$$\Gamma_2 = \frac{2\pi}{p^2 + \epsilon^2} \int \mathrm{d}r\mathrm{d}\phi \, r e^{i\boldsymbol{p}\cdot\boldsymbol{r}} \mathrm{K}_0(\epsilon r) \sigma_{q\bar{q}}(z\boldsymbol{r}, x)$$

$$\Gamma_2 = \frac{(2\pi)^2}{p^2 + \epsilon^2} \int \mathrm{d}r \, r J_0(pr) \mathrm{K}_0(\epsilon r) \sigma_{q\bar{q}}(z\boldsymbol{r}, x)$$

$$\Gamma_2 = \frac{(2\pi)^2}{p^2 + \epsilon^2} I_1(z, p),$$

where

$$I_1(z, p) = \int \mathrm{d}r \, r J_0(pr) \mathrm{K}_0(\epsilon r) \sigma_{q\bar{q}}(z\boldsymbol{r}, x). \tag{226}$$

Thus, returning those results into T_1 definition, eq. (224):

$$T_1 = \frac{(C_f^G)^2 (g_{f,V}^G)^2}{(2\pi)^4} \left\{ \frac{1 + (1-z)^2}{z} \epsilon^2 \frac{(2\pi)^2}{\epsilon} \frac{p}{\left(p^2 + \epsilon^2\right)} I_3(z, p) \right.$$

$$\left. + z \left[(m_b - m_a) + z m_a\right]^2 \frac{(2\pi)^2}{p^2 + \epsilon^2} I_1(z, p) \right\}$$

$$T_1 = \frac{(C_f^G)^2 (g_{f,V}^G)^2}{(2\pi)^2} \left\{ \frac{1 + (1-z)^2}{z} \epsilon \frac{p}{\left(p^2 + \epsilon^2\right)} I_3(z, p) \right.$$

$$\left. + z \left[(m_b - m_a) + z m_a\right]^2 \frac{1}{p^2 + \epsilon^2} I_1(z, p) \right\}. \tag{227}$$

To obtain the parton-target cross-section, we need to evaluate T_2 and T_3 still. So, for T_2:

$$T_2 = \frac{(\mathcal{C}_f^G)^2 (g_{f,V}^G)^2}{(2\pi)^4} \int \mathrm{d}^2 \boldsymbol{r} \int \mathrm{d}^2 \boldsymbol{r}' e^{i\boldsymbol{p}\cdot(\boldsymbol{r}-\boldsymbol{r}')} \left\{ \frac{1+(1-z)^2}{z} \frac{\boldsymbol{r}\cdot\boldsymbol{r}'}{rr'} \epsilon^2 \mathrm{K}_1(\epsilon r) \mathrm{K}_1(\epsilon r') \right.$$

$$\left. + z\left[(m_b - m_a) + zm_a\right]^2 \mathrm{K}_0(\epsilon r) \mathrm{K}_0(\epsilon r') \right\} \sigma_{q\bar{q}}(z\boldsymbol{r}', x),$$

$$T_2 = \frac{(\mathcal{C}_f^G)^2 (g_{f,V}^G)^2}{(2\pi)^4} \left\{ \frac{1+(1-z)^2}{z} \epsilon^2 \Omega_1 + z\left[(m_b - m_a) + zm_a\right]^2 \Omega_2 \right\}, \tag{228}$$

where

$$\Omega_1 = \int \mathrm{d}^2 \boldsymbol{r} \mathrm{d}^2 \boldsymbol{r}' e^{i\boldsymbol{p}\cdot(\boldsymbol{r}-\boldsymbol{r}')} \frac{\boldsymbol{r}\cdot\boldsymbol{r}'}{rr'} \mathrm{K}_1(\epsilon r) \mathrm{K}_1(\epsilon r') \sigma_{q\bar{q}}(z\boldsymbol{r}', x),$$

$$\Omega_2 = \int \mathrm{d}^2 \boldsymbol{r} \mathrm{d}^2 \boldsymbol{r}' e^{i\boldsymbol{p}\cdot(\boldsymbol{r}-\boldsymbol{r}')} \mathrm{K}_0(\epsilon r) \mathrm{K}_0(\epsilon r') \sigma_{q\bar{q}}(z\boldsymbol{r}', x),$$

now we have two more integrals to evaluate, they will be evaluated directly likewise Γ_2 was. Then,

$$\Omega_1 = \int \mathrm{d}^2 \boldsymbol{r} \mathrm{d}^2 \boldsymbol{r}' e^{i\boldsymbol{p}\cdot(\boldsymbol{r}-\boldsymbol{r}')} \frac{1}{2\pi i\epsilon} \int \mathrm{d}^2 \boldsymbol{l}\, e^{i\boldsymbol{l}\cdot\boldsymbol{r}} \frac{\boldsymbol{l}}{l^2 + \epsilon^2} \cdot \frac{\boldsymbol{r}'}{r'} \mathrm{K}_1(\epsilon r') \sigma_{q\bar{q}}(z\boldsymbol{r}', x),$$

$$\Omega_1 = \frac{1}{2\pi i\epsilon} \int \mathrm{d}^2 \boldsymbol{r}' \mathrm{d}^2 \boldsymbol{l} \frac{1}{l^2 + \epsilon^2} e^{-i\boldsymbol{p}\cdot\boldsymbol{r}'} \frac{\boldsymbol{l}\cdot\boldsymbol{r}'}{r'} \mathrm{K}_1(\epsilon r') \sigma_{q\bar{q}}(z\boldsymbol{r}', x) \int \mathrm{d}^2 \boldsymbol{r}\, e^{i\boldsymbol{r}\cdot(\boldsymbol{l}+\boldsymbol{p})},$$

$$\Omega_1 = \frac{1}{2\pi i\epsilon} \int \mathrm{d}^2 \boldsymbol{r}' \mathrm{d}^2 \boldsymbol{l} \frac{1}{l^2 + \epsilon^2} e^{-i\boldsymbol{p}\cdot\boldsymbol{r}'} \frac{\boldsymbol{l}\cdot\boldsymbol{r}'}{r'} \mathrm{K}_1(\epsilon r') \sigma_{q\bar{q}}(z\boldsymbol{r}', x) (2\pi)^2 \delta^{(2)}(\boldsymbol{l}+\boldsymbol{p}),$$

$$\Omega_1 = \frac{2\pi}{i\epsilon} \frac{1}{p^2 + \epsilon^2} \int \mathrm{d}r' \mathrm{d}\phi\, r' e^{-i\boldsymbol{p}\cdot\boldsymbol{r}'} (-p) \cos\phi \mathrm{K}_1(\epsilon r') \sigma_{q\bar{q}}(z\boldsymbol{r}', x),$$

assuming $\boldsymbol{p} = -\boldsymbol{p}$, one have

$$\Omega_1 = \frac{(2\pi)^2}{\epsilon} \frac{p}{p^2 + \epsilon^2} \int \mathrm{d}r'\, r' J_1(pr') \mathrm{K}_1(\epsilon r') \sigma_{q\bar{q}}(z\boldsymbol{r}', x),$$

$$\Omega_1 = \frac{(2\pi)^2}{\epsilon} \frac{p}{p^2 + \epsilon^2} I_3(z, p).$$

Doing the calculations of Ω_2:

$$\Omega_2 = \int \mathrm{d}^2 \boldsymbol{r} \mathrm{d}^2 \boldsymbol{r}' e^{i\boldsymbol{p}\cdot(\boldsymbol{r}-\boldsymbol{r}')} \frac{1}{2\pi} \int \mathrm{d}^2 \boldsymbol{l} \frac{e^{i\boldsymbol{l}\cdot\boldsymbol{r}'}}{l^2 + \epsilon^2} \mathrm{K}_0(\epsilon r') \sigma_{q\bar{q}}(z\boldsymbol{r}', x)$$

$$\Omega_2 = \frac{1}{2\pi} \int \mathrm{d}^2 \boldsymbol{r}' \mathrm{d}^2 \boldsymbol{l}\, e^{-i\boldsymbol{p}\cdot\boldsymbol{r}'} \mathrm{K}_0(\epsilon r') \sigma_{q\bar{q}}(z\boldsymbol{r}', x) \frac{1}{l^2 + \epsilon^2} \int \mathrm{d}^2 \boldsymbol{r} e^{i\boldsymbol{r}\cdot(\boldsymbol{l}+\boldsymbol{p})}$$

$$\Omega_2 = \frac{1}{2\pi} \int \mathrm{d}^2 \boldsymbol{r}' \mathrm{d}^2 \boldsymbol{l}\, e^{-i\boldsymbol{p}\cdot\boldsymbol{r}'} \mathrm{K}_0(\epsilon r') \sigma_{q\bar{q}}(z\boldsymbol{r}', x) \frac{1}{l^2 + \epsilon^2} (2\pi)^2 \delta^{(2)}(\boldsymbol{l}+\boldsymbol{p})$$

$$\Omega_2 = \frac{2\pi}{(-\boldsymbol{p})^2 + \epsilon^2} \int \mathrm{d}r' \mathrm{d}\phi\, r' e^{-i\boldsymbol{p}\cdot\boldsymbol{r}'} \mathrm{K}_0(\epsilon r') \sigma_{q\bar{q}}(z\boldsymbol{r}', x)$$

$$\Omega_2 = \frac{(2\pi)^2}{p^2 + \epsilon^2} \int \mathrm{d}r' \, r' J_0(pr') \mathrm{K}_0\left(\epsilon r'\right) \sigma_{q\bar{q}}(z\boldsymbol{r}', x)$$

$$\Omega_2 = \frac{(2\pi)^2}{p^2 + \epsilon^2} I_1(z, p),$$

returning these results to T_2, eq.(228), then

$$T_2 = \frac{(\mathcal{C}_f^G)^2 (g_{f,V}^G)^2}{(2\pi)^4} \left\{ \frac{1 + (1-z)^2}{z} \epsilon^2 \frac{(2\pi)^2}{\epsilon} \frac{p}{p^2 + \epsilon^2} I_3(z, p) \, , \right.$$

$$\left. + z \left[(m_b - m_a) + z m_a\right]^2 \frac{(2\pi)^2}{p^2 + \epsilon^2} I_1(z, p) \right\}$$

$$T_2 = \frac{(\mathcal{C}_f^G)^2 (g_{f,V}^G)^2}{(2\pi)^2} \left\{ \frac{1 + (1-z)^2}{z} \epsilon \frac{p}{p^2 + \epsilon^2} I_3(z, p) \, , \right.$$

$$\left. + z \left[(m_b - m_a) + z m_a\right]^2 \frac{1}{p^2 + \epsilon^2} I_1(z, p) \right\}. \tag{229}$$

At last, we need to evaluate T_3 (eq.(223)), which is defined as

$$T_3 = -\frac{(\mathcal{C}_f^G)^2 (g_{f,V}^G)^2}{(2\pi)^4} \int \mathrm{d}^2\boldsymbol{r} \int \mathrm{d}^2\boldsymbol{r}' e^{i\boldsymbol{p}\cdot(\boldsymbol{r}-\boldsymbol{r}')} \left\{ \frac{1 + (1-z)^2}{z} \frac{\boldsymbol{r} \cdot \boldsymbol{r}'}{rr'} \epsilon^2 \mathrm{K}_1(\epsilon r) \mathrm{K}_1(\epsilon r') \right.$$

$$\left. + z \left[(m_b - m_a) + z m_a\right]^2 \mathrm{K}_0(\epsilon r) \mathrm{K}_0(\epsilon r') \right\} \sigma_{q\bar{q}}(z|\boldsymbol{r} - \boldsymbol{r}'|, x)$$

$$T_3 = -\frac{(\mathcal{C}_f^G)^2 (g_{f,V}^G)^2}{(2\pi)^4} \left\{ \frac{1 + (1-z)^2}{z} \epsilon^2 \chi_1 + z \left[(m_b - m_a) + z m_a\right]^2 \chi_2 \right\}, \tag{230}$$

where

$$\chi_1 = \int \mathrm{d}^2\boldsymbol{r} \mathrm{d}^2\boldsymbol{r}' e^{i\boldsymbol{p}\cdot(\boldsymbol{r}-\boldsymbol{r}')} \frac{\boldsymbol{r} \cdot \boldsymbol{r}'}{rr'} \mathrm{K}_1(\epsilon r) \mathrm{K}_1(\epsilon r') \sigma_{q\bar{q}}(z|\boldsymbol{r} - \boldsymbol{r}'|, x),$$

$$\chi_2 = \int \mathrm{d}^2\boldsymbol{r} \mathrm{d}^2\boldsymbol{r}' e^{i\boldsymbol{p}\cdot(\boldsymbol{r}-\boldsymbol{r}')} \mathrm{K}_0(\epsilon r) \mathrm{K}_0(\epsilon r') \sigma_{q\bar{q}}(z|\boldsymbol{r} - \boldsymbol{r}'|, x),$$

before we start the calculation of χ_1 and χ_2, is important to do a shift in the integral variables in order to the ride of the angular dependency in the dipole model argument. Let's assume:

$$\boldsymbol{\eta} = \boldsymbol{r} - \boldsymbol{r}'; \qquad \boldsymbol{\eta}' = \boldsymbol{r}'; \qquad \boldsymbol{\eta} + \boldsymbol{\eta}' = \boldsymbol{r}.$$

Thus, χ_1, is rewrite as

$$\chi_1 = \int \mathrm{d}^2\boldsymbol{\eta} \mathrm{d}^2\boldsymbol{\eta}' e^{i\boldsymbol{p}\cdot\boldsymbol{\eta}} \frac{(\boldsymbol{\eta} + \boldsymbol{\eta}') \cdot \boldsymbol{\eta}'}{|\boldsymbol{\eta} + \boldsymbol{\eta}'| \eta'} \mathrm{K}_1(\epsilon |\boldsymbol{\eta} + \boldsymbol{\eta}'|) \mathrm{K}_1(\epsilon \eta') \sigma_{q\bar{q}}(z\boldsymbol{\eta}, x),$$

$$\chi_1 = \int \mathrm{d}^2\boldsymbol{\eta} \mathrm{d}^2\boldsymbol{\eta}' e^{i\boldsymbol{p}\cdot\boldsymbol{\eta}} \frac{1}{2\pi i \epsilon} \int \mathrm{d}^2\boldsymbol{l} e^{i\boldsymbol{l}\cdot(\boldsymbol{\eta}+\boldsymbol{\eta}')} \frac{\boldsymbol{l}}{l^2 + \epsilon^2} \cdot \frac{1}{2\pi i \epsilon} \int \mathrm{d}^2\boldsymbol{l}' e^{i\boldsymbol{l}'\cdot\boldsymbol{\eta}'} \frac{\boldsymbol{l}'}{l'^2 + \epsilon^2} \sigma_{q\bar{q}}(z\boldsymbol{\eta}, x),$$

$$\chi_1 = \int \mathrm{d}^2\boldsymbol{\eta}\mathrm{d}^2\boldsymbol{\eta}' e^{i\boldsymbol{p}\cdot\boldsymbol{\eta}} \frac{1}{2\pi i\epsilon} \int \mathrm{d}^2\boldsymbol{l} e^{i\boldsymbol{l}\cdot(\boldsymbol{\eta}+\boldsymbol{\eta}')} \frac{\boldsymbol{l}}{l^2+\epsilon^2} \cdot \frac{1}{2\pi i\epsilon} \int \mathrm{d}^2\boldsymbol{l}' e^{i\boldsymbol{l}'\cdot\boldsymbol{\eta}'} \frac{\boldsymbol{l}'}{l'^2+\epsilon^2} \sigma_{q\bar{q}}(z\boldsymbol{\eta},x),$$

$$\chi_1 = \frac{1}{(2\pi i\epsilon)^2} \int \mathrm{d}^2\eta e^{i\boldsymbol{p}\cdot\boldsymbol{\eta}} \sigma_{q\bar{q}}(z\boldsymbol{\eta},x) \int \mathrm{d}^2\boldsymbol{l}'\mathrm{d}^2\boldsymbol{l} e^{i\boldsymbol{l}\cdot\boldsymbol{\eta}} \frac{\boldsymbol{l}}{l^2+\epsilon^2} \cdot \frac{\boldsymbol{l}'}{l'^2+\epsilon^2} \int \mathrm{d}^2\eta e^{i\boldsymbol{\eta}\cdot(\boldsymbol{l}+\boldsymbol{l}')}$$

$$\chi_1 = \frac{1}{(2\pi i\epsilon)^2} \int \mathrm{d}^2\eta e^{i\boldsymbol{p}\cdot\boldsymbol{\eta}} \sigma_{q\bar{q}}(z\boldsymbol{\eta},x) \int \mathrm{d}^2\boldsymbol{l}'\mathrm{d}^2\boldsymbol{l} e^{i\boldsymbol{l}\cdot\boldsymbol{\eta}} \frac{\boldsymbol{l}}{l^2+\epsilon^2} \cdot \frac{\boldsymbol{l}'}{l'^2+\epsilon^2} (2\pi)^2 \delta^{(2)}(\boldsymbol{l}+\boldsymbol{l}')$$

$$\chi_1 = \frac{(2\pi)^2}{(2\pi i\epsilon)^2} \int \mathrm{d}^2\eta e^{i\boldsymbol{p}\cdot\boldsymbol{\eta}} \sigma_{q\bar{q}}(z\boldsymbol{\eta},x) \int \mathrm{d}^2\boldsymbol{l} e^{i\boldsymbol{l}\cdot\boldsymbol{\eta}} \frac{-\boldsymbol{l}\cdot\boldsymbol{l}}{(l^2+\epsilon^2)^2}$$

inserting $-\epsilon^2 + \epsilon^2$, i.e., a zero, the equation above become

$$\chi_1 = \frac{(2\pi)^2}{(2\pi i\epsilon)^2} \int \mathrm{d}^2\eta e^{i\boldsymbol{p}\cdot\boldsymbol{\eta}} \sigma_{q\bar{q}}(z\boldsymbol{\eta},x) \int \mathrm{d}^2\boldsymbol{l} e^{i\boldsymbol{l}\cdot\boldsymbol{\eta}} \frac{-(\boldsymbol{l}\cdot\boldsymbol{l}-\epsilon^2+\epsilon^2)}{(l^2+\epsilon^2)^2}$$

$$\chi_1 = \frac{1}{\epsilon^2} \int \mathrm{d}^2\eta e^{i\boldsymbol{p}\cdot\boldsymbol{\eta}} \sigma_{q\bar{q}}(z\boldsymbol{\eta},x) \int \mathrm{d}^2\boldsymbol{l} e^{i\boldsymbol{l}\cdot\boldsymbol{\eta}} \frac{(l^2+\epsilon^2)}{(l^2+\epsilon^2)^2}$$
$$- \frac{1}{\epsilon^2} \int \mathrm{d}^2\eta e^{i\boldsymbol{p}\cdot\boldsymbol{\eta}} \sigma_{q\bar{q}}(z\boldsymbol{\eta},x) \int \mathrm{d}^2\boldsymbol{l} e^{i\boldsymbol{l}\cdot\boldsymbol{\eta}} \frac{\epsilon^2}{(l^2+\epsilon^2)^2}$$

$$\chi_1 = \frac{1}{\epsilon^2} \int \mathrm{d}^2\eta e^{i\boldsymbol{p}\cdot\boldsymbol{\eta}} \sigma_{q\bar{q}}(z\boldsymbol{\eta},x) \int \mathrm{d}^2\boldsymbol{l} e^{i\boldsymbol{l}\cdot\boldsymbol{\eta}} \frac{1}{l^2+\epsilon^2}$$
$$- \int \mathrm{d}^2\boldsymbol{\eta} e^{i\boldsymbol{p}\cdot\boldsymbol{\eta}} \sigma_{q\bar{q}}(z\boldsymbol{\eta},x) \int \mathrm{d}^2\boldsymbol{l} e^{i\boldsymbol{l}\cdot\boldsymbol{\eta}} \frac{1}{(l^2+\epsilon^2)^2}$$

$$\chi_1 = \frac{1}{\epsilon^2} \int \mathrm{d}^2\eta e^{i\boldsymbol{p}\cdot\boldsymbol{\eta}} \sigma_{q\bar{q}}(z\boldsymbol{\eta},x) 2\pi\mathrm{K}_0(\epsilon\eta)$$
$$- \int \mathrm{d}^2\eta e^{i\boldsymbol{p}\cdot\boldsymbol{\eta}} \sigma_{q\bar{q}}(z\boldsymbol{\eta},x) \frac{\pi}{\epsilon} \eta\mathrm{K}_1(\epsilon\eta)$$

$$\chi_1 = \frac{2\pi}{\epsilon^2} \int \mathrm{d}\eta\mathrm{d}\phi \, \eta e^{i\boldsymbol{p}\cdot\boldsymbol{\eta}} \sigma_{q\bar{q}}(z\boldsymbol{\eta},x)\mathrm{K}_0(\epsilon\eta)$$
$$- \frac{\pi}{\epsilon} \int \mathrm{d}\eta\mathrm{d}\phi \, \eta^2 e^{i\boldsymbol{p}\cdot\boldsymbol{\eta}} \sigma_{q\bar{q}}(z\boldsymbol{\eta},x)\mathrm{K}_1(\epsilon\eta)$$

$$\chi_1 = \frac{(2\pi)^2}{\epsilon^2} \int \mathrm{d}\eta \, \eta J_0(p\eta) \mathrm{K}_0(\epsilon\eta) \sigma_{q\bar{q}}(z\boldsymbol{\eta},x)$$
$$- \frac{2\pi^2}{\epsilon} \int \mathrm{d}\eta \, \eta^2 J_0(p\eta) \mathrm{K}_1(\epsilon\eta)\sigma_{q\bar{q}}(z\boldsymbol{\eta},x)$$

$$\chi_1 = \frac{(2\pi)^2}{\epsilon^2} I_1(z,p) - \frac{2\pi^2}{\epsilon} I_2(z,p),$$

where we have used the definition of K_1 in it's two integrals forms. Moreover, we have defined

$$I_2(z,p) = \mathrm{d}\eta \, \eta^2 J_0(p\eta) \mathrm{K}_1(\epsilon\eta)\sigma_{q\bar{q}}(z\boldsymbol{\eta},x).$$

For χ_2:

$$\chi_2 = \int \mathrm{d}^2\boldsymbol{\eta}\mathrm{d}^2\boldsymbol{\eta}' e^{i\boldsymbol{p}\cdot\boldsymbol{\eta}} \mathrm{K}_0(\epsilon\,|\boldsymbol{\eta}+\boldsymbol{\eta}'|)\mathrm{K}_0(\epsilon\eta')\sigma_{q\bar{q}}(z\boldsymbol{\eta},x),$$

$$\chi_2 = \int \mathrm{d}^2\boldsymbol{\eta}\mathrm{d}^2\boldsymbol{\eta}' e^{i\boldsymbol{p}\cdot\boldsymbol{\eta}}\frac{1}{2\pi}\int \mathrm{d}^2\boldsymbol{l}\,\frac{e^{i\boldsymbol{l}\cdot(\boldsymbol{\eta}+\boldsymbol{\eta}')}}{l^2+\epsilon^2}\frac{1}{2\pi}\int \mathrm{d}^2\boldsymbol{l}'\,\frac{e^{i\boldsymbol{l}'\cdot\boldsymbol{\eta}'}}{l'^2+\epsilon^2}\sigma_{q\bar{q}}(z\boldsymbol{\eta},x),$$

$$\chi_2 = \frac{1}{(2\pi)^2}\int \mathrm{d}^2\boldsymbol{\eta}\mathrm{d}^2\boldsymbol{l}\mathrm{d}^2\boldsymbol{l}' e^{i\boldsymbol{p}\cdot\boldsymbol{\eta}}\sigma_{q\bar{q}}(z\boldsymbol{\eta},x)\frac{e^{i\boldsymbol{l}\cdot\boldsymbol{\eta}}}{(l^2+\epsilon^2)(l'^2+\epsilon^2)}\int \mathrm{d}^2\boldsymbol{\eta}'\,e^{i\boldsymbol{\eta}'\cdot(\boldsymbol{l}+\boldsymbol{l}')}$$

$$\chi_2 = \frac{1}{(2\pi)^2}\int \mathrm{d}^2\boldsymbol{\eta}\mathrm{d}^2\boldsymbol{l}\mathrm{d}^2\boldsymbol{l}' e^{i\boldsymbol{p}\cdot\boldsymbol{\eta}}\sigma_{q\bar{q}}(z\boldsymbol{\eta},x)\frac{e^{i\boldsymbol{l}\cdot\boldsymbol{\eta}}}{(l^2+\epsilon^2)(l'^2+\epsilon^2)}(2\pi)^2\,\delta^{(2)}\left(\boldsymbol{l}+\boldsymbol{l}'\right)$$

$$\chi_2 = \int \mathrm{d}^2\boldsymbol{\eta}\mathrm{d}^2\boldsymbol{l} e^{i\boldsymbol{p}\cdot\boldsymbol{\eta}}\sigma_{q\bar{q}}(z\boldsymbol{\eta},x)\frac{e^{-i\boldsymbol{l}\cdot\boldsymbol{\eta}}}{(l^2+\epsilon^2)^2}$$

defining $-\boldsymbol{l}=\boldsymbol{l}$,

$$\chi_2 = \int \mathrm{d}^2\boldsymbol{\eta} e^{i\boldsymbol{p}\cdot\boldsymbol{\eta}}\sigma_{q\bar{q}}(z\boldsymbol{\eta},x)\int \mathrm{d}^2\boldsymbol{l}\,\frac{e^{i\boldsymbol{l}\cdot\boldsymbol{\eta}}}{(l^2+\epsilon^2)^2}$$

$$\chi_2 = \int \mathrm{d}\eta\mathrm{d}\phi\,\eta e^{i\boldsymbol{p}\cdot\boldsymbol{\eta}}\frac{\pi\eta}{\epsilon}\mathrm{K}_1\left(\epsilon\eta\right)\sigma_{q\bar{q}}(z\boldsymbol{\eta},x)$$

$$\chi_2 = \frac{2\pi^2}{\epsilon}\int \mathrm{d}\eta\,\eta^2 J_0\left(p\eta\right)\mathrm{K}_1\left(\epsilon\eta\right)\sigma_{q\bar{q}}(z\boldsymbol{\eta},x)$$

$$\chi_2 = \frac{2\pi^2}{\epsilon}I_2(z,p).$$

Returning to eq.(230),

$$T_3 = -\frac{(\mathcal{C}_f^G)^2(g_{f,V}^G)^2}{(2\pi)^4}\left\{\frac{1+(1-z)^2}{z}\epsilon^2\left[\frac{(2\pi)^2}{\epsilon^2}I_1(z,p)-\frac{2\pi^2}{\epsilon}I_2(z,p)\right]\right.$$

$$\left.+z\left[(m_b-m_a)+zm_a\right]^2\frac{2\pi^2}{\epsilon}I_2(z,p)\right\},$$

$$T_3 = -\frac{(\mathcal{C}_f^G)^2(g_{f,V}^G)^2}{(2\pi)^2}\left\{\frac{1+(1-z)^2}{z}\left[I_1(z,p)-\frac{\epsilon}{2}I_2(z,p)\right]+z\frac{1}{2\epsilon}\left[(m_b-m_a)+zm_a\right]^2 I_2(z,p)\right\}.$$

$$\tag{231}$$

Assemble T_1, T_2 and T_3 (eq. (227), eq. (229) and eq. (231)) together, we get the parton-target cross-section for the transverse-vector contribution which is [1]

$$\frac{\mathrm{d}\sigma_T^f}{\mathrm{d}z\mathrm{d}^2\boldsymbol{p}}\bigg|_V = \frac{\beta}{(2\pi)^2}\frac{1+(1-z)^2}{z}\epsilon\frac{p}{(p^2+\epsilon^2)}I_3(z,p)+\frac{\beta}{(2\pi)^2}z\left[(m_b-m_a)+zm_a\right]^2\frac{1}{p^2+\epsilon^2}I_1(z,p)$$

$$\frac{\beta}{(2\pi)^2}\frac{1+(1-z)^2}{z}\epsilon\frac{p}{(p^2+\epsilon^2)}I_3(z,p)+\frac{\beta}{(2\pi)^2}z\left[(m_b-m_a)+zm_a\right]^2\frac{1}{p^2+\epsilon^2}I_1(z,p)$$

$$-\frac{\beta}{(2\pi)^2}\frac{1+(1-z)^2}{z}I_1(z,p)+\frac{\beta}{(2\pi)^2}\frac{1+(1-z)^2}{z}\frac{\epsilon}{2}I_2(z,p)$$

---

[1] using $\beta=(\mathcal{C}_f^G)^2(g_{f,V}^G)^2$

$$- \frac{\beta}{(2\pi)^2} z \frac{1}{2\epsilon} \left[(m_b - m_a) + z m_a \right]^2 I_2(z, p)$$

gathering the same pre-factor terms, we obtain

$$\frac{\mathrm{d}\sigma_T^f}{\mathrm{d}z\mathrm{d}^2\boldsymbol{p}}\bigg|_V = \frac{\beta}{(2\pi)^2} \left\{ \frac{1 + (1-z)^2}{z} \left[\epsilon \frac{p}{(p^2 + \epsilon^2)} I_3(z,p) + \epsilon \frac{p}{(p^2 + \epsilon^2)} I_3(z,p) - I_1(z,p) + \frac{\epsilon}{2} I_2(z,p) \right] \right.$$
$$\left. + z \left[(m_b - m_a) + z m_a \right]^2 \left(\frac{1}{p^2 + \epsilon^2} I_1(z,p) + \frac{1}{p^2 + \epsilon^2} I_1(z,p) - \frac{1}{2\epsilon} I_2(z,p) \right) \right\}$$

$$z\frac{\mathrm{d}\sigma_T^f}{\mathrm{d}z\mathrm{d}^2\boldsymbol{p}}\bigg|_V = \frac{\beta}{(2\pi)^2} \left\{ \left(1 + (1-z)^2 \right) \epsilon^2 \left[\frac{2}{\epsilon} \frac{p}{(p^2 + \epsilon^2)} I_3(z,p) - \frac{1}{\epsilon^2} I_1(z,p) + \frac{1}{2\epsilon} I_2(z,p) \right] \right.$$
$$\left. + z^2 \left[(m_b - m_a) + z m_a \right]^2 \left(\frac{2}{p^2 + \epsilon^2} I_1(z,p) - \frac{1}{2\epsilon} I_2(z,p) \right) \right\}$$

$$z\frac{\mathrm{d}\sigma_T^f}{\mathrm{d}z\mathrm{d}^2\boldsymbol{p}}\bigg|_V = \frac{\beta}{2\pi^2} \left\{ \left(1 + (1-z)^2 \right) \epsilon^2 \left[\frac{1}{\epsilon} \frac{p}{(p^2 + \epsilon^2)} I_3(z,p) - \frac{1}{2\epsilon^2} I_1(z,p) + \frac{1}{4\epsilon} I_2(z,p) \right] \right.$$
$$\left. + z^2 \left[(m_b - m_a) + z m_a \right]^2 \left(\frac{1}{p^2 + \epsilon^2} I_1(z,p) - \frac{1}{4\epsilon} I_2(z,p) \right) \right\}$$

$$z\frac{\mathrm{d}\sigma_T^f}{\mathrm{d}z\mathrm{d}^2\boldsymbol{p}}\bigg|_V = \frac{(\mathcal{C}_f^G)^2 (g_{f,V}^G)^2}{2\pi^2} \left\{ z^2 \left[(m_b - m_a) + z m_a \right]^2 \mathcal{D}_1(z,p,\epsilon) + \left[1 + (1-z)^2 \right] \epsilon^2 \mathcal{D}_2(z,p,\epsilon) \right\},$$

(232)

where we have defined the auxiliary functions:

$$\mathcal{D}_1(z,p,\epsilon) \equiv \left[\frac{1}{(p^2 + \epsilon^2)} I_1(z,p) - \frac{1}{4\epsilon} I_2(z,p) \right] \tag{233}$$

$$\mathcal{D}_2(z,p,\epsilon) \equiv \left[\frac{1}{\epsilon} \frac{p}{(p^2 + \epsilon^2)} I_3(z,p) - \frac{1}{2\epsilon^2} I_1(z,p) + \frac{1}{4\epsilon} I_2(z,p) \right]. \tag{234}$$

Similarly, doing the step-by-step process shown before, substituting the expression for $\rho_V^A(z, \boldsymbol{r}, \boldsymbol{r}')$, one has that the axial contribution is given by:

$$z\frac{d\sigma_T^f}{dz d^2\boldsymbol{p}}|_A = \frac{(\mathcal{C}_f^G)^2 (g_{a,f}^G)^2}{2\pi^2} \left\{ z^2 [(m_b + m_a) - z m_a]^2 \mathcal{D}_1(z,p,\epsilon) \right.$$
$$\left. + [1 + (1-z)^2] \epsilon^2 \, \mathcal{D}_2(z,p,\epsilon) \right\} \tag{235}$$

Furthermore, for the longitudinal polarization, results that the vector contribution is given by

$$z\frac{d\sigma_L^f}{dz d^2\boldsymbol{p}}|_V = \frac{(\mathcal{C}_f^G)^2 (g_{v,f}^G)^2}{4\pi^2} \left\{ \frac{(z^2 m_a (m_b - m_a) - z(m_b^2 - m_a^2) - 2(1-z) M_G^2)^2}{M_G^2} \mathcal{D}_1(z,p,\epsilon) \right.$$

$$+\frac{z^2(m_b - m_a)^2}{M_G^2}\epsilon^2 \mathcal{D}_2(z,p,\epsilon)\Big\}m \tag{236}$$

while the axial contribution can be written as

$$z\frac{d\sigma_L^f}{dzd^2\boldsymbol{p}}\Big|_A \quad = \quad \frac{(\mathcal{C}_f^G)^2(g_{a,f}^G)^2}{4\pi^2}\Big\{\frac{(z^2 m_a(m_b + m_a) + z(m_b^2 - m_a^2) + 2(1-z)M_G^2)^2}{M_G^2}\mathcal{D}_1(z,p,\epsilon)$$

$$+\frac{\epsilon^2 z^2(m_b + m_a)^2}{M_G^2}\mathcal{D}_2(z,p,\epsilon)\Big\}\,. \tag{237}$$

D.1 Particular cases

D.1.1 Real photon produciton

The simplest case that which we can apply the expressions derived in the previous section is the real photon production in the $qp \to \gamma X$ process. For the production of a real photon, one has that $g_{a,f}^\gamma = 0$, $g_{v,f}^\gamma = 1$, $\mathcal{C}_f^\gamma = \sqrt{\alpha_{em}}e_f$, $M_G^2 = 0$ and $m_a = m_b = m_f$. Moreover, the longitudinal polarization does not contribute. Consequently, the differential cross-section will be given in the impact parameter space by

$$z\frac{d\sigma_T^f}{dzd^2\boldsymbol{p}}\Bigg|_{qp\to\gamma X} \quad = \quad \frac{\alpha_{em}e_f^2}{2\pi^2}\left\{m_f^2 z^4\,\mathcal{D}_1(z,p,\epsilon) + [1 + (1-z)^2]\epsilon^2\,\mathcal{D}_2(z,p,\epsilon)\right\} \tag{238}$$

with $\epsilon^2 = z^2 m_f^2$. Such an expression was used as input in the calculations of the cross-section for the real photon production in pp collisions performed e.g. in Refs. (Kopeliovich; Rezaeian; Pirner; Schmidt, 2007; Kopeliovich; Levin; Rezaeian; Schmidt, 2009; Santos; Silveira; Machado, 2020) using the color dipole formalism.

D.1.1.1 Drell - Yan process

Another possible application of our results is the emission of an off-mass shell gauge boson G^* that decays into a dilepton system with invariant mass M, characteristic of the Drell - Yan (DY) process. For $G^* = \gamma^*$ and Z^*, one has the production of l^+l^- system in the final state and such a process was analyzed largely in the literature using the color dipole and CGC formalisms. The results derived in this appendix can be directly applied for such case, taking into account the DY description shown in Chap. 4,

$$\frac{d\sigma(qp \to [G^* \to l\bar{l}]X)}{dzd^2\boldsymbol{p}dM^2} = \mathcal{F}_G(M)\frac{d\sigma(qp \to G^*X)}{dzd^2\boldsymbol{p}}\,. \tag{239}$$

For the particular case of a virtual photon ($G^* = \gamma^*$) with virtuality M^2, one has that the axial contributions vanishes and differential cross-section for the $qp \to [\gamma^* \to l\bar{l}]X$

process will be given in the impact parameter space by

$$
\begin{aligned}
z\frac{d\sigma^f_{total}}{dzd^2\boldsymbol{p}dM^2}\bigg|_{DY} &= z\frac{d\sigma^f_T}{dzd^2\boldsymbol{p}dM^2}\bigg|_V + z\frac{d\sigma^f_L}{dzd^2\boldsymbol{p}dM^2}\bigg|_V \\
&= \frac{\alpha_{em}e_f^2}{2\pi^2}\mathcal{F}_\gamma(M)\Big\{\big[m_f^2z^4 + 2M^2\left(1-z\right)^2\big]\,\mathcal{D}_1(z,p,\epsilon) \\
&\quad + [1+(1-z)^2]\epsilon^2\,\mathcal{D}_2(z,p,\epsilon)\Big\}
\end{aligned}
\tag{240}
$$

with $\epsilon^2 = (1-z)M^2 + z^2m_f^2$. Such an expression was used e.g. in Ref. (Kopeliovich; Raufeisen; Tarasov, 2001; Raufeisen; Peng; Nayak, 2002; Kopeliovich; Raufeisen; Tarasov; Johnson, 2003; Betemps; Gay ducati, 2004; Betemps; Ducati; Machado; Raufeisen, 2003; Golec-biernat; Lewandowska; Stasto, 2010; Ducati; Griep; Machado, 2014; Schäfer; Szczurek, 2016; Ducloué, 2017) to estimate the DY production in hadronic collisions at the LHC, assuming different models for the dipole - target cross-section.

D.2 The color transparency regime

The behavior of the spectrum for the electroweak gauge boson production is strongly dependent on the dipole–proton cross–section, which is determined by the QCD dynamics at high energies. In recent years, several groups have proposed distinct models for this quantity, some derived from the solutions of the Balitsky–Kovchegov equation (Albacete; Armesto; Milhano; Salgado, 2009; Albacete; Armesto; Milhano; Quiroga-arias; Salgado, 2011) or inspired by its solutions in the saturation and linear regimes (Iancu; Itakura; Munier, 2004), and others based on a particular phenomenological ansatz (Kowalski; Teaney, 2003; Kowalski; Motyka; Watt, 2006; Watt; Kowalski, 2008). In general, the dependence on r^2 is non-trivial and energy dependent, which makes the calculation of the auxiliary functions $\mathcal{D}_i$'s present in the spectrum a hard task due to the presence of oscillatory functions in its definitions. Here we will analyze in more detail the color transparency regime, predicted to be valid when $\boldsymbol{r} \to 0$, which implies that the dipole–proton cross–section can be approximated by $\sigma_{q\bar{q}} \propto \boldsymbol{r}^2$. Such behavior is also denoted in the literature by r^2–approximation, and is expected to be valid when the impact of the saturation corrections is negligible. As we will demonstrate below, in this regime, it is possible to derive analytical expressions for the spectrum, which can be used to study the z and $\boldsymbol{p}$ dependencies in the linear regime and can be considered as a baseline for future comparisons with the results derived using more sophisticated models for the dipole–proton cross–section.

In order to perform our calculations, we will consider the linear prediction of the GBW model (Golec-biernat; Wusthoff, 1998, 1999), in which $\sigma_{q\bar{q}}(\boldsymbol{r},x) = \mathcal{C}(x)\boldsymbol{r}^2$ with $\mathcal{C}(x) = \sigma_0Q_s^2(x)/4$, where $Q_s = (x_0/x)^{\lambda/2}$ is the saturation scale and the parameters

σ_0, x_0 and λ are determined by a fit to the HERA data. In this approximation the $r-$integrals in the functions I_1, I_2 and I_3 can be performed analytically and are given by

$$I_1(z,p) = \int dr r \mathrm{J}_0(pr)\mathrm{K}_0(\epsilon r)\sigma_{q\bar{q}}(z\boldsymbol{r}) = \mathcal{C}(x)\frac{4z^2(\epsilon^2 - p^2)}{(p^2 + \epsilon^2)^3} \tag{241}$$

$$I_2(z,p) = \int dr r^2 \mathrm{J}_0(pr)\mathrm{K}_1(\epsilon r)\sigma_{q\bar{q}}(z\boldsymbol{r}) = \mathcal{C}(x)\frac{16z^2\epsilon(\epsilon^2 - 2p^2)}{(p^2 + \epsilon^2)^4} \tag{242}$$

$$I_3(z,p) = \int dr r \mathrm{J}_1(pr)\mathrm{K}_1(\epsilon r)\sigma_{q\bar{q}}(z\boldsymbol{r}) = \mathcal{C}(x)\frac{8z^2\epsilon p}{(p^2 + \epsilon^2)^3} \tag{243}$$

As a consequence, the auxiliary functions $\mathcal{D}_1(z,p,\epsilon)$ and $\mathcal{D}_2(z,p,\epsilon)$ can be expressed as follows

$$\mathcal{D}_1(z,p,\epsilon) = \frac{1}{(p^2+\epsilon^2)}\mathcal{C}(x)\frac{4z^2(\epsilon^2-p^2)}{(p^2+\epsilon^2)^3} - \frac{1}{4\epsilon}\mathcal{C}(x)\frac{16z^2\epsilon(\epsilon^2-2p^2)}{(p^2+\epsilon^2)^4} \tag{244}$$

$$\begin{aligned}\mathcal{D}_2(z,p,\epsilon) = & \frac{1}{\epsilon}\frac{p}{(p^2+\epsilon^2)}\mathcal{C}(x)\frac{8z^2\epsilon p}{(p^2+\epsilon^2)^3} \\ & -\frac{1}{2\epsilon^2}\mathcal{C}(x)\frac{4z^2(\epsilon^2-p^2)}{(p^2+\epsilon^2)^3} + \frac{1}{4\epsilon}\mathcal{C}(x)\frac{16z^2\epsilon(\epsilon^2-2p^2)}{(p^2+\epsilon^2)^4} \;,\end{aligned} \tag{245}$$

which can be simplified as

$$\mathcal{D}_1(z,p,\epsilon) = \mathcal{C}(x)\frac{4z^2p^2}{(p^2+\epsilon^2)^4} \tag{246}$$

$$\mathcal{D}_2(z,p,\epsilon) = \mathcal{C}(x)\frac{2z^2\epsilon^2}{(p^2+\epsilon^2)^4}\left[1+\frac{p^4}{\epsilon^4}\right] \;. \tag{247}$$

Such expressions can be used in eqs. (232)), (235), (236) and (237) to obtain the distinct contributions for the differential cross-section in the color transparency regime.

APPENDIX E – Frame transformation

In eq. (112) we present the full expression for the angular distribution in terms of density matrix elements, however using the eq. (114) one can connect the density matrix elements with the structure functions elements. Therefore, the angular distribution in terms of the structure functions at a given production plane frame F is:

$$\frac{dN}{d\Omega} \;=\; \frac{3}{8\pi}\frac{1}{2W_T + W_L}\left[g_T W_T + g_L W_L + g_\Delta W_\Delta + g_{\Delta\Delta} W_{\Delta\Delta} \right.$$

$$\left. + c_G g_{T_P} W_{T_P} + c_G g_{\nabla_P} W_{\nabla_P} + c_G g_\nabla W_\nabla + g_{\Delta\Delta_P} W_{\Delta\Delta_P} + g_{\Delta_P} W_{\Delta_P} \right], \quad (248)$$

where

$$g_T = 1 + \cos^2\theta\,, \qquad g_L = 1 - \cos^2\theta\,, \qquad g_{T_P} = 2\cos\theta\,,$$

$$g_{\Delta\Delta} = \sin^2\theta\cos 2\phi\,, \qquad g_\Delta = \sin 2\theta\cos\phi\,, \qquad g_{\nabla_P} = 2\sin\theta\cos\phi\,,$$

$$g_{\Delta\Delta_P} = \sin^2\theta\sin 2\phi\,, \qquad g_{\Delta_P} = \sin 2\theta\sin\phi\,, \qquad g_\nabla = 2\sin\theta\sin\phi\,. \quad (249)$$

We can parameterize the transformation from one observation frame to another by a single angle, describing a rotation around the y axis. The rotation matrix

$$R_y(\gamma) \;=\; \begin{pmatrix} \cos\gamma & 0 & -\sin\gamma \\ 0 & 1 & 0 \\ \sin\gamma & 0 & \cos\gamma \end{pmatrix} \quad (250)$$

transforms the components of a vector, reproducing the effect of a rotation of the Z and x axis in the production plane. The coordinates of the unit vector indicating the positive lepton direction in the *old* frame,

$$\hat{r} \;=\; (\sin\theta\cos\phi,\ \sin\theta\sin\phi,\ \cos\theta)\,, \quad (251)$$

can be expressed as a function of the coordinates in the new frame as

$$\sin\theta\cos\phi = \cos\gamma\sin\theta'\cos\phi' + \sin\gamma\cos\theta', \tag{252}$$

$$\sin\theta\sin\phi = \sin\theta\sin\phi, \tag{253}$$

$$\cos\theta = -\sin\gamma\sin\theta'\cos\phi' + \cos\gamma\cos\theta'. \tag{254}$$

Substituing eq. (252) into eq. (248), we obtain the angular distribution in the rotated frame

$$
\begin{aligned}
\frac{dN}{d\Omega} = {} & \frac{3}{8\pi}\frac{1}{2W_T + W_L}\Bigg\{ g_T\Big[\Big(1 - \frac{\sin^2\gamma}{2}\Big)W_T + \frac{\sin^2\gamma}{2}W_L + \frac{\sin 2\gamma}{2}W_\Delta + \frac{\sin^2\gamma}{2}W_{\Delta\Delta}\Big] \\
& + g_L\Big[\sin^2\gamma W_T + \cos^2\gamma W_L - \sin 2\gamma W_\Delta - \sin^2\gamma W_{\Delta\Delta}\Big] \\
& + g_\Delta\Big[-\frac{\sin 2\gamma}{2}W_T + \frac{\sin 2\gamma}{2}W_L + \cos 2\gamma W_\Delta + \frac{\sin 2\gamma}{2}W_{\Delta\Delta}\Big] \\
& + g_{\Delta\Delta}\Big[\frac{\sin^2\gamma}{2}W_T - \frac{\sin^2\gamma}{2}W_L - \frac{\sin 2\gamma}{2}W_\Delta + \Big(\frac{1-\sin^2\gamma}{2}\Big)W_{\Delta\Delta}\Big] \\
& + c_G g_{T_p}\Big[\cos\gamma W_{T_p} + \sin\gamma W_{\nabla_p}\Big] \\
& + c_G g_{\nabla_p}\Big[-\sin\gamma W_{T_p} + \cos\gamma W_{\nabla_p}\Big] \\
& + g_{\Delta\Delta_p}\Big[\cos\gamma W_{\Delta\Delta_p} - \sin\gamma W_{\Delta_p}\Big] \\
& + g_{\Delta_p}\Big[\sin\gamma W_{\Delta\Delta_p} + \cos\gamma W_{\Delta_p}\Big] \\
& + c_G g_\nabla W_\nabla\Bigg\}.
\end{aligned}
\tag{255}
$$

Therefore, comparing eq. (248) and eq. (255), we obtain the relation between the structure function in different frames,

$$
\begin{pmatrix} W_T \\ W_L \\ W_\Delta \\ W_{\Delta\Delta} \\ W_{T_p} \\ W_{\nabla_p} \\ W_{\Delta\Delta_p} \\ W_{\Delta_p} \\ W_\nabla \end{pmatrix}_F
=
\begin{pmatrix}
1 - \frac{\sin^2\gamma}{2} & \frac{\sin^2\gamma}{2} & \frac{\sin 2\gamma}{2} & \frac{\sin^2\gamma}{2} & 0 & 0 & 0 & 0 & 0 \\
\sin^2\gamma & \cos^2\gamma & -\sin 2\gamma & -\sin^2\gamma & 0 & 0 & 0 & 0 & 0 \\
-\frac{\sin 2\gamma}{2} & \frac{\sin 2\gamma}{2} & \cos 2\gamma & \frac{\sin 2\gamma}{2} & 0 & 0 & 0 & 0 & 0 \\
\frac{\sin^2\gamma}{2} & -\frac{\sin^2\gamma}{2} & -\frac{\sin 2\gamma}{2} & \frac{1-\sin^2\gamma}{2} & 0 & 0 & 0 & 0 & 0 \\
0 & 0 & 0 & 0 & \cos\gamma & \sin\gamma & 0 & 0 & 0 \\
0 & 0 & 0 & 0 & -\sin\gamma & \cos\gamma & 0 & 0 & 0 \\
0 & 0 & 0 & 0 & 0 & 0 & \cos\gamma & -\sin\gamma & 0 \\
0 & 0 & 0 & 0 & 0 & 0 & \sin\gamma & \cos\gamma & 0 \\
0 & 0 & 0 & 0 & 0 & 0 & 0 & 0 & 1
\end{pmatrix}
\begin{pmatrix} W_T \\ W_L \\ W_\Delta \\ W_{\Delta\Delta} \\ W_{T_p} \\ W_{\nabla_p} \\ W_{\Delta\Delta_p} \\ W_{\Delta_p} \\ W_\nabla \end{pmatrix}_{F'},
\tag{256}
$$

To connect the GJ frame with the CS frame, the angular relation is

$$\cos\gamma = \frac{1}{\sqrt{1+\beta^2}}, \qquad \sin\gamma = \frac{\beta}{\sqrt{1+\beta^2}} \tag{257}$$

for $\beta = q/M$. Therefore,

$$
\begin{pmatrix} W_T \\ W_L \\ W_\Delta \\ W_{\Delta\Delta} \\ W_{T_p} \\ W_{\nabla_p} \\ W_{\Delta\Delta_p} \\ W_{\Delta_p} \\ W_\nabla \end{pmatrix}_{CS}
= \frac{1}{1+\beta^2}
\begin{pmatrix}
1+\frac{\beta^2}{2} & \frac{\beta^2}{2} & \beta & \frac{\beta^2}{2} & 0 & 0 & 0 & 0 & 0 \\
\beta^2 & 1 & -2\beta & -\beta^2 & 0 & 0 & 0 & 0 & 0 \\
-\beta & \beta & 1-\beta^2 & \beta & 0 & 0 & 0 & 0 & 0 \\
\frac{\beta^2}{2} & -\frac{\beta^2}{2} & -\beta & 1+\frac{\beta^2}{2} & 0 & 0 & 0 & 0 & 0 \\
0 & 0 & 0 & 0 & \sqrt{1+\beta^2} & \beta\sqrt{1+\beta^2} & 0 & 0 & 0 \\
0 & 0 & 0 & 0 & -\beta\sqrt{1+\beta^2} & \sqrt{1+\beta^2} & 0 & 0 & 0 \\
0 & 0 & 0 & 0 & 0 & 0 & \sqrt{1+\beta^2} & -\beta\sqrt{1+\beta^2} & 0 \\
0 & 0 & 0 & 0 & 0 & 0 & \beta\sqrt{1+\beta^2} & \sqrt{1+\beta^2} & 0 \\
0 & 0 & 0 & 0 & 0 & 0 & 0 & 0 & 1+\beta^2
\end{pmatrix}
\begin{pmatrix} W_T \\ W_L \\ W_\Delta \\ W_{\Delta\Delta} \\ W_{T_p} \\ W_{\nabla_p} \\ W_{\Delta\Delta_p} \\ W_{\Delta_p} \\ W_\nabla \end{pmatrix}_{GJ}
\tag{258}
$$

APPENDIX F – The angular coefficients

In eq. (112) we present the angular distribution parametrization, nevertheless one need connects it with the angular distribution which given us the A_i ($i = 0, 1, 2, 3, 4, 5, 6, 7$) values in terms of the structure functions W_j (for $j = T, L, \Delta, \Delta\Delta, T_P, \nabla_P, \nabla, \Delta\Delta_P, \Delta_P$). In what follows, we'll show how to obtain such connection. Therefore, starting from the angular distribution which is written as

$$\frac{dN}{d\Omega} = \frac{3}{8\pi} \frac{1}{2W_T + W_L} \Bigg[g_T W_T + g_L W_L + g_\Delta W_\Delta + g_{\Delta\Delta} W_{\Delta\Delta}$$

$$+ c_G g_{T_P} W_{T_P} + c_G g_{\nabla_P} W_{\nabla_P} + c_G g_\nabla W_\nabla + g_{\Delta\Delta_P} W_{\Delta\Delta_P} + g_{\Delta_P} W_{\Delta_P} \Bigg], \quad (259)$$

where

$$g_T = 1 + \cos^2\theta, \qquad g_L = 1 - \cos^2\theta, \qquad g_{T_P} = 2\cos\theta,$$

$$g_{\Delta\Delta} = \sin^2\theta\cos 2\phi, \qquad g_\Delta = \sin 2\theta\cos\phi, \qquad g_{\nabla_P} = 2\sin\theta\cos\phi,$$

$$g_{\Delta\Delta_P} = \sin^2\theta\sin 2\phi, \qquad g_{\Delta_P} = \sin 2\theta\sin\phi, \qquad g_\nabla = 2\sin\theta\sin\phi. \quad (260)$$

Multiplying the angular distribution by $(W_T + W_L)/(W_T + W_L)$, one gets

$$\frac{dN}{d\Omega} = \frac{3}{4\pi} \frac{1}{\lambda + 3} \Bigg[1 + \lambda\cos^2\theta + \mu\sin 2\theta\cos\phi + \frac{\nu}{2}\sin^2\theta\cos 2\phi$$

$$+ \tau\sin\theta\cos\phi + \eta\cos\theta + \xi\sin^2\theta\sin 2\phi + \zeta\sin 2\theta\sin\phi + \chi\sin\theta\sin\phi \Bigg], (261)$$

where

$$\lambda = \frac{W_T - W_L}{W_T + W_L}, \quad \mu = \frac{W_\Delta}{W_T + W_L}, \quad \nu = \frac{2W_{\Delta\Delta}}{W_T + W_L}, \quad \tau = \frac{2c_G W_{\nabla_P}}{W_T + W_L},$$

$$\eta = \frac{2c_G W_{T_P}}{W_T + W_L}, \quad \xi = \frac{W_{\Delta\Delta_P}}{W_T + W_L}, \quad \zeta = \frac{W_{\Delta_P}}{W_T + W_L}, \quad \chi = \frac{2c_G W_\nabla}{W_T + W_L}. \quad (262)$$

The eq. (261) is a usual parametrization for the angular distribution, this form is quite often present in theoretical papers (see for instance (Boer; Vogelsang, 2006; Faccioli; Lourenco; Seixas; Wohri, 2010; Faccioli; Lourenco; Seixas, 2010; Faccioli; Lourenco;

Seixas; Wohri, 2011; Lyubovitskij; Zhevlakov; Anikin, 2024)). However, the most used parametrization found in experimental works is

$$
\begin{aligned}
\frac{\mathrm{d}N}{\mathrm{d}\Omega} &= \frac{3}{16\pi}\Bigg(1 + \cos^2\theta + \frac{A_0}{2}\left(1 - 3\cos^2\theta\right) + A_1\sin 2\theta\cos\phi + \frac{A_2}{2}\sin^2\theta\cos 2\phi \\
&+ A_3\sin\theta\cos\phi + A_4\cos\theta + A_5\sin^2\theta\sin 2\phi + A_6\sin 2\theta\sin\phi + A_7\sin\theta\sin\phi\Bigg).
\end{aligned}
\tag{263}
$$

Therefore, by comparison, one has that these two parametrization connects trough

$$
\begin{aligned}
A_0 &= \frac{2(1-\lambda)}{\lambda+3} = \frac{2W_L}{2W_T + W_L}\,, & A_1 &= \frac{4\mu}{\lambda+3} = \frac{2W_\Delta}{2W_T + W_L}\,, \\
A_2 &= \frac{4\nu}{\lambda+3} = \frac{4W_{\Delta\Delta}}{2W_T + W_L}\,, & A_3 &= \frac{4\tau}{\lambda+3} = \frac{4c_G W_{\nabla_P}}{2W_T + W_L}\,, \\
A_4 &= \frac{4\eta}{\lambda+3} = \frac{4c_G W_{T_P}}{2W_T + W_L}\,, & A_5 &= \frac{4\xi}{\lambda+3} = \frac{2W_{\Delta\Delta_P}}{2W_T + W_L}\,, \\
A_6 &= \frac{4\zeta}{\lambda+3} = \frac{2W_{\Delta_P}}{2W_T + W_L}\,, & A_7 &= \frac{4\chi}{\lambda+3} = \frac{4c_G W_\nabla}{2W_T + W_L}\,.
\end{aligned}
\tag{264}
$$

where we have used that

$$
\begin{aligned}
\frac{4}{\lambda+3}\left(1 + \lambda\cos^2\theta\right) &= \frac{1}{\lambda+3}\left(4 + (\lambda + 3\lambda)\cos^2\theta\right)\,, \\
\frac{4}{\lambda+3}\left(1 + \lambda\cos^2\theta\right) &= \frac{1}{\lambda+3}\left(4 + \lambda - \lambda + (\lambda + 3\lambda + 3 - 3)\cos^2\theta\right)\,, \\
\therefore \frac{4}{\lambda+3}\left(1 + \lambda\cos^2\theta\right) &= 1 + \cos^2\theta + \frac{(1-\lambda)}{\lambda+3}(1 - 3\cos^2\theta)\,.
\end{aligned}
\tag{265}
$$